School of Mathematics and Statistics

MATHEMATICAL MODELS AND NUMERICAL TECHNIQUES FOR PLASTICITY FLOWS OF GRANULAR MEDIA

Roger Collinson

This thesis is presented as part of the requirements for
the award of the Degree of Doctor of Philosophy
of the
Curtin University of Technology

August 1998

ABSTRACT

A mathematical study has been undertaken to model various kinds of granular flows including the perfect plasticity flow and the viscous elasto-plasticity flow. The work is mainly based on the double-shearing theory originated by Spencer and developed by many others. The focus of the project is on the formulation of the theory, the construction of mathematical models and the development of robust simulation techniques.

Based on a general formulation of the double-shearing theory, the perfect plasticity flow is shown to be governed by a set of highly nonlinear first order hyperbolic partial differential equations with two distinct characteristics. A sophisticated numerical algorithm is then developed based on the method of characteristics to determine the stress discontinuity and the velocity and stress fields. With the method developed, a numerical study is then undertaken to model the flow of granular materials in a hopper in the presence of stress discontinuity and to investigate the influence of various parameters on the distribution of hopper wall pressures.

Utilising the double shearing theory, a set of stress-strain constitutive equations in explicit form has been derived, which makes it possible to formulate the double-shearing theory within the framework of the finite element method. Thus, consequently, a sophisticated finite element technique has been developed to solve the general boundary value problem governing the viscous elasto-plasticity flows obeying the double-shearing theory. Numerical implementation of the frictional boundary condition is also presented. The model is then illustrated with a numerical example demonstrating the influence of wall friction on the distribution of pressures on silo walls throughout the dynamic process of material discharge from silos.

CERTIFICATION

I certify that the work presented in this thesis is my own work and that all references are duly acknowledged. This work has not been submitted, in whole or in part, in respect of any academic award at Curtin University of Technology or elsewhere.

ACKNOWLEDGEMENTS

I would like to express my appreciation to my supervisor, Dr. Yong-Hong Wu, for his support, enthusiasm, and encouragement throughout the entire project. I would also like to thank my associate supervisor, Dr. Peg-Foo Siew, for his constructive comments and suggestions.

A project of this magnitude has a profound impact on one's personal life. I would like to extend my special thanks to my parents for their love, support, and encouragement throughout this time-consuming endeavour and throughout my entire education.

Finally, I am grateful to the Australian Government for providing me with the Australian Postgraduate Award, without which it would have been difficult to undertake this study. Also, I wish to thank Curtin University of Technology for giving me financial support to present part of this work at the MODSIM97 World Congress.

Roger Collinson
Perth, Western Australia.

TABLE OF CONTENTS

LIST OF FIGURES

LIST OF TABLES

NOTATION

Latin letters

$\boldsymbol{D}$	elastic matrix
$\boldsymbol{D}_{ep}$	elastic-plastic matrix
D^{λ}	defined by Eq. (3.57)
D^{Λ}	defined by Eq. (3.59)
E	elastic modulus
G	viscous matrix
$H^1(\ )$	Sobolev space
$\boldsymbol{J}$, J	Jacobian matrix and its determinant
$L^2(\ )$	square integrable function space
N_b	number of nodes on $\partial\Omega_a$ and $\partial\Omega_f$
X , Y	body forces, per unit volume, in the x- and y-directions respectively
b_r, b_θ	components of the body force in the r- and θ - directions
c	cohesion
$c_{\alpha 1}$, $c_{\alpha 2}$	defined on page 52
$c_{\beta 1}$, $c_{\beta 2}$	defined on page 52
$\boldsymbol{d}$	rate of deformation tensor
$\boldsymbol{e}_\alpha$, $\boldsymbol{e}_\beta$	unit vectors in α- and β- directions respectively
$\overline{\boldsymbol{f}}$	prescribed traction
$\boldsymbol{f}_v$	body force vector
g	acceleration due to gravity
g_P	plastic potential
h	defined by Eq. (4.72)
$\boldsymbol{n}$	outward unit normal
p	mean pressure defined by Eq. (2.4)

q	maximum shear stress defined by Eq. (2.5)
s	deviatoric stress tensor
$s_{\alpha 1}$, $s_{\alpha 2}$	defined on page 52
$s_{\beta 1}$, $s_{\beta 2}$	defined on page 52
t_α, t_β	defined on page 52
v	velocity vector
v_i	velocity component in x_i-direction
v_n	normal component of velocity
v'	particle velocity relative to (ξ, η)-system
w	spin tensor

Greek letters

γ	defined by Eq. (4.50)
Δt	time increments
η	angle between the x-axis and outward normal to the surface
θ	$0 \le \theta \le \theta_w$
θ_w	hopper half-angle
μ	viscous constant
μ_w	coefficient of wall friction
ν	angle of dilation
ρ	density
σ	stress tensor
σ_s	rate-independent part of stress
σ_v	rate-dependent part of stress
σ_z	intermediate principal stress
σ_1, σ_2	principal stresses
$\overset{\circ}{\sigma}_m$	defined by Eq. (3.68)
υ	Poisson's ratio

ϕ	angle of internal friction
ϕ_k	interpolating functions
ϕ_w	angle of wall friction
ψ	angle between positive x-direction and σ_1-direction
ψ_w	ψ value at wall
$\overline{\psi}$	angle between the algebraically greatest principal stress and the radial direction
$\overline{\psi}_w$	value of $\overline{\psi}$ at the wall
ω_j	weight functions

Mathematical symbols

$\partial\Omega_a$	adhesion contact boundary
$\partial\Omega_f$	frictional boundary
$\partial\Omega_t$	boundary with prescribed tractions
R	set of real numbers
∇	gradient operator
$\nabla\cdot(\ )$	$(\ )_{ij,j}$
$\nabla(\ )$	$(\ )_{ij,k}$
$\dot{(\ )}=\frac{D(\ )}{Dt}$	material derivative
$\mathring{(\ )}$	co-rotational time derivative

Subscripts

$(\ )_{ij}$	tensor indices
$(\ )_{,j}$	partial derivative with respect to x_j
$(\ )_D$	value at a point on the line of discontinuity
$(\ )_p$	value along α-line

$( )_Q$ value along β-line

$( )_R$ value at the intersection of α- and β-lines

Superscripts

$( )^i$ ith iteration

$( )^n$ nth time step

$( )^-$ denotes values below the discontinuity

$( )^+$ denotes values above the discontinuity

CHAPTER ONE

INTRODUCTION

1.1 BACKGROUND

A granular material can be defined as a collection of a large number of discrete macroscopic solid particles in contact with each other. The interstices are usually filled with a fluid, most often air, which usually can be neglected in the study of most properties of the system. In general, granular materials cannot be classified as any of the usual states of matter - solids, liquids or gases, and have to be considered as an additional state of matter. Under extreme conditions, granular materials are polymorphous - they can sustain shear like a solid (up to a point) but they can also flow like fluids. Due to this dual nature, the behaviours of granular materials are extremely complex and their modelling constitutes one of the outstanding problems of continuum mechanics (Jaeger *et al.*, 1996).

The storage and flow of granular materials are essential in many industrial processes and engineering applications. For example, materials to be handled in mining and mineral industries such as coal and mineral ores are granular materials. In the chemical industry, about one-half of the products and at least three-quarters of the raw materials are in granular form. Many other industries also deal with granular materials such as food, pharmaceuticals and cement. Geophysical processes such as avalanches, river sedimentation, dune formation and tectonic faulting, also involve granular materials. A good understanding of the properties of granular materials and

the behaviour of granular flows will enable one to control natural processes and to optimise industrial processes involving granular materials.

Despite the prevalence of granular flows in the process industries, the underlying principles are poorly understood. It is estimated that up to forty percent capacity of many industrial plants is wasted due to problems in transporting these materials from one part of factory floor to another (Jaeger *et al.*, 1996). Most problems are related to the storage and flow of granular materials in silos. A silo is a storage structure usually consisting of a vertical bin section and a converging hopper section as shown in Fig. 1.1. The size of a silo can be up to 20 metres in diameter and 60 metres in height (see Nedderman, 1992). Problems in silo operation mainly include erratic flow or blockage, dead zones and material ageing, wall adhesion, wear of the silo wall, dust explosions, and the complete collapse of silos (often with loss of life). These difficulties cause enormous financial losses.

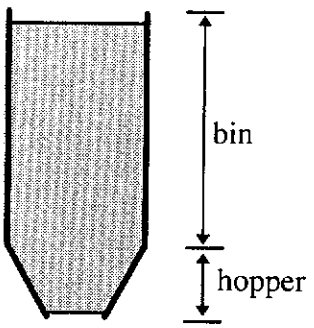

Fig. 1.1 A typical silo

Although many studies have been undertaken, the physics of granular flows is still not fully understood due to its complexity and, as a result, there is no generally accepted flow theory of granular media. Spencer (1982) has suggested that different models may be required, not only for different materials, but also for the same material under different conditions. Therefore at the current stage of development, it is important to investigate the physics of granular flow and thus to develop new

robust flow theory and mathematical models. It is equally important to formulate the existing flow theories and thus to develop robust numerical methods for solving general granular flow problems, which are not only technologically important, but also essential to the validation of flow theories.

1.2 OBJECTIVE

At present, the study of plasticity flows of granular materials is mainly dominated by the plastic-flow rule theory and the double-shearing type theory. Over the last two decades, many sophisticated constitutive equations and finite element methods based on the plastic flow rule theory have been developed and used to study the stress fields in hoppers and bins, but in general, velocity predictions do not agree well with experimental results. Great efforts have also been devoted to the development of double-shearing type models and to the solution of various problems using the theory. It has also been shown that the double-shearing theory possesses certain advantages over the more classical plastic flow rule theory. For example, under certain conditions, a double shearing model may include the plastic flow rule model as a special case. In addition, the theory is inherently capable of describing the discontinuity characteristics of stress fields in granular materials. However, very few attempts have been made to develop constitutive equations and sophisticated numerical methods based on the double shearing theory for solving general granular flow problems.

The objective of this thesis is to develop robust mathematical models and sophisticated numerical techniques for various kinds of granular flows based on the double shearing flow theory with a particular application to the study of granular flows in silos. More specifically, the project aims to

- formulate the dilatant double shearing theory to establish a set of double-shearing type constitutive equations for perfect plasticity flows and elastic- plasticity flows;

- develop a characteristic method and numerical algorithm for solving the hyperbolic system governing the double-shearing perfect-plasticity flow of granular materials in hoppers;

- develop a general finite element technique for modelling the double-shearing plasticity flows incorporating the viscous effect and elastic deformation with an application to the study of pressures on silo walls.

1.3 OUTLINE OF THE THESIS

This thesis briefly reviews previous work on the modelling of granular flows, describes the mathematical models and numerical algorithms developed for perfect plasticity flows and viscous elastic-plasticity flows and presents results and conclusions gained from various numerical investigations.

Chapter one introduces the background of research and presents the objectives of the research program.

Chapter two reviews some of the voluminous literature on the subject of granular materials that is pertinent to the proposed research, and highlights areas that require further investigation and development.

Chapter three is concerned with the derivation of constitutive equations for perfect plasticity flows and viscous elastic-plasticity flows based on the *double-shearing* theory. In particular, an elastic-plastic matrix based on the double-shearing theory is derived.

Chapter four is concerned with the development of a characteristics method and numerical algorithm for solving the highly nonlinear hyperbolic partial

differential equations governing the perfect plasticity flow of granular materials in hoppers.

Chapter five is concerned with the development of a finite element method for solving the highly nonlinear boundary value problem governing the viscous elastic-plasticity flow of granular materials utilising the double-shearing type constitutive equations derived in chapter three.

Chapter six presents conclusions gained from the present study and highlights areas for further research.

CHAPTER TWO

REVIEW OF THE LITERATURE

2.1 GENERAL OVERVIEW

Granular flow may occur in several regions, which can be subdivided into slow and rapid flows. In slow flows, particles stay in contact and interact frictionally with their neighbours over a long period of time. Particle motion continues in this manner as long as the deformation remains fairly slow. This is the so-called *quasi-static* regime of granular flows. On the other hand, in rapid flows, each particle moves freely and independently of even its nearest neighbours. Particles interact by fast impacts occurring during their collisions by transfer of particle kinetic energy and momentum, the nature of which governs the material flow property.

Over the last few decades, extensive research has been carried out to study the properties and flows of granular materials. Early research mainly focused on experimental investigation and deriving approximate analytical methods and empirical formulae suitable for engineering design. Typical results developed include Walker (1966), Walker & Blanchard (1967), Walters (1973a, 1973b) and Jenike's (1961) formulae for the prediction of silo pressures and Savage (1965), Davidson & Nedderman (1973) and McLean's (1979) formulae for the prediction of flow rates of granular materials flowing out of silos. To investigate the complex flow behaviour and phenomena related to granular flows, in the last two decades, many researchers have concentrated on investigating granular flows theoretically

and a number of flow theories have been developed for analysis. Essentially, these theories can be classified into three categories:

- discrete element simulation models for both rapid and shear flows,
- statistical collision models for rapid flows,
- frictional plasticity models for slow flows.

The discrete element method is based on the molecular dynamic simulation approach. In such kind of models, a granular material is assumed as an assembly of macro-particles, each containing many actual granules, connected by springs and dashpots. The motion of each individual particle is governed by the principle of linear momentum and the principle of angular momentum. By calculating the interaction forces between particles in contact and integrating the equations of motion for each particle with respect to time, one can determine the velocity and position of every particle at any instant of time and thus analyse the granular flow behaviour. Over the last few decades, many different discrete element models have been developed. These models can be classified into two categories, namely the hard particle model (Campbell & Brennen, 1985a; 1985b; Cambell & Gong, 1986) and the soft particle model (Walton & Braun, 1985; 1987). The hard particle model generally is only applicable to rapid flows with low bulk density. While the soft particle model is applicable to both rapid and slow flows. Many attempts have also been made to incorporate statistical mechanics methods with the discrete element model and in this kind of models, the flow of particles is simulated using either the Markov process (Kitamura, 1980; Roco *et al.*, 1990) or the Monte Carlo methods (Hopkins & Shen, 1988). Recently, the discrete element method has also been applied to the problem of granular material flows in silos. An investigation of hopper wall stresses has been carried out by Rong (1994) and Langston *et al.* (1995) among others. Rong also presented a comprehensive review of the method and its applications in the field of granular materials. This approach is gaining popularity with increasing computer power. However, the big disadvantage of the method is that it is computationally expensive and so only fewer that 20000 particles are

usually considered. In addition, the particles usually have to be assumed to have particular shapes such as circular discs, spheres, polygonal blocks, or super-elliptic discs and etc. It is still not possible at present to consider any irregular shapes, which limits the application of the method as it has been well established that the granular flow behaviour greatly depends on particle shape and size distribution.

The statistical collision method is a continuum approach based on micro-mechanics analysis of particle collisions and statistical averaging. In this kind of models, a granular material is assumed as an assembly of microscopic solid particles and the flow is dominated by random motion and binary collisions of particles usually assumed as rigid or near elastic smooth discs or spheres. The stress in the material is assumed to be created by particle collisions. Early models of this type include those due to Bagnold (1954), McTigue (1978), Shen & Ackermann (1982), and Haff (1983). Models that explore the similarity of rapid granular flows and compressible flows of dense gas have also been proposed such as those by Blinowski (1978) and Ahmadi (1985). Recent developments of this kind of theory are mainly based on the kinetic Boltzmann-Enskog equation. The Chapman Enskog method for the dense gas kinetic theory was modified to derive the dynamic equation for granular flows. The physical similarity between rapid granular flows and the kinetic theory view of dense gases has led to a number of models for granular rapid flows and the continuum equations are similar to those for dense gases. Typical theories of this type include those by Jenkins & Savage (1983), Campbell (1990), Goldshtein & Shapiro (1995), and Brey *et al.* (1997). Several attempts have also been made to develop theories considering the frictional effect, such as those due to Johnson & Jackson (1987) and Savage (1988). These theories are based on the argument that stresses due to different mechanisms can simply be added together. Thus, total stresses are then the sum of collisional stresses and frictional contributions. The collision theory has been applied to model various kinds of granular flows, such as the plane shear-flow between parallel plates and the flow down an inclined plane. However, in general, the existing theories of this type are limited in several aspects. Firstly, they only apply to rapid granular flows with

low bulk density. Secondly, most existing models are limited to idealised materials consisting of circular disc and spherical particles only.

Plasticity models are based on the assumption that the material flows according to a constitutive law if the stress state satisfies a yield condition. Many different yield conditions have been established (see Farley & Valentin, 1968; Matsuoka, 1984; Hill & Wu, 1993) and two different theories have been proposed to derive the constitutive equations for granular materials, i.e., the conventional plastic flow rule theory and the so-called double-shearing theory originated by Spencer and developed by Spencer and others (see Spencer, 1982; Hill & Wu, 1992; Harris, 1993; 1995). Sophisticated constitutive equations and numerical techniques based on the plastic flow rule theory have been developed and used with considerable success to investigate granular flows in hoppers and bins (Rombach & Eibl, 1995; Schmidt & Wu, 1989). It has also been found that under certain conditions, the double-shearing theory includes the plastic flow rule theory as a special case (see Hill & Wu, 1992; Harris, 1995). From the features of plasticity models and in comparison with other types of models/theories, it is believed that proper models for slow granular flows are within the framework of nonlinear plasticity theory. However, the plasticity theory for granular flows at present is still at the stage of development. There does not exist a generally accepted theory and thus further work to develop more accurate theory, to unify all existing theory and to implement these theories numerically is essential for the development of the subject.

The current project is focused on further development of mathematical models and numerical techniques for slow granular flow based on the plasticity theory. Thus we will introduce in the rest of this chapter the fundamental continuum equations and plasticity theories governing the flow of granular materials. Prior work on granular flows based on other types of theories will not be presented here.

2.2 YIELD FUNCTION AND YIELD CRITERION

The yield criterion constitutes an essential part of plasticity theory. Granular materials deform or yield when there is a relative slipping motion of adjacent particles. This slipping is resisted by frictional forces which are overcome only when the shear stress attains a sufficiently large magnitude in comparison with the normal stress. The criterion under which yield occurs is referred to as a yield criterion.

In the present study, we consider plane deformations relative to a rectangular Cartesian coordinate system $Oxyz$ such that the displacements are parallel to the (x,y)-plane and independent of the coordinate z. We assume that the intermediate principal stress is directed in the z-direction. We also use the usual sign convention for continuum mechanics that tensile stresses are positive. Let $\sigma_1 > \sigma_z > \sigma_2$ be the principal stress components of the stress tensor σ and ψ be the angle between the positive x direction and the σ_1 direction. Then from tensor transformation, we have

$$\sigma_{xx} = -p + q\cos 2\psi, \tag{2.1}$$

$$\sigma_{yy} = -p - q\cos 2\psi, \tag{2.2}$$

$$\sigma_{xy} = q\sin 2\psi, \tag{2.3}$$

where p and q are defined as

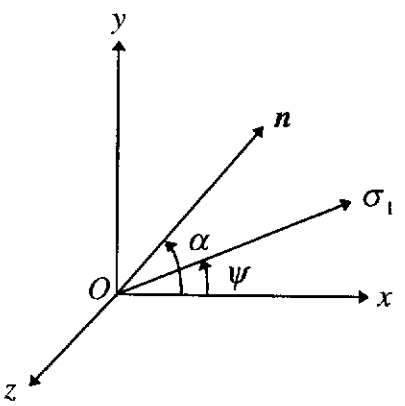

Fig. 2.1 Eulerian frame of reference $Oxyz$ and principal stress σ_i

$$p = -\frac{1}{2}(\sigma_1 + \sigma_2), \tag{2.4}$$

$$q = \frac{1}{2}(\sigma_1 - \sigma_2). \tag{2.5}$$

Consider an element of surface with normal $\boldsymbol{n}$ which lies in the Oxy plane. Let α be the angle that $\boldsymbol{n}$ makes with the x direction as shown in Fig. 2.1. Then the normal stress and shear stress acting on the element surface are respectively given by

$$\sigma_{nn} = p - q\cos 2(\alpha - \psi),$$

$$\sigma_{nt} = q\sin 2(\alpha - \psi).$$

The locus of the values of $(\sigma_{nn}, \sigma_{nt})$ at which permanent deformation or yield occurs is called the yield locus. For a stress state represented by the Mohr circle A, which does not touch the yield locus, the frictional forces are not fully mobilised and the solid is rigid or elastic. When the stress state changes so that the corresponding Mohr circle A' is tangent to the yield locus then two slip planes are formed, inclined at angles $\pm\left(\frac{\pi}{4} + \frac{\phi}{2}\right)$ to σ_1, represented by s_1 and s_2. These slip planes are also referred to as α- and β-lines. The material is then said to be in a state of plastic equilibrium. The extent of slip may be large during steady flow or

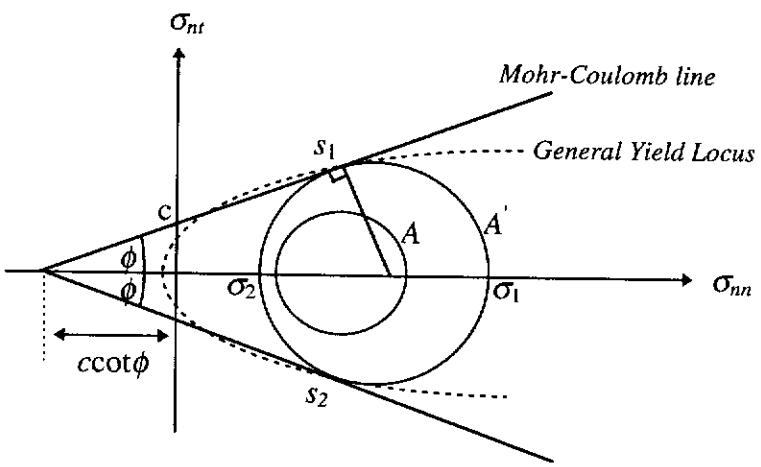

Fig. 2.2 The Mohr-Coulomb failure criterion

infinitesimal in a static material. The criterion gives an upper limit on the magnitude of the shear stress on a plane, it does not, however, give the direction of slip.

The most simple and wildly used yield condition is the so-called Coulomb-Mohr yield condition which states that the material fails when the shear (tangential) stress σ_{nt} acting on the surface of a material element attains the critical value, namely

$$|\sigma_{nt}| = c + \sigma_{nn} \tan\phi, \tag{2.6}$$

where the parameters c and ϕ are constants which characterise the mechanical properties of the material. The parameter c is called the cohesion and ϕ is called the angle of internal friction; both parameters are determined by experiment. The Coulomb-Mohr yield criterion can be represented by a pair of straight lines as shown in Fig. 2.2. In the special case of frictionless materials, for which $\phi = 0$, Eq. (2.6) reduces to the Tresca yield condition. If $c = 0$, the material is referred to as cohesionless material.

In terms of the stress invariants p and q, the Coulomb-Mohr yield criterion (2.6) can be shown to become

$$f = 2q - 2p\sin\phi - 2c\cos\phi = 0, \tag{2.7}$$

from which it can be noted that yielding is uninfluenced by the intermediate principal stress.

For most granular materials the angle of internal friction is not constant along the yield locus (see for example Stainforth *et al.*, 1970). Kingston and Spencer (1970) have presented a discussion on the general yield criteria for plane strain materials. Various nonlinear (in terms of p and q) yield functions have been

developed to describe the yielding property of granular materials. Such as those by Hill (1950), Sokolovskii (1965) and Hill & Wu (1993).

2.3 STRESS EQUATIONS OF MOTION AND KINEMATIC EQUATIONS

In the Eulerian frame of reference $Oxyz$ as shown in Fig. 2.1, the stress equations of motion can be expressed in invariant form as

$$\nabla \cdot \sigma + f_v = \rho\left(\dot{v} + \nabla v \cdot v\right) \text{ in } \Omega,$$

or in index notation,

$$\sigma_{ji,j} + f_{vi} = \rho\left(v_{i,t} + v_j v_{i,j}\right). \tag{2.8}$$

Assuming that the material obeys the Coulomb-Mohr yield criterion, then in terms of p and q, Eqs. (2.8) become

$$-(1-\sin\phi\cos 2\psi)\frac{\partial p}{\partial x} + \sin\phi\sin 2\psi\frac{\partial p}{\partial y} - 2(p\sin\phi + c\cos\phi)\sin 2\psi\frac{\partial \psi}{\partial x}$$
$$+2(p\sin\phi + c\cos\phi)\cos 2\psi\frac{\partial \psi}{\partial y} + X = \rho\left(\frac{\partial v_x}{\partial t} + v_x\frac{\partial v_x}{\partial x} + v_y\frac{\partial v_x}{\partial y}\right), \tag{2.9}$$

$$\sin\phi\sin 2\psi\frac{\partial p}{\partial x} - (1+\sin\phi\cos 2\psi)\frac{\partial p}{\partial y} + 2(p\sin\phi + c\cos\phi)\cos 2\psi\frac{\partial \psi}{\partial x}$$
$$+2(p\sin\phi + c\cos\phi)\sin 2\psi\frac{\partial \psi}{\partial y} + Y = \rho\left(\frac{\partial v_y}{\partial t} + v_x\frac{\partial v_y}{\partial x} + v_y\frac{\partial v_y}{\partial y}\right). \tag{2.10}$$

Let $v = \left(v_x, v_y\right)$ be the granular velocity, then the rate of deformation tensor $\boldsymbol{d}$, and the spin tensor $\boldsymbol{w}$ are related to v by the usual kinematic equations as follows

$$\boldsymbol{d} = \frac{1}{2}\left(\nabla v + (\nabla v)^T\right),\ \boldsymbol{w} = \frac{1}{2}\left(\nabla v - (\nabla v)^T\right), \tag{2.11}$$

or in component form

$$d_{ij} = \frac{1}{2}\left(v_{i,j} + v_{j,i}\right),\ w_{ij} = \frac{1}{2}\left(v_{i,j} - v_{j,i}\right), \tag{2.12}$$

where the superscript T denotes transpose.

2.4 PLASTIC POTENTIAL FLOW RULE THEORIES

Once the yield condition is satisfied, the material will flow obeying a set of constitutive equations describing the relation between the stress tensor σ and the deformation and spin tensors $\boldsymbol{d}$ and $\boldsymbol{w}$. The plastic potential flow rule theory is one of the principal theories for establishing the constitutive equations. Models of this kind are developed in the context of civil and geotechnical engineering (Harris, 1993). The necessary kinematic assumption postulated for plastic deformation or plastic flow is called the flow rule. The theory is based on a plastic potential g_p, having the unit of stress and being a function of stresses. The flow rule states that the plastic strain rates d_{ij}^{p} are proportional to the derivatives of the plastic potential with respect to the corresponding stress, that is

$$d_{ij}^{p} = \lambda \frac{\partial g_p}{\partial \sigma_{ij}}, \tag{2.13}$$

where λ is a scalar that may be called a plastic multiplier and depends on the flow rate. The flow rule is called associated if g_p is identical to the yield function f and nonassociated otherwise. In the case of associated flow rule, plastic flow develops along the normal to the yield surface.

Numerous plastic potential models have been proposed. The common features of these models are that they either use the associated flow rule or some modification of it and the characteristics of stress and velocity do not coincide in general. Some examples of the most significant works utilising the associated flow rule models are those by Drucker & Prager (1952), Drucker, Gibson & Henkel

(1957), and Cox, Eason & Hopkins (1961). The major criticism of these theories is that this approach predicts unrealistically large dilatation rates (Collins, 1990). Also Balendran & Nemat-Nasser (1993) pointed out that since a granular material is dilatant and pressure sensitive, the above flow rules do not apply. Roscoe, Schofield & Wroth (1958) and Atkinson & Bransby (1978) abandon the Coulomb-Mohr yield criterion and replace it by a hardening model described by the associated plastic flow rule with a new family of yield functions as the plastic potential. The criticism of non-coincidence of stress and velocity characteristics in this model is addressed by Collins (1990), who shows that when the density changes are properly allowed for then the velocity and stress characteristics will always coincide. Various attempts have also been made to develop non-associated flow rule models. Typical examples include those by Hill (1950), Johanson (1964) and Lade (1977).

Generally, in elastic-plastic analysis, one assumes that the total deformation consists of an elastic component and a plastic component, namely

$$\boldsymbol{d} = \boldsymbol{d}^e + \boldsymbol{d}^p, \tag{2.14}$$

and $\boldsymbol{d}^e$ can be related to stress through an elastic matrix $\boldsymbol{D}$, namely

$$\sigma = \boldsymbol{D}\boldsymbol{d}^e. \tag{2.15}$$

From Eqs. (2.13) and (2.15), together with the condition $f = 0$, one can derive a set of constitutive equations of the form

$$\sigma = \boldsymbol{D}_{ep}\boldsymbol{d}. \tag{2.16}$$

Thus by substituting Eq. (2.16) into the stress equations of motion (2.8) and using the kinematic Eqs. (2.12), one obtains a system of two equations for the solution of two unknown variables v_x and v_y. The deformation $\boldsymbol{d}$ and stress σ can be determined from (2.12) and (2.16).

2.5 DOUBLE SHEARING FLOW THEORIES

The double shearing theory is an alternative flow theory parallel to the plastic flow rule theory. The basic form of the theory is based on the Mohr yield condition and

assumes that deformation arises by shear on surfaces on which the critical shear traction is mobilised and that the shear direction coincides with that of the shear traction.

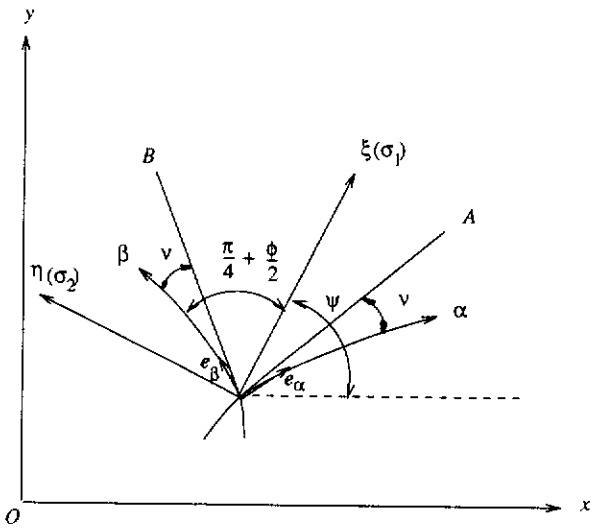

Fig. 2.3 Relation of α and β lines with the σ_1 axis

The most significant pioneering work in the development of the double shearing theory is due to de Jong (1959) and Spencer (1964). In 1959, de Josselin de Jong, from a review of the experimental evidence, postulated that deformation of granular materials occurs by simultaneous sliding along two families of stress characteristics. However, de Jong considered only graphical methods for solving boundary value problems and did not formulate the theory to derive the general constitutive equations. Thus, Spencer (1964), motivated by de Jong's ideas, developed a general double shearing theory for plane deformations of isotropic incompressible granular materials. Spencer's double shearing theory assumes that the complete deformation at any point of the body consists of two shearing motions occurring simultaneously on the $\alpha-$ and $\beta-$ stress characteristic lines and which are superposed on one another. More specifically, using the notation as shown in Fig. (2.3), the double shearing assumption can be expressed as

$$\frac{\partial v'}{\partial s_\alpha} = a e_\beta \,, \quad \frac{\partial v'}{\partial s_\beta} = b e_\alpha \tag{2.17}$$

where v' is the particle velocity relative to the (ξ,η) system the origin of which is fixed on the particle P and its axes rotate with angular velocity $\Omega = \frac{D\psi}{Dt}$ about the instantaneous position P relative to the fixed coordinate system (x,y). So that the α and β lines are independent of time relative to the (ξ,η) system. Based on the assumption described by Eqs. (2.17), Spencer derived two kinematic equations usually known as velocity equations for the flow of granular materials, namely

$$\frac{\partial v_x}{\partial x} + \frac{\partial v_y}{\partial y} = 0, \tag{2.18}$$

$$\left(\frac{\partial v_x}{\partial y} + \frac{\partial v_y}{\partial x}\right)\cos 2\psi - \left(\frac{\partial v_x}{\partial x} - \frac{\partial v_y}{\partial y}\right)\sin 2\psi + \sin\phi\left(\frac{\partial v_x}{\partial y} - \frac{\partial v_y}{\partial x} + 2\Omega\right) = 0, \tag{2.19}$$

where $v = (v_x, v_y)$ is the velocity relative to the (x,y) system and ϕ is the angle of internal friction. The first equation is the incompressibility condition and the second equation relates the spin component to the components of the strain-rate tensor. The principal axes of stress and strain-rate will only coincide if $\phi = 0$. Also, the second equation is form-invariant under transformations of rectangular Cartesian coordinates and is independent of superimposed rigid-body motions.

Following Spencer's work, many studies have been carried out to further examine the theory (de Jong, 1971; Mandl and Luque, 1970) and to extend the theory in various aspects. Various authors extended the theory to axially symmetric cases (eg. Spencer, 1982 & 1986; Hill & Wu, 1992) and three dimensional cases (eg. Spencer, 1982; and Ostrowska-Maciejewska & Harris, 1990).

Another important extension of the theory is to include the dilatancy of granular materials. Spencer & Kingston (1973) proposed a dilatant model based on the hypothesis that the volume of a granular material will increase during flow by expanding an amount which is equal in all spacial directions. Thus the density is

considered as a state variable and is related to the stress and deformation history, namely

$$\frac{d\rho}{dp} = f(\rho, p, \kappa_R), \quad R = 1,2,\ldots,N,$$

where p is as defined by Eq. (2.4) and κ_R depends on stress and deformation history. The constitutive Eq. (2.19) is still valid while the incompressible condition (2.18) is replaced by the usual continuity equation for compressible fluids. Following Spencer, another form of dilatant double shearing model was proposed by de Josselin de Jong (1977). He assumed that sliding is accompanied by volume change as the sliding planes are saw-tooth shaped. The saw teeth are inclined at an angle θ to the average direction α^* of a sliding plane. Sliding occurs along the faces of the steps in the direction $(\alpha^*+\theta)$ as shown in Fig. 2.4. Based on this assumption, de Jong derived a set of equations including his double sliding, free rotating model as a special case.

Another type of double shearing model for dilatant granular material is due to Mehrabadi & Cowin (1978), Harris (1985), and Hill & Wu (1993). These models are based on the kinematic proposal of Butterfield & Harkness (1972) which states that any change in velocity relative to the slip-line field that occurs between successive points is in a direction inclined at ν to the conjugate slip-line. Using the same notation as defined in Fig. 2.3, the kinematic proposal can be expressed by

$$\frac{\partial v'}{\partial s_\alpha} = a e_B, \frac{\partial v'}{\partial s_\beta} = b e_A. \tag{2.20}$$

From Eq. (2.18) and (2.19), a set of constitutive equations can be derived, namely

$$\sin\nu\left[\left(\frac{\partial v_x}{\partial x} - \frac{\partial v_y}{\partial y}\right)\cos 2\psi + \left(\frac{\partial v_x}{\partial y} + \frac{\partial v_y}{\partial x}\right)\sin 2\psi\right] - \left(\frac{\partial v_x}{\partial x} + \frac{\partial v_y}{\partial y}\right)\cos(\phi - \nu) = 0, \tag{2.21}$$

$$\cos\nu\left[\left(\frac{\partial v_x}{\partial x}-\frac{\partial v_y}{\partial y}\right)\sin 2\psi-\left(\frac{\partial v_x}{\partial y}+\frac{\partial v_y}{\partial x}\right)\cos 2\psi\right]-\left(\frac{\partial v_x}{\partial y}-\frac{\partial v_y}{\partial x}+2\Omega\right)\sin(\phi-\nu)=0. \tag{2.22}$$

These equations reduce to Spencer's (1964) velocity equations when $\nu = 0$ (Eqs. (2.16) and (2.17) in Spencer (1964)). When $\nu = \phi$, Eqs. (2.21) and (2.22) together with the Coulomb yield condition are equivalent to the plastic flow rule proposed by Drucker & Prager (1952).

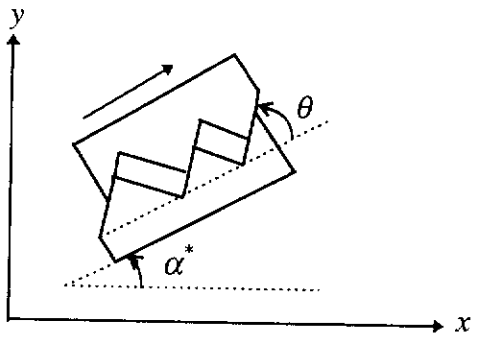

Fig. 2.4 Mechanism of material dilation

2.6 BOUNDARY CONDITIONS

Typically, a hopper is subjected to two different pressure states commonly referred to as the active and passive stress states. The active stress state develops during filling and persists until discharge. In the filling stage, the only load applied to the material is its weight and so the main load is directed downwards. The passive stress state applies to convergent flow during discharge. In this case the flowing material deforms plastically in a way that it contracts horizontally and expands vertically so that the main load is directed horizontally.

The required boundary conditions for both the active and passive stress states include a symmetry condition on the axis of symmetry, a frictional boundary

condition on the wall, and a traction condition on the top surface. On the centre-line, the geometric symmetry requires that $\overline{\psi} = \pi/2$ for the active case and $\overline{\psi} = 0$ for the passive case, where we have assumed that x is in the vertical axial direction and $\overline{\psi}$ denotes the angle between the algebraically greatest principal stress and the radial direction.

We assume that, at the hopper walls, frictional forces are fully mobilised and can be described by Coulomb's law of friction, i.e.

$$\sigma_{r\theta} = \sigma_{\theta\theta} \tan\phi_w \,, \qquad \text{at } \theta = -\theta_w \,, \tag{2.23}$$

$$\sigma_{r\theta} = -\sigma_{\theta\theta} \tan\phi_w \,, \qquad \text{at } \theta = \theta_w \,. \tag{2.24}$$

Now, considering the left hopper wall $(\theta = \theta_w)$, we have

$$\sin 2\overline{\psi}_w = \tan\phi_w \left(\csc\phi + \cos 2\overline{\psi}_w\right),$$

which on multiplying by $\cos\phi_w$, results in

$$\sin\left(2\overline{\psi}_w - \phi_w\right) = \frac{\sin\phi_w}{\sin\phi}. \tag{2.25}$$

Thus, we have

$$\overline{\psi}_w = \frac{1}{2}\left[\phi_w + \omega\right], \tag{2.26}$$

where

$$\omega = \sin^{-1}\left(\frac{\sin\phi_w}{\sin\phi}\right).$$

Also, we have

$$\sin\left[\pi - \left(2\overline{\psi}_w - \phi_w\right)\right] = \sin\left(2\overline{\psi}_w - \phi_w\right),$$

which on using Eq. (2.25) results in

$$\overline{\psi}_w = \frac{1}{2}\left[\phi_w + \pi - \omega\right]. \tag{2.27}$$

Condition (2.26) is applicable in the passive state and (2.27) in the active state. This situation can be better illustrated using the Mohr circle as shown in Fig. 2.6

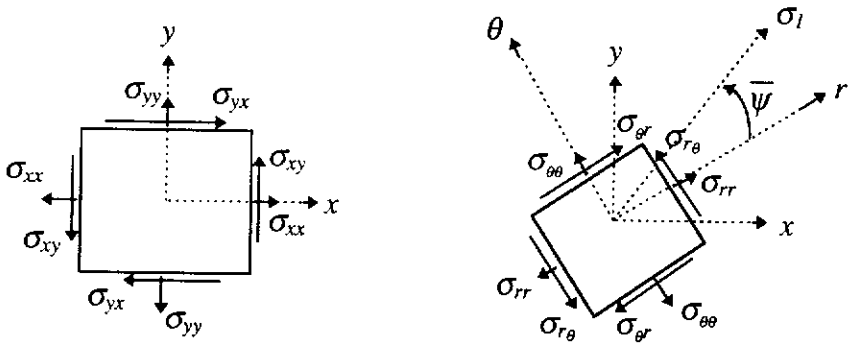

Fig. 2.5 Stresses acting on an infinitesimal element

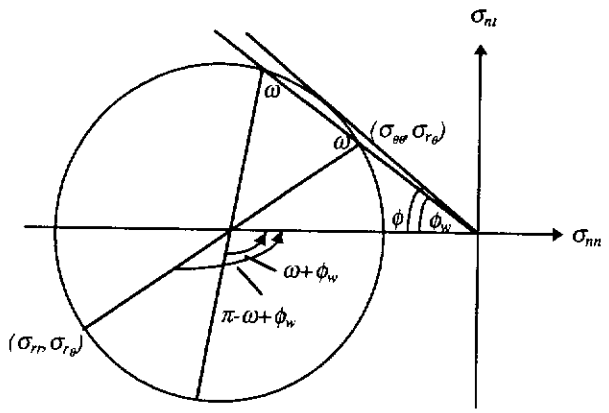

Fig. 2.6 The Mohr circle representation of active and passive stress states

For a moving granular material, the governing equations have to be supplemented by conditions that must be satisfied at the surfaces bounding the material. For a solid non-deformable surface, the necessary boundary condition is simply that the material cannot penetrate the solid surface. Hence, given that the surface is at rest, we have

$$v_n = 0. \tag{2.28}$$

2.7 NUMERICAL STUDIES

Using the continuum mechanics approach, the flow of a granular material in general can be modelled by the following boundary value problem.

BVP: find the stress tensor σ and velocity/displacement vector v such that the stress equations of motion, the kinematic equation, the continuity equation, the constitutive equations and the traction and velocity/displacement boundary conditions are all satisfied.

The constitutive equations are the major field equations which distinguish granular flow from other kinds of material flows. In addition, granular flow also possesses certain special features. For example, there may exist stress and velocity discontinuities in the flow region. Unlike in fluid dynamics, where the no-slip boundary condition is usually used, we have nonlinear frictional boundary conditions to deal with for granular flows.

Due to the complexity of the governing field equations, it is extremely difficult to solve the boundary value problem for granular flows. So far, only several simple exact solutions associated with the double shearing theories have been derived. Although these exact solutions provide a means for validating theories, they are only applicable to idealised problems and cannot be generalised to general problems with boundary conditions sensible to industrial processes and engineering practice. This difficulty in obtaining solutions explains why early studies on granular flow are only focused on deriving approximate analytical solutions.

With the development of computer technology, great effort has been made to develop numerical methods to solve the BVP numerically and to investigate the granular flow behaviour. Numerical methods for solving the boundary value problem for granular flows using the plastic flow rule theory have been studied by many researchers. Typical examples are those by Haussler & Eibl (1984), Ooi &

Rotter (1986, 1987), Schmidt & Wu (1989), Wu & Schmidt (1992), Rombach & Eibl (1995). However, only a few attempts have been made to study numerical methods for double shearing theories.

2.8 CONCLUDING REMARKS

Unlike many other areas of continuum mechanics disciplines, the flow of granular materials remains controversial. Granular materials possess many features other than solid and liquid and thus existing solid mechanics theories and fluid dynamics theories cannot be simply used to model granular flows. Different theories are needed to deal with the special features of granular flows, such as internal friction, frictional boundary conditions and possible change of phase from solid-like to fluid-like state.

Although many mathematical models and theories have been proposed for granular flows, there is no generally accepted theory at present and thus intensive study on various aspects is still needed. Firstly, any new development of flow theory and flow models will contribute significantly to the subject. Secondly, as so far no criterion has been developed to distinguish among different flow regimes, it is important to develop such a criterion. Thirdly, as granular materials are so diverse in their properties and existing flow theories are controversial, it is important to identify the application domain of each theory. Finally, in order to validate the flow theories and to apply them to solve real problems, it is necessary to develop robust numerical techniques for the most promising theories.

The present study focuses on the modelling of slow flow of granular materials. Based on the nature of different types of models, it is believed that the actual flow behaviour can be best simulated by developing a proper plasticity model. Therefore, this study focuses on the development of mathematical equations and numerical techniques based on the double-shearing plasticity model.

CHAPTER THREE

CONSTITUTIVE EQUATIONS FOR GRANULAR MATERIALS FLOWS

3.1 GENERAL

This chapter is concerned with the development of constitutive relations for granular flows obeying the dilatant double shearing flow theory. In Section 3.2, we present a general formulation of the theory based on Butterfield and Harkness' kinematic proposal. We allow the angle of internal friction and the angle of dilatancy to be a function of stresses. We also present the constitutive relations in two forms, namely along the (x,y) Cartesian coordinates and along the characteristics. The present derivation is parallel to the derivation by Harris (1985) and our work shows that the derived constitutive equations allow the use of any model for the angle of dilatancy and the use of a yield criterion of the form described by Teunissen & Vermeer (1988) . In addition, motivated by Harris' (1992) formulas, we also formulated the dilatant double shearing model to incorporate elastic deformation. A set of constitutive equations are derived to relate the stress rate with the deformation rate in explicit form. This development makes it possible to use the *finite element method* to solve the general boundary value problems of granular flows obeying the double shearing model, which will be presented in chapter five.

3.2 GENERAL CONSTITUTIVE RELATIONS DERIVED FROM DILATANT DOUBLE SHEARING MODEL

Consider a granular material, if the stress state in the material reaches the yielding condition, flow occurs by shearing along two families of planes namely the α and β characteristics. These two planes are inclined at angles $\pm(\pi/4+\phi/2)$ to the direction of the principal stress σ_1 where ϕ is the angle of internal friction. The dilatant double-shearing model postulates that the shearing along the α and β slip planes is accompanied by an expansion of material along the normal direction of the planes. This flow mechanism is described clearly by Butterfield and Harkness' kinematic proposal which states that any changes of velocity in the two successive points along the α and β slip-lines are along the B and A directions respectively. The A-direction makes an angle ν with the tangent to the α slip-line at P; and the B direction makes an angle $-\nu$ with the tangent to the β slip-line at P, as illustrated in Fig. 3.1.

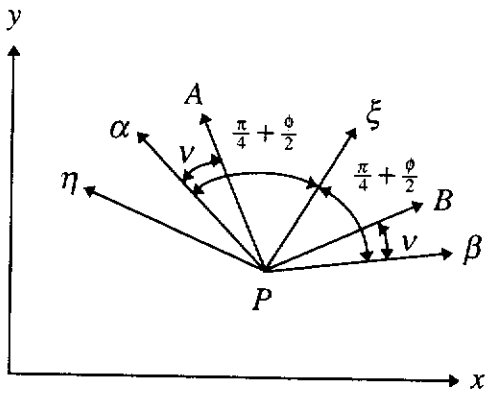

Fig. 3.1 Deformation at material particle P

To formulate the dilatant double shearing theory, we choose two sets of rectangular Cartesian coordinate systems, as proposed by Spencer (1964). The first set (Oxy) is fixed in space while the second set ($P\xi\eta$) is fixed on the particle and is in motion relative to the first set with rotating speed Ω and translational velocity (v_x, v_y).

Let $\boldsymbol{v} = (v_\xi, v_\eta)$ denote the velocity of particle P relative to the (ξ, η) system, then Butterfield and Harkness' proposal can be expressed as

$$\frac{\partial \boldsymbol{v}}{\partial s_\alpha} = a\boldsymbol{e}_B \,, \quad \frac{\partial \boldsymbol{v}}{\partial s_\beta} = b\boldsymbol{e}_A \,, \tag{3.1}$$

where s_α and s_β are measured along the slip-surface, $\boldsymbol{e}_A$ and $\boldsymbol{e}_B$ denote unit vectors along the directions of A and B respectively; and a and b are constants. Therefore, from Eq. (3.1) and Fig. 3.1 we have

$$\frac{\partial v_\eta}{\partial s_\alpha} \Big/ \frac{\partial v_\xi}{\partial s_\alpha} = -\tan\theta_\beta \quad , \quad \frac{\partial v_\eta}{\partial s_\beta} \Big/ \frac{\partial v_\xi}{\partial s_\beta} = \tan\theta_\beta \,, \tag{3.2}$$

or

$$\frac{\partial v_\eta}{\partial s_\alpha}\cos\theta_\beta + \frac{\partial v_\xi}{\partial s_\alpha}\sin\theta_\beta = 0 \quad , \quad \frac{\partial v_\eta}{\partial s_\beta}\cos\theta_\beta - \frac{\partial v_\xi}{\partial s_\beta}\sin\theta_\beta = 0 \,, \tag{3.3}$$

where

$$\theta_\beta = \frac{\pi}{4} + \frac{\phi}{2} - \nu \,.$$

The directional derivatives along the α and β lines are given by

$$\frac{\partial}{\partial s_\alpha} = \cos\theta_\alpha \frac{\partial}{\partial \xi} + \sin\theta_\alpha \frac{\partial}{\partial \eta} \,, \quad \frac{\partial}{\partial s_\beta} = \cos\theta_\alpha \frac{\partial}{\partial \xi} - \sin\theta_\alpha \frac{\partial}{\partial \eta} \,,$$

where

$$\theta_\alpha = \frac{\pi}{4} + \frac{\phi}{2} \,.$$

Then it follows from Eq. $(3.3)_1$ and Eq. $(3.3)_2$ that

$$\frac{\partial v_\eta}{\partial \xi}\cos\theta_\alpha\cos\theta_\beta + \frac{\partial v_\eta}{\partial \xi}\sin\theta_\alpha\cos\theta_\beta + \frac{\partial v_\xi}{\partial \xi}\cos\theta_\alpha\sin\theta_\beta + \frac{\partial v_\xi}{\partial \eta}\sin\theta_\alpha\sin\theta_\beta = 0 \,, \tag{3.4}$$

$$\frac{\partial v_\eta}{\partial \xi}\cos\theta_\alpha\cos\theta_\beta - \frac{\partial v_\eta}{\partial \eta}\sin\theta_\alpha\cos\theta_\beta - \frac{\partial v_\xi}{\partial \xi}\cos\theta_\alpha\sin\theta_\beta + \frac{\partial v_\xi}{\partial \eta}\sin\theta_\alpha\sin\theta_\beta = 0\,. \tag{3.5}$$

Subtracting Eq. (3.5) from Eq. (3.4) gives

$$2\frac{\partial v_\eta}{\partial \eta}\sin\theta_\alpha\cos\theta_\beta + 2\frac{\partial v_\xi}{\partial \xi}\cos\theta_\alpha\sin\theta_\beta = 0. \tag{3.6}$$

Noting that

$$\sin\theta_\alpha\cos\theta_\beta = \frac{1}{2}[\sin\nu + \cos(\phi-\nu)],$$

$$\sin\theta_\beta\cos\theta_\alpha = \frac{1}{2}[\cos(\phi-\eta) - \sin\nu],$$

Eq. (3.6) can be written as

$$\frac{\partial v_\xi}{\partial \xi} + K(\phi)\frac{\partial v_\eta}{\partial \eta} = 0\ , \tag{3.7}$$

where

$$K(\phi) = \frac{\cos(\phi-\nu)+\sin\nu}{\cos(\phi-\nu)-\sin\nu}.$$

Adding Eq. (3.4) and Eq. (3.5) results in

$$\frac{\partial v_\eta}{\partial \xi}[-\sin(\phi-\nu)+\cos\nu] + \frac{\partial v_\xi}{\partial \eta}[\sin(\phi-\nu)+\cos\nu] = 0\,,$$

which can be written in the form

$$\left(\frac{\partial v_\xi}{\partial \eta} + \frac{\partial v_\eta}{\partial \xi}\right) + \left(\frac{\partial v_\xi}{\partial \eta} - \frac{\partial v_\eta}{\partial \xi}\right)\frac{\sin(\phi-\nu)}{\cos\nu} = 0. \tag{3.8}$$

Let $\boldsymbol{d}$ and $\boldsymbol{w}$ denote respectively the rate of strain tensor and spin tensor. Then, relative to the (ξ,η) system, we have

$$d_{\xi\xi}=\frac{\partial v_\xi}{\partial \xi},\ d_{\eta\eta}=\frac{\partial v_\eta}{\partial \eta},\ d_{\xi\eta}=\frac{1}{2}\left(\frac{\partial v_\xi}{\partial \eta}+\frac{\partial v_\eta}{\partial \xi}\right),\ w_{\xi\eta}=\frac{1}{2}\left(\frac{\partial v_\xi}{\partial \eta}-\frac{\partial v_\eta}{\partial \xi}\right),$$

and Eqs. (3.7) and (3.8) become

$$d_{\xi\xi}+K(\phi)d_{\eta\eta}=0,\ d_{\xi\eta}+\frac{\sin(\phi-\nu)}{\cos\nu}w_{\xi\eta}=0. \tag{3.9}$$

Since the (ξ,η) system rotates with angular speed Ω relative to the (x,y) system, we have

$$w_{\xi\eta}=w_{xy}+\Omega.$$

Using the above equations together with the following standard tensor transformation formulae,

$$\begin{bmatrix} d_{\xi\xi} & d_{\xi\eta} \\ d_{\xi\eta} & d_{\eta\eta} \end{bmatrix}=\begin{bmatrix} \cos\psi & \sin\psi \\ -\sin\psi & \cos\psi \end{bmatrix}\begin{bmatrix} d_{xx} & d_{xy} \\ d_{xy} & d_{yy} \end{bmatrix}\begin{bmatrix} \cos\psi & -\sin\psi \\ \sin\psi & \cos\psi \end{bmatrix}$$

equations (3.9) become

$$\left(d_{xx}-d_{yy}\right)\cos 2\psi+2d_{xy}\sin 2\psi=\frac{\cos(\phi-\nu)}{\sin\nu}\left(d_{xx}+d_{yy}\right), \tag{3.10}$$

$$\left(d_{xx}-d_{yy}\right)\sin 2\psi-2d_{xy}\cos 2\psi=\frac{2\sin(\phi-\nu)}{\cos\nu}\left(w_{xy}+\Omega\right). \tag{3.11}$$

Equations (3.10) and (3.11) were originally proposed by Mehrabadi & Cowin (1978). Harris (1985) proposed another method for deriving the formulae and the present method is another alternative derivation. It is clear from the current derivation that the angle of internal friction is allowed to be any function of stress and there is no restriction on the angle of dilatancy.

Using the following standard formulae,

$$d_{xx}=\frac{\partial v_x}{\partial x},\quad d_{yy}=\frac{\partial v_y}{\partial y},\quad d_{xy}=\frac{1}{2}\left(\frac{\partial v_x}{\partial y}+\frac{\partial v_y}{\partial x}\right),\quad w_{xy}=\frac{1}{2}\left(\frac{\partial v_x}{\partial y}-\frac{\partial v_y}{\partial x}\right),$$

Eqs (3.10) and (3.11) can be expressed in terms of velocity components, namely

$$\left(\frac{\partial v_x}{\partial x}-\frac{\partial v_y}{\partial y}\right)\cos 2\psi+\left(\frac{\partial v_y}{\partial x}+\frac{\partial v_x}{\partial y}\right)\sin 2\psi=\frac{\cos(\phi-\nu)}{\sin\nu}\left(\frac{\partial v_x}{\partial x}+\frac{\partial v_y}{\partial y}\right), \quad (3.12)$$

$$\left(\frac{\partial v_x}{\partial x}-\frac{\partial v_y}{\partial y}\right)\sin 2\psi-\left(\frac{\partial v_y}{\partial x}+\frac{\partial v_x}{\partial y}\right)\cos 2\psi=\frac{\sin(\phi-\nu)}{\cos\nu}\left(\frac{\partial v_x}{\partial y}-\frac{\partial v_y}{\partial x}+2\Omega\right). \quad (3.13)$$

In the rest of this section, we formulate the constitutive relations along the α and β characteristics for the cases where both ϕ and ν are functions of stresses.

Let

$$\theta_\alpha=\psi-\frac{\pi}{4}-\frac{\phi}{2},$$

$$\theta_\beta=\psi+\frac{\pi}{4}+\frac{\phi}{2}.$$

Noting that directional derivatives along the α- and β-lines are given by

$$\frac{\partial}{\partial s_\alpha}=\cos\theta_\alpha\frac{\partial}{\partial x}+\sin\theta_\alpha\frac{\partial}{\partial y}, \quad (3.14)$$

$$\frac{\partial}{\partial s_\beta}=\cos\theta_\beta\frac{\partial}{\partial x}+\sin\theta_\beta\frac{\partial}{\partial y}, \quad (3.15)$$

we have

$$\cos\phi\frac{\partial}{\partial x}=\sin\theta_\beta\frac{\partial}{\partial s_\alpha}-\sin\theta_\alpha\frac{\partial}{\partial s_\beta}, \quad (3.16)$$

$$\cos\phi\frac{\partial}{\partial y}=-\cos\theta_\beta\frac{\partial}{\partial s_\alpha}+\cos\theta_\alpha\frac{\partial}{\partial s_\beta}. \tag{3.17}$$

Relative to the fixed (x,y) system, the velocity components in the x - and y-directions in terms of the components in the α- and β- directions are given by

$$v_x=v_\alpha\cos\theta_\alpha+v_\beta\cos\theta_\beta, \tag{3.18}$$

$$v_y=v_\alpha\sin\theta_\alpha+v_\beta\sin\theta_\beta. \tag{3.19}$$

Using Eqs. (3.16) - (3.19), we have

$$\begin{aligned}\cos\phi\left(\frac{\partial v_x}{\partial x}+\frac{\partial v_y}{\partial y}\right)=&\frac{\partial v_\alpha}{\partial s_\alpha}\cos\phi+v_\alpha\frac{\partial\theta_\alpha}{\partial s_\alpha}\sin\phi-v_\beta\frac{\partial\theta_\beta}{\partial s_\alpha}+v_\alpha\frac{\partial\theta_\alpha}{\partial s_\beta}\\&+\frac{\partial v_\beta}{\partial s_\beta}\cos\phi-v_\beta\frac{\partial\theta_\beta}{\partial s_\beta}\sin\phi,\end{aligned} \tag{3.20}$$

$$\begin{aligned}\cos\phi\left(\frac{\partial v_x}{\partial x}-\frac{\partial v_y}{\partial y}\right)=&\frac{\partial v_\alpha}{\partial s_\alpha}\sin 2\psi+v_\alpha\frac{\partial\theta_\alpha}{\partial s_\alpha}\cos 2\psi-\frac{\partial v_\beta}{\partial s_\alpha}\sin 2\psi\sin\phi\\&+\frac{\partial v_\beta}{\partial s_\alpha}\cos 2\psi\cos\phi-v_\beta\frac{\partial\theta_\beta}{\partial s_\alpha}\cos 2\psi\sin\phi\\&-v_\beta\frac{\partial\theta_\beta}{\partial s_\alpha}\sin 2\psi\cos\phi+\frac{\partial v_\alpha}{\partial s_\beta}\sin 2\psi\sin\phi\\&+\frac{\partial v_\alpha}{\partial s_\beta}\cos 2\psi\cos\phi+v_\alpha\frac{\partial\theta_\alpha}{\partial s_\beta}\cos 2\psi\sin\phi\\&-v_\alpha\frac{\partial\theta_\alpha}{\partial s_\beta}\sin 2\psi\cos\phi-\frac{\partial v_\beta}{\partial s_\beta}\sin 2\psi\\&-v_\beta\frac{\partial\theta_\beta}{\partial s_\beta}\cos 2\psi,\end{aligned} \tag{3.21}$$

$$\cos\phi\left(\frac{\partial v_x}{\partial y}+\frac{\partial v_y}{\partial x}\right)=-\frac{\partial v_\alpha}{\partial s_\alpha}\cos 2\psi+v_\alpha\frac{\partial\theta_\alpha}{\partial s_\alpha}\sin 2\psi+\frac{\partial v_\beta}{\partial s_\alpha}\cos 2\psi\sin\phi$$

$$+\frac{\partial v_\beta}{\partial s_\alpha}\sin 2\psi\cos\phi - v_\beta\frac{\partial \theta_\beta}{\partial s_\alpha}\sin 2\psi\sin\phi$$

$$+v_\beta\frac{\partial \theta_\beta}{\partial s_\alpha}\cos 2\psi\cos\phi - \frac{\partial v_\alpha}{\partial s_\beta}\cos 2\psi\sin\phi$$

$$+\frac{\partial v_\alpha}{\partial s_\beta}\sin 2\psi\cos\phi + v_\alpha\frac{\partial \theta_\alpha}{\partial s_\beta}\sin 2\psi\sin\phi$$

$$+v_\alpha\frac{\partial \theta_\alpha}{\partial s_\beta}\cos 2\psi\cos\phi + \frac{\partial v_\beta}{\partial s_\beta}\cos 2\psi$$

$$-v_\beta\frac{\partial \theta_\beta}{\partial s_\beta}\sin 2\psi, \tag{3.22}$$

$$\cos\phi\left(\frac{\partial v_x}{\partial y}-\frac{\partial v_y}{\partial x}\right)=\frac{\partial v_\alpha}{\partial s_\alpha}\sin\phi - v_\alpha\frac{\partial \theta_\alpha}{\partial s_\alpha}\cos\phi - \frac{\partial v_\beta}{\partial s_\alpha}+\frac{\partial v_\alpha}{\partial s_\beta}$$

$$-\frac{\partial v_\beta}{\partial s_\beta}\sin\phi - v_\beta\frac{\partial \theta_\beta}{\partial s_\beta}\cos\phi. \tag{3.23}$$

Substituting Eqs. (3.20) - (3.22) into Eq. (3.12) produces

$$v_\alpha\frac{\partial \theta_\alpha}{\partial s_\alpha}+\frac{\partial v_\beta}{\partial s_\alpha}\cos\phi - v_\beta\frac{\partial \theta_\beta}{\partial s_\alpha}\sin\phi + \frac{\partial v_\alpha}{\partial s_\beta}\cos\phi + v_\alpha\frac{\partial \theta_\alpha}{\partial s_\beta}\sin\phi - v_\beta\frac{\partial \theta_\beta}{\partial s_\beta}$$

$$-\frac{\cos(\phi-\nu)}{\sin\nu}\left(\frac{\partial v_\alpha}{\partial s_\alpha}\cos\phi + v_\alpha\frac{\partial \theta_\alpha}{\partial s_\alpha}\sin\phi - v_\beta\frac{\partial \theta_\beta}{\partial s_\alpha}+v_\alpha\frac{\partial \theta_\alpha}{\partial s_\beta}\right.$$

$$\left.-v_\beta\frac{\partial \theta_\beta}{\partial s_\beta}\sin\phi+\frac{\partial v_\beta}{\partial s_\beta}\cos\phi\right)=0 \tag{3.24}$$

Substituting Eqs. (3.21) - (3.23) into Eq. (3.13) gives

$$\frac{\partial v_\alpha}{\partial s_\alpha}-\frac{\partial v_\beta}{\partial s_\alpha}\sin\phi - v_\beta\frac{\partial \theta_\beta}{\partial s_\alpha}\cos\phi + \frac{\partial v_\alpha}{\partial s_\beta}\sin\phi - v_\alpha\frac{\partial \theta_\alpha}{\partial s_\beta}\cos\phi - \frac{\partial v_\beta}{\partial s_\beta}$$

$$-\frac{\sin(\phi-\nu)}{\cos\nu}\left(\frac{\partial v_\alpha}{\partial s_\alpha}\sin\phi - v_\alpha\frac{\partial\theta_\alpha}{\partial s_\alpha}\cos\phi - \frac{\partial v_\beta}{\partial s_\alpha} + \frac{\partial v_\alpha}{\partial s_\beta} - \frac{\partial v_\beta}{\partial s_\beta}\sin\phi\right.$$

$$\left. - v_\beta\frac{\partial\theta_\beta}{\partial s_\beta}\cos\phi + 2\Omega\cos\phi\right) = 0. \quad (3.25)$$

Multiplying Eq. (3.24) by $\sin\nu$ and Eq. (3.25) by $\cos\nu$ and adding the resulting equations gives

$$\frac{\partial v_\alpha}{\partial s_\beta}\sin\nu - v_\alpha\frac{\partial\theta_\alpha}{\partial s_\beta}\cos\nu + v_\beta\frac{\partial\theta_\beta}{\partial s_\beta}\sin(\phi-\nu) - \frac{\partial v_\beta}{\partial s_\beta}\cos(\phi-\nu) - \Omega\sin(\phi-\nu) = 0. \quad (3.26)$$

Multiplying Eq. (3.24) by $\sin\nu$ and Eq. (3.25) by $\cos\nu$ and taking the difference of the resulting equations gives

$$-v_\alpha\frac{\partial\theta_\alpha}{\partial s_\alpha}\sin(\phi-\nu) + \frac{\partial v_\beta}{\partial s_\alpha}\sin\nu + v_\beta\frac{\partial\theta_\beta}{\partial s_\alpha}\cos\nu - \frac{\partial v_\alpha}{\partial s_\alpha}\cos(\phi-\nu) + \Omega\sin(\phi-\nu) = 0. \quad (3.27)$$

Finally, given that Ω can be expressed in the form of

$$\Omega = \frac{\partial\psi}{\partial t} + v_\alpha\frac{\partial\psi}{\partial s_\alpha} + v_\beta\frac{\partial\psi}{\partial s_\beta},$$

we may deduce from Eq. (3.26) and Eq. (3.27) the following two velocity equations

$$\frac{\partial v_\beta}{\partial s_\beta}\cos(\phi-\nu) - \frac{\partial v_\alpha}{\partial s_\beta}\sin\nu + v_\alpha\left[\frac{\partial\psi}{\partial s_\beta}\cos\nu + \frac{\partial\psi}{\partial s_\alpha}\sin(\phi-\nu)\right] + \frac{\partial\psi}{\partial t}\sin(\phi-\nu)$$

$$-\frac{1}{2}\left[v_\alpha\cos\nu + v_\beta\sin(\phi-\nu)\right]\frac{\partial\phi}{\partial s_\beta} = 0, \quad (3.28)$$

$$\frac{\partial v_\alpha}{\partial s_\alpha}\cos(\phi-\nu) - \frac{\partial v_\beta}{\partial s_\alpha}\sin\nu - v_\beta\left[\frac{\partial\psi}{\partial s_\alpha}\cos\nu + \frac{\partial\psi}{\partial s_\beta}\sin(\phi-\nu)\right] - \frac{\partial\psi}{\partial t}\sin(\phi-\nu)$$

$$-\frac{1}{2}\left[v_\alpha\sin(\phi-\nu) + v_\beta\cos\nu\right]\frac{\partial\phi}{\partial s_\alpha} = 0, \quad (3.29)$$

which reduce to equations (3.15) in Spencer's (1964) paper when $\nu = 0$ and ϕ is constant.

When ϕ is constant and the deformation is in steady-state, Eqs. (3.28) and (3.29) reduce to

$$\frac{\partial v_\beta}{\partial s_\beta}\cos(\phi-\nu)-\frac{\partial v_\alpha}{\partial s_\beta}\sin\nu+v_\alpha\left[\frac{\partial \psi}{\partial s_\beta}\cos\nu+\frac{\partial \psi}{\partial s_\alpha}\sin(\phi-\nu)\right]=0, \qquad (3.30)$$

$$\frac{\partial v_\alpha}{\partial s_\alpha}\cos(\phi-\nu)-\frac{\partial v_\beta}{\partial s_\alpha}\sin\nu-v_\beta\left[\frac{\partial \psi}{\partial s_\alpha}\cos\nu+\frac{\partial \psi}{\partial s_\beta}\sin(\phi-\nu)\right]=0. \qquad (3.31)$$

3.3 CONSTITUTIVE EQUATIONS FOR DOUBLE SHEARING PLASTIC FLOW

In this section, we construct a set of constitutive equations for granular flows consisting of both elastic and plastic deformation governed by the double shearing mechanism.

Denote the Cauchy stress tensor by σ, then the deviatoric stress and strain-rate tensors are respectively given by

$$\boldsymbol{s} = \sigma - \left(\tfrac{1}{2}\mathrm{tr}\sigma\right)\boldsymbol{I}, \quad \boldsymbol{e} = \boldsymbol{d} - \left(\tfrac{1}{2}\mathrm{tr}\boldsymbol{d}\right)\boldsymbol{I},$$

where tr is the trace of a matrix and $\boldsymbol{I}$ is the identity tensor. The co-rotational time derivative of the Cauchy stress and deviatoric stress, denoted by $\overset{\circ}{\sigma}$ and $\overset{\circ}{s}$, respectively, are defined by

$$\overset{\circ}{\sigma} = \dot{\sigma} + \sigma\boldsymbol{w} - \boldsymbol{w}\sigma, \quad \overset{\circ}{\boldsymbol{s}} = \dot{\boldsymbol{s}} + \boldsymbol{s}\boldsymbol{w} - \boldsymbol{w}\boldsymbol{s},$$

where $\overset{\circ}{\sigma}$ and $\overset{\circ}{s}$ are the material time derivatives of σ and s, respectively. The co-rotational, or Jaumann, time derivative has the property (Green & Adkins, 1960) that it is independent of superposed rigid-body motions.

Based on a representation theorem of Wineman and Pipkin (1964), Harris (1992) showed that many theories in the mechanics of granular materials (theories presented in chapter two) can be incorporated into a single mathematical formulation. Harris deduced that it is possible to formulate a relation of the form

$$\boldsymbol{d}^{p} = \beta_{00}\boldsymbol{I} + \beta_{10}\boldsymbol{s} + \beta_{01}\overset{\circ}{\boldsymbol{s}} + \beta_{20}\boldsymbol{s}^{2}, \tag{3.32}$$

where the scalar functions β_{00}, β_{10}, β_{01} and β_{20} are assumed to be functions of some or all of the scalar invariants in the set

$$\mathcal{R} = \left\{\mathrm{tr}\sigma, \mathrm{tr}\boldsymbol{s}^{2}, \mathrm{tr}\boldsymbol{s}^{3}, \mathrm{tr}\overset{\circ}{\sigma}, \mathrm{tr}\boldsymbol{d}, \mathrm{tr}\boldsymbol{e}^{2}, \mathrm{tr}(\boldsymbol{s}\overset{\circ}{\boldsymbol{s}}), \mathrm{tr}(\boldsymbol{e}\boldsymbol{s}), \mathrm{tr}(\boldsymbol{s}^{2}\overset{\circ}{\boldsymbol{s}})\right\}.$$

To derive the double shearing based constitutive equations relating stress rate with strain rate in explicit form, we assume that the plastic strain component can be expressed by

$$\boldsymbol{d}^{p} = \alpha\boldsymbol{s} - \beta\overset{\circ}{\boldsymbol{s}}. \tag{3.33}$$

In the following, we describe how to determine α and β using the constitutive relation derived from the double shearing theory. We will consider here the cases where the angle of dilatancy ν is zero and the Mohr - Coulomb function is used. Under these conditions, the double shearing based constitutive relation is

$$d^{p}_{xx} + d^{p}_{yy} = 0, \tag{3.34}$$

$$\sin 2\psi\left(d^{p}_{xx} - d^{p}_{yy}\right) - 2d^{p}_{xy}\cos 2\psi - 2\sin\phi\left(w_{xy} + \Omega\right) = 0, \tag{3.35}$$

and the stress components can be expressed by

$$\sigma_{xx} = -p + q\cos 2\psi\,, \tag{3.36a}$$

$$\sigma_{yy} = -p - q\cos 2\psi\,, \tag{3.36b}$$

$$\sigma_{xy} = q\sin 2\psi\,, \tag{3.36c}$$

From Eqs. (3.36), we can deduce the following relations

$$\sin 2\psi = \frac{\sigma_{xy}}{q},\quad \cos 2\psi = \frac{\sigma_{xx} - \sigma_{yy}}{2q},\quad \tan 2\psi = \frac{2\sigma_{xy}}{\sigma_{xx} - \sigma_{yy}}. \tag{3.37}$$

Substitution of Eqs. $(3.37)_1$ and Eq. $(3.37)_2$ into Eq. (3.35) leads to

$$\sigma_{xy}\left(d^{p}_{xx} - d^{p}_{yy}\right) - d^{p}_{xy}\left(\sigma_{xx} - \sigma_{yy}\right) - 2q\sin\phi\left(w_{xy} + \Omega\right) = 0\,. \tag{3.38}$$

Taking the material derivative of Eq. $(3.37)_3$ with respect to time, that is

$$\frac{D}{Dt}\left(\tan 2\psi\right) = \frac{D}{Dt}\left(\frac{2\sigma_{xy}}{\sigma_{xx} - \sigma_{yy}}\right),$$

we have

$$2\Omega\sec^2 2\psi = \frac{2\dot{\sigma}_{xy}}{\sigma_{xx} - \sigma_{yy}} + 2\sigma_{xy}\frac{D}{Dt}\left(\sigma_{xx} - \sigma_{yy}\right)^{-1},$$

which implies that

$$\Omega = \frac{\dot{\sigma}_{xy}\left(\sigma_{xx} - \sigma_{yy}\right) - \sigma_{xy}\left(\dot{\sigma}_{xx} - \dot{\sigma}_{yy}\right)}{\left(\sigma_{xx} - \sigma_{yy}\right)^2}\cos^2 2\psi\,, \tag{3.39}$$

where $\Omega = \dfrac{D\psi}{Dt}$, and the superposed dots denote material times derivatives.

Squaring the difference of Eq. (3.36a) and Eq. (3.36b) results in

$$\left(\sigma_{xx}-\sigma_{yy}\right)^2 = 4q^2\cos^2 2\psi, \tag{3.40}$$

Substitution of Eq. (3.40) into Eq. (3.39) gives

$$4q^2\Omega = \dot{\sigma}_{xy}\left(\sigma_{xx}-\sigma_{yy}\right)-\sigma_{xy}\left(\dot{\sigma}_{xx}-\dot{\sigma}_{yy}\right), \tag{3.41}$$

As

$$\begin{bmatrix} \mathring{\sigma}_{xx} & \mathring{\sigma}_{xy} \\ \mathring{\sigma}_{xy} & \mathring{\sigma}_{yy} \end{bmatrix} = \begin{bmatrix} \dot{\sigma}_{xx}-2\sigma_{xy}w_{xy} & \dot{\sigma}_{xy}+w_{xy}\left(\sigma_{xx}-\sigma_{yy}\right) \\ \dot{\sigma}_{xy}+w_{xy}\left(\sigma_{xx}-\sigma_{yy}\right) & \dot{\sigma}_{yy}-2\sigma_{xy}w_{xy} \end{bmatrix}, \tag{3.42}$$

we have

$$\dot{\sigma}_{xy} = \mathring{\sigma}_{xy}-w_{xy}\left(\sigma_{xx}-\sigma_{yy}\right), \quad \mathring{\sigma}_{xx}-\mathring{\sigma}_{yy} = \dot{\sigma}_{xx}-\dot{\sigma}_{yy}-4\sigma_{xy}w_{xy} \tag{3.43}$$

which can be written as

$$\dot{\sigma}_{xx}-\dot{\sigma}_{yy} = \mathring{\sigma}_{xx}-\mathring{\sigma}_{yy}+4\sigma_{xy}w_{xy}. \tag{3.44}$$

Substituting Eq. $(3.43)_1$ and Eq. (3.44) into Eq. (3.41), we have

$$\begin{aligned} 4q^2\Omega &= \left(\sigma_{xx}-\sigma_{yy}\right)\left[\mathring{\sigma}_{xy}-w_{xy}\left(\sigma_{xx}-\sigma_{yy}\right)\right]-\sigma_{xy}\left(\mathring{\sigma}_{xx}-\mathring{\sigma}_{yy}+4\sigma_{xy}w_{xy}\right) \\ &= \left(\sigma_{xx}-\sigma_{yy}\right)\mathring{\sigma}_{xy}-\sigma_{xy}\left(\mathring{\sigma}_{xx}-\mathring{\sigma}_{yy}\right)-4w_{xy}\left[\tfrac{1}{4}\left(\sigma_{xx}-\sigma_{yy}\right)^2+\sigma_{xy}^2\right]. \end{aligned} \tag{3.45}$$

Using

$$\frac{1}{4}\left(\sigma_{xx}-\sigma_{yy}\right)^2+\sigma_{xy}^2 = q^2,$$

equation (3.45) becomes

$$w_{xy}+\Omega = \frac{\left(\sigma_{xx}-\sigma_{yy}\right)\mathring{\sigma}_{xy}-\sigma_{xy}\left(\mathring{\sigma}_{xx}-\mathring{\sigma}_{yy}\right)}{4q^2}. \tag{3.46}$$

Substitution of Eq. (3.46) into Eq. (3.38) gives

$$\sigma_{xy}\left(d_{xx}^{p}-d_{yy}^{p}\right)-d_{xy}^{p}\left(\sigma_{xx}-\sigma_{yy}\right)=\frac{\sin\phi}{2q}\left[\left(\sigma_{xx}-\sigma_{yy}\right)\overset{\circ}{\sigma}_{xy}-\sigma_{xy}\left(\overset{\circ}{\sigma}_{xx}-\overset{\circ}{\sigma}_{yy}\right)\right], \tag{3.47}$$

From Eq. (3.33), the components of the strain-rate tensor are given by

$$d_{xx}^{p}=\alpha s_{xx}-\beta\overset{\circ}{s}_{xx}=\alpha\left(\frac{\sigma_{xx}-\sigma_{yy}}{2}\right)-\beta\overset{\circ}{s}_{xx}, \tag{3.48a}$$

$$d_{yy}^{p}=\alpha s_{yy}-\beta\overset{\circ}{s}_{yy}=\alpha\left(\frac{\sigma_{yy}-\sigma_{xx}}{2}\right)-\beta\overset{\circ}{s}_{yy}, \tag{3.48b}$$

$$d_{xy}^{p}=\alpha s_{xy}-\beta\overset{\circ}{s}_{xy}=\alpha\sigma_{xy}-\beta\left[\overset{\bullet}{\sigma}_{xy}+w_{xy}\left(\sigma_{xx}-\sigma_{yy}\right)\right], \tag{3.48c}$$

Substitution of Eqs. (3.48) into Eq. (3.47) leads to

$$\sigma_{xy}\left[\alpha\left(\sigma_{xx}-\sigma_{yy}\right)-\beta\left(\overset{\circ}{s}_{xx}-\overset{\circ}{s}_{yy}\right)\right]-\left(\alpha\sigma_{xy}-\beta\overset{\circ}{s}_{xy}\right)\left(\sigma_{xx}-\sigma_{yy}\right)$$

$$=\frac{\sin\phi}{2q}\left[\left(\sigma_{xx}-\sigma_{yy}\right)\overset{\circ}{\sigma}_{xy}-\sigma_{xy}\left(\overset{\circ}{\sigma}_{xx}-\overset{\circ}{\sigma}_{yy}\right)\right]$$

which can be written as

$$\alpha\left[\sigma_{xy}\left(\sigma_{xx}-\sigma_{yy}\right)-\sigma_{xy}\left(\sigma_{xx}-\sigma_{yy}\right)\right]-\beta\left[\sigma_{xy}\left(\overset{\circ}{s}_{xx}-\overset{\circ}{s}_{yy}\right)-\overset{\circ}{s}_{xy}\left(\sigma_{xx}-\sigma_{yy}\right)\right]$$

$$=\frac{\sin\phi}{2q}\left[\left(\sigma_{xx}-\sigma_{yy}\right)\overset{\circ}{\sigma}_{xy}-\sigma_{xy}\left(\overset{\circ}{\sigma}_{xx}-\overset{\circ}{\sigma}_{yy}\right)\right].$$

The coefficient of α is identically equal to zero and hence β can be determined as follows

$$\beta = -\frac{\sin\phi\left[\left(\sigma_{xx}-\sigma_{yy}\right)\overset{\circ}{\sigma}_{xy}-\sigma_{xy}\left(\overset{\circ}{\sigma}_{xx}-\overset{\circ}{\sigma}_{yy}\right)\right]}{2q\left[\sigma_{xy}\left(\overset{\circ}{s}_{xx}-\overset{\circ}{s}_{yy}\right)-\overset{\circ}{s}_{xy}\left(\sigma_{xx}-\sigma_{yy}\right)\right]}$$

$$= -\frac{\sin\phi\left[\left(\sigma_{xx}-\sigma_{yy}\right)\overset{\circ}{\sigma}_{xy}-\sigma_{xy}\left(\overset{\circ}{\sigma}_{xx}-\overset{\circ}{\sigma}_{yy}\right)\right]}{2q\left[\sigma_{xy}\left(\overset{\circ}{\sigma}_{xx}-\overset{\circ}{\sigma}_{yy}\right)-\overset{\circ}{\sigma}_{xy}\left(\sigma_{xx}-\sigma_{yy}\right)\right]}$$

$$= \frac{\sin\phi}{2q}. \tag{3.49}$$

To solve for α, we assume that the total strain-rate can be decomposed into an elastic (reversible) part and a plastic (irreversible) part. Thus the total deformation can be written as

$$\boldsymbol{d} = \boldsymbol{d}^e + \boldsymbol{d}^p, \tag{3.50}$$

or

$$\boldsymbol{d}^e = \boldsymbol{d} - \boldsymbol{d}^p. \tag{3.51}$$

We then assume that a Hookean relationship between the stress and the elastic strain-rates exists, thus

$$\overset{\circ}{\boldsymbol{\sigma}} = \boldsymbol{D}\boldsymbol{d}^e, \tag{3.52}$$

where $\boldsymbol{D}$ is a Hookean elasticity matrix. As at yielding, stress stays on the yield surface $f(\sigma) = 0$, we have the following consistency condition

$$\left(\frac{\partial f}{\partial \sigma}\right)^T \overset{\circ}{\sigma} = 0. \tag{3.53}$$

Substitution of Eq. (3.51) and Eq. (3.52) into Eq. (3.53) leads to

$$\left(\frac{\partial f}{\partial \sigma}\right)^T \boldsymbol{D}\left(\boldsymbol{d} - \boldsymbol{d}^p\right) = 0. \tag{3.54}$$

Substituting Eq. (3.33) into Eq. (3.54) yields

$$\left(\frac{\partial f}{\partial \sigma}\right)^T \boldsymbol{D}\boldsymbol{d} - \left(\frac{\partial f}{\partial \sigma}\right)^T \boldsymbol{D}\alpha\boldsymbol{s} + \left(\frac{\partial f}{\partial \sigma}\right)^T \boldsymbol{D}\beta\overset{\circ}{s} = 0. \tag{3.55}$$

Rearranging Eq. (3.55) and solving for α gives

$$\alpha = \frac{1}{\lambda}\left(\frac{\partial f}{\partial \sigma}\right)^T \boldsymbol{D}\left(\boldsymbol{d} + \beta\overset{\circ}{s}\right), \tag{3.56}$$

where

$$\lambda = \left(\frac{\partial f}{\partial \sigma}\right)^T \boldsymbol{D}\boldsymbol{s}.$$

Now from Eq. (3.52), we have

$$\begin{aligned}
\overset{\circ}{\sigma} &= \boldsymbol{D}\left(\boldsymbol{d} - \boldsymbol{d}^p\right) \\
&= \boldsymbol{D}\left\{\boldsymbol{d} - \frac{1}{\lambda}\left[\left(\frac{\partial f}{\partial \sigma}\right)^T \boldsymbol{D}\left(\boldsymbol{d} + \beta\overset{\circ}{s}\right)\right]\boldsymbol{s} + \beta\overset{\circ}{s}\right\} \\
&= \boldsymbol{D}\left\{\boldsymbol{d} - \frac{1}{\lambda}\left[\left(\frac{\partial f}{\partial \sigma}\right)^T \boldsymbol{D}\boldsymbol{d}\right]\boldsymbol{s} - \frac{1}{\lambda}\left[\left(\frac{\partial f}{\partial \sigma}\right)^T \boldsymbol{D}\beta\overset{\circ}{s}\right]\boldsymbol{s} + \beta\overset{\circ}{s}\right\} \\
&= \boldsymbol{D}\left\{\boldsymbol{d} - \frac{1}{\lambda}\boldsymbol{s}\left(\frac{\partial f}{\partial \sigma}\right)^T \boldsymbol{D}\boldsymbol{d} - \frac{1}{\lambda}\boldsymbol{s}\left(\frac{\partial f}{\partial \sigma}\right)^T \boldsymbol{D}\beta\overset{\circ}{s} + \beta\overset{\circ}{s}\right\} \\
&= \boldsymbol{D}^\lambda \boldsymbol{d} + \boldsymbol{D}^\lambda \beta\overset{\circ}{s},
\end{aligned} \tag{3.57}$$

where

$$\boldsymbol{D}^\lambda = \boldsymbol{D}\left\{\boldsymbol{I} - \frac{1}{\lambda}\boldsymbol{s}\left(\frac{\partial f}{\partial \sigma}\right)^T \boldsymbol{D}\right\}.$$

Equation (3.57) can be written as

$$\overset{\circ}{\sigma} - \boldsymbol{D}^\lambda \beta\overset{\circ}{s} = \boldsymbol{D}^\lambda \boldsymbol{d}, \tag{3.58}$$

the left-hand side of Eq. (3.58) can be written as

$$\boldsymbol{D}^{\Lambda}\overset{\circ}{\boldsymbol{\sigma}}, \tag{3.59}$$

where

$$\boldsymbol{D}^{\Lambda}=\begin{bmatrix}\left(1-\frac{D_{11}^{\lambda}}{2}\beta+\frac{D_{12}^{\lambda}}{2}\beta\right) & \left(\frac{D_{11}^{\lambda}}{2}\beta-\frac{D_{12}^{\lambda}}{2}\beta\right) & -D_{13}^{\lambda}\beta \\ \left(\frac{D_{22}^{\lambda}}{2}\beta-\frac{D_{21}^{\lambda}}{2}\beta\right) & \left(1+\frac{D_{21}^{\lambda}}{2}\beta-\frac{D_{22}^{\lambda}}{2}\beta\right) & -D_{23}^{\lambda}\beta \\ \left(\frac{D_{32}^{\lambda}}{2}\beta-\frac{D_{31}^{\lambda}}{2}\beta\right) & \left(\frac{D_{31}^{\lambda}}{2}\beta-\frac{D_{32}^{\lambda}}{2}\beta\right) & 1-D_{33}^{\lambda}\beta\end{bmatrix},$$

in which D_{ij}^{λ} are the components of $\boldsymbol{D}^{\lambda}$.

Substitution of Eq. (3.59) into Eq. (3.58) gives

$$\boldsymbol{D}^{\Lambda}\overset{\circ}{\boldsymbol{\sigma}}=\boldsymbol{D}^{\lambda}\boldsymbol{d},$$

from which, one obtains

$$\overset{\circ}{\boldsymbol{\sigma}}=\boldsymbol{H}\boldsymbol{d}, \tag{3.60}$$

where $\boldsymbol{H}$ is the elastic-plastic matrix given by

$$\boldsymbol{H}=\left(\boldsymbol{D}^{\Lambda}\right)^{-1}\boldsymbol{D}^{\lambda}. \tag{3.61}$$

The inverse matrix in Eq. (3.61) can be found by the following standard formula

$$\left(\boldsymbol{D}^{\Lambda}\right)^{-1}=\frac{1}{\det\left(\boldsymbol{D}^{\Lambda}\right)}\mathrm{adj}\left(\boldsymbol{D}^{\Lambda}\right), \tag{3.62}$$

where det denotes the determinant and adj denotes the adjoint of a matrix.

3.4 CONSTITUTIVE EQUATIONS FOR DILATANT DOUBLE SHEARING FLOW

In this Section, we derive an elastic-plastic matrix that incorporates the angle of dilatancy and thus allows for compressible flows of granular materials.

We now assume that the total strain rate tensor has the representation

$$\boldsymbol{d} = \alpha \boldsymbol{s} - \beta \overset{\circ}{\boldsymbol{s}}, \tag{3.63}$$

Substitution of equations $(3.37)_1$, $(3.37)_2$, (3.46), and (3.63) into Eqs. (3.10) and (3.11) results in

$$4\alpha q^2 + \beta\left[\left(\overset{\circ}{s}_{yy} - \overset{\circ}{s}_{xx}\right)\left(\sigma_{xx} - \sigma_{yy}\right) - 4\overset{\circ}{s}_{xy}\sigma_{xy}\right] = 0, \tag{3.64}$$

$$\beta\left[\left(\overset{\circ}{s}_{yy} - \overset{\circ}{s}_{xx}\right)\sigma_{xy} + \overset{\circ}{s}_{xy}\left(\sigma_{xx} - \sigma_{yy}\right)\right] - \frac{\sin(\phi - \nu)}{2q\cos\nu}\left[\left(\sigma_{xx} - \sigma_{yy}\right)\overset{\circ}{\sigma}_{xy} - \sigma_{xy}\left(\overset{\circ}{\sigma}_{xx} - \overset{\circ}{\sigma}_{yy}\right)\right] = 0. \tag{3.65}$$

These are two linear equations in terms of variables α and β. From Eq. (3.65), we can solve for β by inspection, i.e.

$$\beta = \frac{\sin(\phi - \nu)}{2q\cos(\nu)}. \tag{3.66}$$

Substitution of Eq. (3.66) into Eq. (3.64) leads to

$$\alpha = -\frac{\sin(\phi - \nu)}{8q^3\cos\nu}\left[\left(\overset{\circ}{s}_{yy} - \overset{\circ}{s}_{xx}\right)\left(\sigma_{xx} - \sigma_{yy}\right) - 4\overset{\circ}{s}_{xy}\sigma_{xy}\right]. \tag{3.67}$$

The corotational rate of stress, in terms of the deviatoric stress tensor, is given by

$$\overset{\circ}{\boldsymbol{\sigma}} = \overset{\circ}{\boldsymbol{s}} + \overset{\circ}{\sigma}_m \boldsymbol{I}. \tag{3.68}$$

Now, using the consistency condition (3.53), we have

$$\overset{\circ}{\sigma}_m = -\frac{1}{\lambda}\left(\frac{\partial f}{\partial \sigma_{xx}}\overset{\circ}{s}_{xx} + \frac{\partial f}{\partial \sigma_{yy}}\overset{\circ}{s}_{yy} + \frac{\partial f}{\partial \sigma_{xy}}\overset{\circ}{s}_{xy}\right),$$

where

$$\lambda = \frac{\partial f}{\partial \sigma_{xx}} + \frac{\partial f}{\partial \sigma_{yy}}.$$

Rewriting Eq. (3.63) and then substituting it into Eq. (3.68) results in

$$\overset{\circ}{\boldsymbol{\sigma}} = \frac{\alpha}{\beta}\boldsymbol{s} - \frac{1}{\beta}\boldsymbol{d} + \overset{\circ}{\sigma}_m \boldsymbol{I},$$

which can be written as

$$\overset{\circ}{\boldsymbol{\sigma}} = \boldsymbol{H}\boldsymbol{d},$$

where the entries h_{ij} of the inverse of $\boldsymbol{H}$, $\boldsymbol{H}^{-1}$, are given by

$$h_{11} = \beta\left[\frac{1}{2\lambda}\left(\frac{\partial f}{\partial \sigma_{yy}} - \frac{\partial f}{\partial \sigma_{xx}}\right) + \frac{1}{8q^2}\left(\sigma_{xx} - \sigma_{yy}\right)^2 - 1\right], \quad h_{12} = -\left(h_{11} + 2\beta\right),$$

$$h_{13} = \beta\left[\frac{1}{2q^2}\sigma_{xy}\left(\sigma_{xx} - \sigma_{yy}\right) - \frac{1}{\lambda}\frac{\partial f}{\partial \sigma_{xy}} - 1\right],$$

$$h_{21} = -\beta\left[\frac{1}{8q^2}\left(\sigma_{xx} - \sigma_{yy}\right)^2 + \frac{1}{2\lambda}\left(\frac{\partial f}{\partial \sigma_{xx}} - \frac{\partial f}{\partial \sigma_{yy}}\right) + 1\right], \quad h_{22} = -\left(h_{21} + 2\beta\right),$$

$$h_{23} = \beta\left[\frac{1}{2q^2}\sigma_{xy}\left(\sigma_{yy} - \sigma_{xx}\right) - \frac{1}{\lambda}\frac{\partial f}{\partial \sigma_{xy}} - 1\right],$$

$$h_{31}=\beta\left[\frac{1}{4q^2}\sigma_{xy}\left(\sigma_{xx}-\sigma_{yy}\right)-1\right],\quad h_{32}=-\left(h_{31}+2\beta\right),\quad h_{33}=\beta\left[\left(\frac{\sigma_{xy}}{q}\right)^2-1\right].$$

3.5 CONCLUDING REMARKS

An alternative method has been used to formulate Butterfield and Harkness' kinematic proposal. The derivation shows that the resulting constitutive relations allow the use of any model for the angle of dilatancy. This finding is very important. In shear flow, material expansion usually occurs in the initial stage and ceases when shearing develops, which means that the angle of dilatancy depends on the shear amount. With this finding, one would be able to improve the model accuracy by using a variable angle of dilatancy. In addition, a set of constitutive equations has been derived to relate the stress rate with the deformation rate in explicit form. This development is extremely important as it makes it possible to implement the double shearing theory using the finite element method. With the use of the finite element method, it becomes possible to solve boundary value problems related to granular flows using the double shearing theory and thus to test the validity of the theory by comparing numerical results with experimental observations.

CHAPTER FOUR

SOLUTION BY THE METHOD OF CHARACTERISTICS

4.1 GENERAL

The equations governing the steady-state double-shearing perfect plasticity flow are the stress equations of motion (2.9) and (2.10) and the velocity equations (3.12) and (3.13). In matrix form, these equations are as follows

$$\boldsymbol{A}\frac{\partial \boldsymbol{u}}{\partial x}+\boldsymbol{B}\frac{\partial \boldsymbol{u}}{\partial y}+\boldsymbol{d}=\boldsymbol{0}, \tag{4.1}$$

where

$$\boldsymbol{A}=\begin{bmatrix} -(1-\sin\phi\cos 2\psi) & -2(p\sin\phi+c\cos\phi)\sin 2\psi & -\rho v_x & 0 \\ \sin\phi\sin 2\psi & 2(p\sin\phi+c\cos\phi)\cos 2\psi & 0 & -\rho v_x \\ 0 & 0 & \left(\cos 2\psi-\dfrac{\cos(\phi-\nu)}{\sin\nu}\right) & \sin 2\psi \\ 0 & -2v_x\dfrac{\sin(\phi-\nu)}{\cos\nu} & \sin 2\psi & \left(\dfrac{\sin(\phi-\nu)}{\cos\nu}-\cos 2\psi\right) \end{bmatrix}$$

$$\boldsymbol{B}=\begin{bmatrix} \sin\phi\sin 2\psi & 2(p\sin\phi+c\cos\phi)\cos 2\psi & -\rho v_y & 0 \\ -(1+\sin\phi\cos 2\psi) & 2(p\sin\phi+c\cos\phi)\sin 2\psi & 0 & -\rho v_y \\ 0 & 0 & \sin 2\psi & -\left(\cos 2\psi+\dfrac{\cos(\phi-\nu)}{\sin\nu}\right) \\ 0 & -2v_y\dfrac{\sin(\phi-\nu)}{\cos\nu} & -\left(\cos 2\psi+\dfrac{\sin(\phi-\nu)}{\cos\nu}\right) & -\sin 2\psi \end{bmatrix}$$

$$\boldsymbol{u}=\begin{pmatrix} p \\ \psi \\ v_x \\ v_y \end{pmatrix},\ \boldsymbol{d}=\begin{pmatrix} X \\ Y \\ 0 \\ 0 \end{pmatrix}.$$

This chapter concerns the numerical solution of system (4.1) under quasi-static conditions. In section 4.2, we show that under quasi-static conditions, system (4.1) is hyperbolic regardless of the dependence of the angle of internal friction on stress. The stress and velocity characteristics are then determined and the method of characteristics is thus used for the solution of the system. Sections 4.3-4.6 present a numerical technique for generating the characteristic mesh and the stress solution. Firstly, the general equations along the characteristics are deduced in section 4.3 and then discretised in section 4.4. Then, starting from the initial value determined in section 4.5, an algorithm for generating the characteristic mesh and stress field is developed in section 4.6. With the characteristic mesh determined, the velocity field is then determined by integrating the velocity equations directly along the characteristics, In section 4.8, a numerical algorithm for finding the stress discontinuity line and the corresponding stress and velocity fields is developed. Finally, in section 4.9, a numerical study is undertaken to demonstrate the fundamental features of the double shearing model through a study of granular flows in a hopper. Investigation on the effect of various parameters on silo pressures is also presented.

4.2 STRESS AND VELOCITY CHARACTERISTICS FOR QUASI-STATIC FLOWS

For quasi-static flow of a granular material, the inertial terms in the stress equilibrium equations are neglected. Thus system (4.1) reduces to

$$\boldsymbol{A}\frac{\partial \boldsymbol{u}}{\partial x}+\boldsymbol{B}\frac{\partial \boldsymbol{u}}{\partial y}+\boldsymbol{d}=\boldsymbol{0}, \tag{4.2}$$

with $\boldsymbol{A}$ and $\boldsymbol{B}$ now defined by

$$\boldsymbol{A}=\begin{bmatrix} -(1-\sin\phi\cos 2\psi) & -2(p\sin\phi+c\cos\phi)\sin 2\psi & 0 & 0 \\ \sin\phi\sin 2\psi & 2(p\sin\phi+c\cos\phi)\cos 2\psi & 0 & 0 \\ 0 & 0 & \left(\cos 2\psi-\dfrac{\cos(\phi-\nu)}{\sin\nu}\right) & \sin 2\psi \\ 0 & -2v_x\dfrac{\sin(\phi-\nu)}{\cos\nu} & \sin 2\psi & \left(\dfrac{\sin(\phi-\nu)}{\cos\nu}-\cos 2\psi\right) \end{bmatrix}$$

$$\boldsymbol{B}=\begin{bmatrix} \sin\phi\sin 2\psi & 2(p\sin\phi+c\cos\phi)\cos 2\psi & 0 & 0 \\ -(1+\sin\phi\cos 2\psi) & 2(p\sin\phi+c\cos\phi)\sin 2\psi & 0 & 0 \\ 0 & 0 & \sin 2\psi & -\left(\cos 2\psi+\dfrac{\cos(\phi-\nu)}{\sin\nu}\right) \\ 0 & -2v_y\dfrac{\sin(\phi-\nu)}{\cos\nu} & -\left(\cos 2\psi+\dfrac{\sin(\phi-\nu)}{\cos\nu}\right) & -\sin 2\psi \end{bmatrix}$$

For convenience, rewrite matrices $\boldsymbol{A}$ and $\boldsymbol{B}$ as follows

$$\boldsymbol{A}=\begin{bmatrix} \boldsymbol{A}_1 & 0 \\ \boldsymbol{A}_2 & \boldsymbol{A}_3 \end{bmatrix}, \boldsymbol{B}=\begin{bmatrix} \boldsymbol{B}_1 & 0 \\ \boldsymbol{B}_2 & \boldsymbol{B}_3 \end{bmatrix},$$

where the top right entry represents the 2×2 matrix with zero components.

The characteristic equation of system (4.2) is

$$\det(\boldsymbol{A}-\lambda\boldsymbol{B})=0, \tag{4.3}$$

which, in terms of $\boldsymbol{A}_i$ and $\boldsymbol{B}_i$ becomes

$$\begin{vmatrix} \boldsymbol{A}_1 - \lambda \boldsymbol{B}_1 & 0 \\ \boldsymbol{A}_2 - \lambda \boldsymbol{B}_2 & \boldsymbol{A}_3 - \lambda \boldsymbol{B}_3 \end{vmatrix} = 0. \tag{4.4}$$

By the Laplace expansion, this results in

$$|\boldsymbol{A}_1 - \lambda \boldsymbol{B}_1||\boldsymbol{A}_3 - \lambda \boldsymbol{B}_3| = 0,$$

therefore

$$|\boldsymbol{A}_1 - \lambda \boldsymbol{B}_1| = 0\,, \quad |\boldsymbol{A}_3 - \lambda \boldsymbol{B}_3| = 0. \tag{4.5}$$

Once λ is determined, the characteristics of system (4.2) can be determined, namely

$$\frac{dx}{dy} = \lambda\,.$$

4.2.1 Stress characteristics

The stress characteristics of system (4.2) are given by Eq. $(4.5)_1$, which in expanded form can be written as

$$\begin{vmatrix} -1 + \sin\phi(\cos 2\psi - \lambda \sin 2\psi) & -2(p\sin\phi + c\cos\phi)(\sin 2\psi + \lambda \cos 2\psi) \\ \lambda + \sin\phi(\sin 2\psi + \lambda \cos 2\psi) & 2(p\sin\phi + c\cos\phi)(\cos 2\psi - \lambda \sin 2\psi) \end{vmatrix} = 0\,,$$

and, after some simplification, becomes

$$(\sin\phi + \cos 2\psi)\lambda^2 + 2\lambda \sin 2\psi - \cos 2\psi + \sin\phi = 0. \tag{4.6}$$

Thus the values of λ can be obtained as follows

$$\lambda = \frac{-\sin 2\psi \pm \cos\phi}{\cos 2\psi + \sin\phi} = \frac{-\sin 2\psi \pm \sin\left(\frac{\pi}{2} + \phi\right)}{\cos 2\psi + \cos\left(\frac{\pi}{2} - \phi\right)} = \cot\left(\psi \pm \frac{\pi}{4} \pm \frac{\phi}{2}\right), \quad (4.7)$$

where we have used the following relations

$$\pm 2\sin\left(\mp\psi + \frac{\pi}{4} + \frac{\phi}{2}\right)\cos\left(\pm\psi + \frac{\pi}{4} + \frac{\phi}{2}\right) = -\sin 2\psi \pm \sin\left(\frac{\pi}{2} + \phi\right),$$

$$2\cos\left(\psi + \frac{\pi}{4} - \frac{\phi}{2}\right)\cos\left(\psi - \frac{\pi}{4} + \frac{\phi}{2}\right) = \cos 2\psi + \cos\left(\frac{\pi}{2} - \phi\right),$$

which were derived by using the identities for products of trigonometric functions.

Hence there are two real characteristics given by

$$\frac{dy}{dx} = \tan\left(\psi \pm \frac{\pi}{4} \pm \frac{\phi}{2}\right). \quad (4.8)$$

The family corresponding to the + and - signs in Eq. (4.8) is usually called the β- and α-family, respectively.

4.2.2 Velocity characteristics

For the velocity characteristics, we expand Eq. $(4.5)_2$ and thus

$$\begin{vmatrix} \cos 2\psi - \dfrac{\cos(\phi - \nu)}{\sin\nu} - \lambda \sin 2\psi & \sin 2\psi + \lambda\left(\cos 2\psi + \dfrac{\cos(\phi - \nu)}{\sin\nu}\right) \\ \sin 2\psi + \lambda\left(\cos 2\psi + \dfrac{\sin(\phi - \nu)}{\cos\nu}\right) & \dfrac{\sin(\phi - \nu)}{\cos\nu} - \cos 2\psi + \lambda \sin 2\psi \end{vmatrix} = 0,$$

and upon multiplying out, we have

$$\left[1+\frac{\cos(2\nu-\phi)}{\sin\nu\cos\nu}\cos 2\psi+\frac{\cos(\phi-\nu)\sin(\phi-\nu)}{\sin\nu\cos\nu}\right]\lambda^2+\left[\frac{2\cos(2\nu-\phi)}{\sin\nu\cos\nu}\sin 2\psi\right]\lambda$$
$$+1-\frac{\cos(2\nu-\phi)}{\sin\nu\cos\nu}\cos 2\psi+\frac{\cos(\phi-\nu)\sin(\phi-\nu)}{\sin\nu\cos\nu}=0.$$

Now, by multiplying this equation by $2\sin\nu\cos\nu=\sin 2\nu$ and noting that $\sin 2\nu+\sin(2\phi-2\nu)=2\sin\phi\cos(2\nu-\phi)$, the above equation results in Eq. (4.6). Therefore the velocity characteristics are the same as the stress characteristics and are given by Eq. (4.8).

4.3 STRESS EQUATIONS ALONG CHARACTERISTICS

Since system (4.2) is hyperbolic, the method of characteristics is chosen for the solution of the problem. The method of characteristics is the most nearly exact numerical technique for solving hyperbolic PDE's. It utilises the property of hyperbolic PDE's that they have a limited domain of dependence. For a given point, the domain of dependence is bounded by the characteristics through that point. The solution at the given point is uninfluenced by any disturbances that may happen outside the domain of dependence.

The characteristics are (curved) lines along which the discontinuities in the initial conditions are propagated and the dependent variables vary in a prescribed manner. The characteristics are used to determine the unknown dependent variables provided that their values are known along some initial curve.

The stress field is governed by four differential equations. These are given by the two parametric equations describing the characteristic curves, namely

$$\frac{dy}{dx}=\tan\left(\psi-\frac{\pi}{4}-\frac{\phi}{2}\right) \qquad \text{along } \alpha\text{-line,} \qquad (4.9)$$

$$\frac{dy}{dx} = \tan\left(\psi + \frac{\pi}{4} + \frac{\phi}{2}\right) \qquad \text{along } \beta\text{-line.} \qquad (4.10)$$

Using Eqs. (3.14) and (3.15), we can deduce from the first two equations of (4.2)

$$\cos\phi \frac{\partial p}{\partial s_\alpha} + 2(p\sin\phi + c\cos\phi)\frac{\partial \psi}{\partial s_\alpha} = X\sin\left(\psi + \frac{\pi}{4} + \frac{\phi}{2}\right) - Y\cos\left(\psi + \frac{\pi}{4} + \frac{\phi}{2}\right), \qquad (4.11)$$

along α-line

$$\cos\phi \frac{\partial p}{\partial s_\beta} - 2(p\sin\phi + c\cos\phi)\frac{\partial \psi}{\partial s_\beta} = Y\cos\left(\psi - \frac{\pi}{4} - \frac{\phi}{2}\right) - X\sin\left(\psi - \frac{\pi}{4} - \frac{\phi}{2}\right), \qquad (4.12)$$

along β-line.

Since the parameter ψ is an unknown, Eqs. (4.9)-(4.12) must be solved simultaneously for x, y, p, and ψ. Therefore we will simultaneously construct the characteristic grid and solve the differential equations at the grid points.

4.4 DISCRETISATION AND COMPUTATIONAL METHOD

Suppose that the initial values of x, y, p, and ψ are prescribed along a curve Γ in the physical plane. Now consider two adjacent points P and Q, a small distance apart, in the discretisation such that the α-characteristic through P intersects the β-characteristic through Q at the point R (see Fig. 4.1).

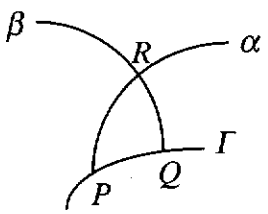

Fig. 4.1 Generation of grid point R

The method of characteristics generates the values of x, y, p, and ψ at the point R. To do this we first discretise Eqs. (4.9)-(4.12) and the derivatives in Eqs. (4.9) and (4.10) can be approximated by

$$\frac{dy}{dx} \approx \frac{\delta y}{\delta x} = \frac{y_R - y_P}{x_R - x_P} \qquad \text{along } PR, \tag{4.13}$$

and

$$\frac{dy}{dx} \approx \frac{\delta y}{\delta x} = \frac{y_R - y_Q}{x_R - x_Q} \qquad \text{along } QR, \tag{4.14}$$

where (x_R, y_R), (x_P, y_P), (x_Q, y_Q) are the coordinates at the points R, P and Q respectively. The partial derivatives in Eqs. (4.11) and (4.12) are approximated by the first order finite differences as follows

$$\frac{\partial p}{\partial s_\alpha} \approx \frac{p_R - p_P}{\delta s_\alpha} \qquad \text{along } PR, \tag{4.15}$$

$$\frac{\partial \psi}{\partial s_\alpha} \approx \frac{\psi_R - \psi_P}{\delta s_\alpha} \qquad \text{along } PR, \tag{4.16}$$

$$\frac{\partial p}{\partial s_\beta} \approx \frac{p_R - p_Q}{\delta s_\beta} \qquad \text{along } QR, \tag{4.17}$$

$$\frac{\partial \psi}{\partial s_\beta} \approx \frac{\psi_R - \psi_Q}{\delta s_\beta} \qquad \text{along } QR. \tag{4.18}$$

The parametric Eqs. of (4.9) and (4.10) can then be written in terms of the arc lengths s_α and s_β as follows

$$\begin{aligned} \frac{dy}{ds_\alpha} &= \sin\left(\psi - \frac{\pi}{4} - \frac{\phi}{2}\right), \quad \frac{dy}{ds_\beta} = \sin\left(\psi + \frac{\pi}{4} + \frac{\phi}{2}\right), \\ \frac{dx}{ds_\alpha} &= \cos\left(\psi - \frac{\pi}{4} - \frac{\phi}{2}\right), \quad \frac{dx}{ds_\beta} = \cos\left(\psi + \frac{\pi}{4} + \frac{\phi}{2}\right). \end{aligned} \tag{4.19}$$

From Eqs. (4.19), we can deduce the following approximations

$$\delta s_\alpha \approx \frac{x_R - x_P}{\cos\left(\psi_R - \frac{\pi}{4} - \frac{\phi}{2}\right)}, \quad \delta s_\beta \approx \frac{x_R - x_Q}{\cos\left(\psi_R + \frac{\pi}{4} + \frac{\phi}{2}\right)}. \tag{4.20}$$

Substituting Eqs. (4.13) and (4.14) into Eqs. (4.9) and (4.10) and Eqs. (4.15) -(4.18) into Eqs. (4.11) and (4.12) and replacing each function by the average value along the given arc (see Smith, 1978) leads to

$$y_R - y_P = t_\alpha\left(x_R - x_P\right) \qquad \text{along } PR, \tag{4.21}$$

$$y_R - y_Q = t_\beta\left(x_R - x_Q\right) \qquad \text{along } QR, \tag{4.22}$$

$$\cos\phi c_{\alpha 1}\left(p_R - p_P\right) + c_{\alpha 1} q_\alpha \left(\psi_R - \psi_P\right) = \left(Xs_{\alpha 2} - Yc_{\alpha 2}\right)\left(x_R - x_P\right) \tag{4.23}$$

along PR,

$$\cos\phi c_{\beta 2}\left(p_R - p_Q\right) - c_{\beta 2} q_\beta \left(\psi_R - \psi_Q\right) = \left(Yc_{\beta 1} - Xs_{\beta 1}\right)\left(x_R - x_Q\right) \tag{4.24}$$

along QR,

where

$$t_\alpha = \tan\left(\frac{1}{2}\left(\psi_R + \psi_P\right) - \varepsilon\right), \; t_\beta = \tan\left(\frac{1}{2}\left(\psi_R + \psi_Q\right) + \varepsilon\right),$$

$$\varepsilon = \frac{\pi}{4} + \frac{\phi}{2},$$

$$c_{\alpha 1} = \cos\left(\frac{1}{2}\left(\psi_R + \psi_P\right) - \varepsilon\right), \; c_{\alpha 2} = \cos\left(\frac{1}{2}\left(\psi_R + \psi_P\right) + \varepsilon\right),$$

$$c_{\beta 1} = \cos\left(\frac{1}{2}\left(\psi_R + \psi_Q\right) - \varepsilon\right), \; c_{\beta 2} = \cos\left(\frac{1}{2}\left(\psi_R + \psi_Q\right) + \varepsilon\right),$$

$$s_{\alpha 1} = \sin\left(\frac{1}{2}\left(\psi_R + \psi_P\right) - \varepsilon\right), \; s_{\alpha 2} = \sin\left(\frac{1}{2}\left(\psi_R + \psi_P\right) + \varepsilon\right),$$

$$s_{\beta 1} = \sin\left(\frac{1}{2}\left(\psi_R + \psi_Q\right) - \varepsilon\right), \; s_{\beta 2} = \sin\left(\frac{1}{2}\left(\psi_R + \psi_Q\right) + \varepsilon\right),$$

$$q_\alpha = \left(p_P + p_R\right)\sin\phi \; , \; q_\beta = \left(p_Q + p_R\right)\sin\phi \; .$$

In deriving the above equations, we have assumed that the material is cohesionless and so $c = 0$.

Equations (4.21)-(4.24) can be written in matrix form as follows

$$\boldsymbol{A}(\boldsymbol{x})\boldsymbol{x} = \boldsymbol{b}(\boldsymbol{x}), \tag{4.25}$$

where

$$\boldsymbol{A} = \begin{bmatrix} -t_\alpha & 1 & 0 & 0 \\ -t_\beta & 1 & 0 & 0 \\ -\left(Xs_{\alpha 2} - Yc_{\alpha 2}\right) & 0 & \cos\phi c_{\alpha 1} & c_{\alpha 1} q_\alpha \\ -\left(Yc_{\beta 1} - Xs_{\beta 1}\right) & 0 & \cos\phi c_{\beta 1} & -c_{\beta 2} q_\beta \end{bmatrix},$$

$$\boldsymbol{b} = \begin{pmatrix} y_P - t_\alpha x_P \\ y_Q - t_\beta x_Q \\ \cos\phi c_{\alpha 1} p_P + c_{\alpha 1} q_\alpha \psi_P - \left(Xs_{\alpha 2} - Yc_{\alpha 2}\right) x_P \\ \cos\phi c_{\beta 2} p_Q - c_{\beta 2} q_\beta \psi_Q - \left(Yc_{\beta 1} - Xs_{\beta 1}\right) x_Q \end{pmatrix}, \quad \boldsymbol{x} = \begin{pmatrix} x_R \\ y_R \\ p_R \\ \psi_R \end{pmatrix},$$

which is a system of four nonlinear equations in four unknowns. Various classical methods, such as the fixed-point iteration and Newton-Raphson method can be used to solve this system. In the following, we present the detailed iterative algorithms for generating unknown variables at inner mesh points, points on the centre-line and points on the wall.

4.4.1 Data generation at inner mesh points

The values of x_R, y_R, p_R and ψ_R at the internal points can be generated directly by solving system (4.25) using Newton's method. Alternatively, we can use the following iterative scheme.

$$y_R^{(i+1)} - y_P = t_\alpha^{(i)}\left(x_R^{(i+1)} - x_P\right) \quad \text{along } PR, \tag{4.26}$$

$$y_R^{(i+1)} - y_Q = t_\beta^{(i)}\left(x_R^{(i+1)} - x_Q\right) \quad \text{along } QR, \tag{4.27}$$

where the superscript i denotes the iteration number. These are two equations in terms of two unknowns $x_R^{(i+1)}$ and $y_R^{(i+1)}$. Their solution is given by

$$x_R^{(i+1)} = \frac{x_P t_\alpha^{(i)} - x_Q t_\beta^{(i)} + y_Q - y_P}{t_\alpha^{(i)} - t_\beta^{(i)}}, \tag{4.28}$$

$$y_R^{(i+1)} = \frac{\left[\left(x_P - x_Q\right)t_\alpha^{(i)} - y_P\right]t_\beta^{(i)} + y_Q t_\alpha^{(i)}}{t_\alpha^{(i)} - t_\beta^{(i)}}, \tag{4.29}$$

Similarly, Eqs. (4.23) and (4.24) can be written as

$$\cos\phi c_{\alpha 1}^{(i)}\left(p_R^{(i+1)} - p_P\right) + c_{\alpha 1}^{(i)} q_\alpha^{(i)}\left(\psi_R^{(i+1)} - \psi_P\right) = \left(Xs_{\alpha 2}^{(i)} - Yc_{\alpha 2}^{(i)}\right)\left(x_R^{(i+1)} - x_P\right) \tag{4.30}$$

along PR,

$$\cos\phi c_{\beta 2}^{(i)}\left(p_R^{(i+1)} - p_Q\right) - c_{\beta 2}^{(i)} q_\beta^{(i)}\left(\psi_R^{(i+1)} - \psi_Q\right) = \left(Yc_{\beta 1}^{(i)} - Xs_{\beta 1}^{(i)}\right)\left(x_R^{(i+1)} - x_Q\right) \tag{4.31}$$

along QR,

which can be solved for the two unknowns $p_R^{(i+1)}$ and $\psi_R^{(i+1)}$. Here we have used the latest update of x_R in Eqs. (4.30) and (4.31) since it has already been calculated in Eq. (4.28). Hence the solution of Eqs. (4.30) and (4.31) is

$$\psi_R^{(i+1)} = \frac{\dfrac{1}{c_{\alpha 1}^{(i)}}\left(Xs_{\alpha 2}^{(i)} - Yc_{\alpha 2}^{(i)}\right)\left(x_R^{(i+1)} - x_P\right) - \dfrac{1}{c_{\beta 2}^{(i)}}\left(Yc_{\beta 1}^{(i)} - Xs_{\beta 1}^{(i)}\right)\left(x_R^{(i+1)} - x_Q\right) + q_\beta^{(i)}\psi_Q - \cos\phi\left(p_Q - p_P\right) + q_\alpha^{(i)}\psi_P}{q_\alpha^{(i)} + q_\beta^{(i)}}, \tag{4.32}$$

$$p_R^{(i+1)} = \frac{\dfrac{q_\alpha^{(i)}}{c_{\beta 2}^{(i)}}\left(Yc_{\beta 1}^{(i)} - Xs_{\beta 1}^{(i)}\right)\left(x_R^{(i+1)} - x_Q\right) + q_\beta^{(i)}\left[\dfrac{1}{c_{\alpha 1}^{(i)}}\left(Xs_{\alpha 2}^{(i)} - Yc_{\alpha 2}^{(i)}\right)\left(x_R^{(i+1)} - x_P\right) + \cos\phi p_P\right] + q_\alpha^{(i)} q_\beta^{(i)}\left(\psi_P - \psi_Q\right) + q_\alpha^{(i)} \cos\phi p_Q}{\left(q_\alpha^{(i)} + q_\beta^{(i)}\right)\cos\phi}.$$

(4.33)

4.4.2 Data generation at points on centre line

On the centre line, $y_R = 0$ and $\psi_R = 0$ due to symmetry. The solution is given by the intersection of a β-line through Q and the x-axis as shown in Fig. 4.2.

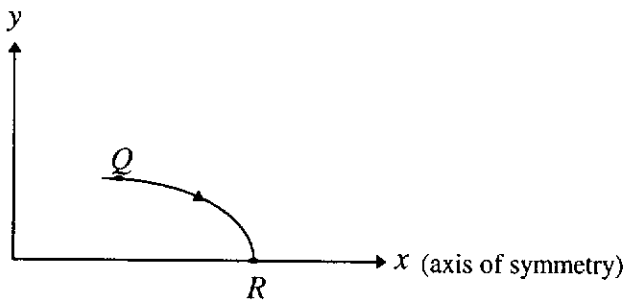

Fig. 4.2 Intersection of β-line with x-axis

From Eq. (4.22), we have

$$x_R = \frac{-y_Q}{t_\beta} + x_Q, \tag{4.34}$$

where

$$t_\beta = \tan\left(\frac{\psi_Q}{2} + \varepsilon\right).$$

From Eq. (4.24) we have

$$p_R^{(i+1)} = \frac{\left(Yc_{\beta 1} - Xs_{\beta 1}\right)\left(x_R - x_Q\right) - c_{\beta 2} q_\beta^{(i)} \psi_Q}{\cos\phi c_{\beta 2}} + p_Q. \tag{4.35}$$

4.4.3 Data generation at points on the wall

The data on the wall are defined by the intersection of the α-line through P and the wall as shown in Fig. 4.3.

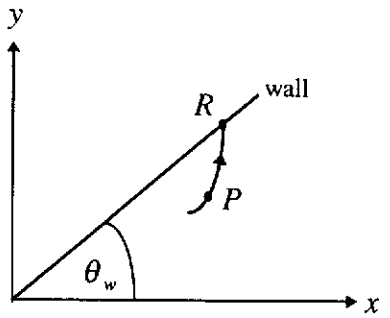

Fig. 4.3 Intersection of α-line with wall

By noting that $\psi_w = \overline{\psi}_w + \theta$ as shown in Fig. 2.5, the condition at the wall in the (x,y) coordinate system can be determined from Eq. (2.26) for the passive state, thus

$$\psi_R = \psi_w = \frac{1}{2}\left[\phi_w + \sin^{-1}\left(\frac{\sin\phi_w}{\sin\phi}\right)\right] + \theta_w . \tag{4.36}$$

As the value of ψ and the relation between x and y on the wall are known, we only have two unknowns at the point R. Let the values of ψ, x and y on the wall point be respectively ψ_w, x_R and y_R and the hopper half-angle be θ_w then,

$$y_R = \tan\theta_w x_R . \tag{4.37}$$

From Eq. (4.21), we have

$$x_R = \frac{y_P - t_\alpha x_P}{\tan\theta_w - t_\alpha}, \tag{4.38}$$

where

$$t_\alpha = \tan\left(\frac{\psi_w + \psi_P}{2} - \varepsilon\right),$$

From Eq. (4.23), we have

$$p_R^{(i+1)} = \frac{(Xs_{\alpha 2} - Yc_{\alpha 2})(x_R - x_P) - c_{\alpha 1} q_\alpha^{(i)} (\psi_w - \psi_P)}{\cos\phi c_{\alpha 1}} + p_P . \tag{4.39}$$

4.5 COMPUTATION DOMAIN AND INITIAL CONDITIONS

Our model hopper is symmetric and we assume that both the flow and stress fields are symmetric about the centre line $\theta = 0$, where θ denotes the angle between the x-axis and the hopper wall. Therefore, only half the domain need to be considered for computational purposes. It is configured such that the axis of symmetry lies along the x-axis and the hopper wall is inclined at an angle θ_w to the x-axis. The virtual apex is located at the origin, as shown in Fig. 4.4. The gravitational force acts in the negative x direction.

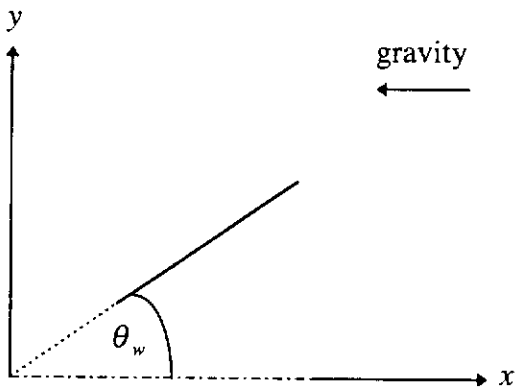

Fig. 4.4 Configuration of model hopper

Since an iterative process is being employed and the solution in the computation domain is generated from prescribed conditions at a given boundary, we must state the initial values of x, y, p and ψ. We must also specify the values of these variables on the initial curve Γ.

4.5.1 Initial values at *R*

As a first approximation of the unknowns at point R, where R is neither on the wall nor on the centre line, we treat arcs PR and QR in Fig. 4.1 as straight lines of slopes $\tan(\psi_P - \varepsilon)$ and $\tan(\psi_Q + \varepsilon)$ respectively. Then Eqs. (4.9) and (4.10) can be approximated by

$$x_R^{(0)} = \frac{\tan(\psi_Q + \varepsilon)x_Q - y_Q + y_P - \tan(\psi_P - \varepsilon)x_P}{\tan(\psi_Q + \varepsilon) - \tan(\psi_P - \varepsilon)}, \tag{4.40}$$

$$y_R^{(0)} = \frac{\tan(\psi_Q + \varepsilon)\left[\tan(\psi_P - \varepsilon)(x_P - x_Q) - y_P\right] + \tan(\psi_P - \varepsilon)y_Q}{\tan(\psi_P - \varepsilon) - \tan(\psi_Q + \varepsilon)}, \tag{4.41}$$

where the superscript (0) denotes the initial value. The values of p and ψ are taken as the average values at points P and Q, that is

$$p_R^{(0)} = \frac{p_P + p_Q}{2}, \psi_R^{(0)} = \frac{\psi_P + \psi_Q}{2}. \tag{4.42}$$

The values on the wall are approximated by

$$x_R^{(0)} = \frac{y_p - \tan(\psi_p - \varepsilon)x_p}{\tan\theta_w - \tan(\psi_p - \varepsilon)}, y_R^{(0)} = x_R^{(0)}\tan\theta_w, p_R^{(0)} = p_P. \tag{4.43}$$

Similarly, values on the centre line are approximated by

$$x_R^{(0)} = x_Q - \frac{y_Q}{\tan(\psi_Q + \varepsilon)}, p_R^{(0)} = p_Q. \tag{4.44}$$

4.5.2 Values on the initial curve Γ

The values on the initial curve are prescribed using the radial stress field solution or some multiple of it. The solution to the radial stress field is summarised as follows.

In polar coordinates and under static case the equilibrium equations (2.8) become

$$\frac{\partial \sigma_{rr}}{\partial r}+\frac{1}{r}\frac{\partial \sigma_{r\theta}}{\partial \theta}+\frac{\sigma_{rr}-\sigma_{\theta\theta}}{r}+\rho b_r=0, \tag{4.45}$$

$$\frac{\partial \sigma_{r\theta}}{\partial r}+\frac{1}{r}\frac{\partial \sigma_{\theta\theta}}{\partial \theta}+\frac{2\sigma_{r\theta}}{r}+\rho b_\theta=0. \tag{4.46}$$

For a material obeying the Mohr-Coulomb yield criterion, we have from section (2.2)

$$\sigma_{rr}=-q\left(\csc\phi-\cos 2\overline{\psi}\right), \tag{4.47}$$

$$\sigma_{\theta\theta}=-q\left(\csc\phi+\cos 2\overline{\psi}\right), \tag{4.48}$$

$$\sigma_{r\theta}=q\sin 2\overline{\psi}, \tag{4.49}$$

where $\overline{\psi}$ is the angle which the axis of the algebraically greatest principal stress makes with the radial direction, so that $\psi=\overline{\psi}+\theta$. In terms of the new variables $\overline{\psi}$ and q, Eqs. (4.45) and (4.46) admit solutions of the form

$$\overline{\psi}=\overline{\psi}(\theta),\quad q=r\rho g\gamma(\theta). \tag{4.50}$$

On substituting Eqs.(4.50) into Eqs. (4.45) and (4.46), we can derive,

$$\frac{d\overline{\psi}}{d\theta}=\frac{\left(\csc\phi-2\cos 2\overline{\psi}-3\sin\phi\right)\gamma+\cos\theta+\sin\phi\cos\left(2\overline{\psi}+\theta\right)}{2\left(\cos 2\overline{\psi}+\sin\phi\right)\gamma}, \tag{4.51}$$

$$\frac{d\gamma}{d\theta}=\frac{\sin 2\overline{\psi}\gamma+\sin\phi\sin\left(2\overline{\psi}+\theta\right)}{\sin\phi+\cos 2\overline{\psi}}, \tag{4.52}$$

which constitute a closed system of two ordinary differential equations in terms of two unknowns $\overline{\psi}$ and γ. The boundary conditions for the problem are the conditions of $\overline{\psi}$ on the axis of symmetry and on the wall, namely

$$\overline{\psi}(\theta_0)=\overline{\psi}_0,\ \ \gamma(\theta_0)=\gamma_0. \tag{4.53}$$

On the axis of symmetry, $\theta_0=0$ and $\overline{\psi}_0=0$. While on the hopper wall, $\overline{\psi}_w$ is known as described in section 2.6. Equations (4.51) and (4.52) together with boundary conditions (4.53) constitute a two-point boundary value problem. Various methods can be used to solve the problem and in this study the shooting method is used. By solving the problem we can obtain the values of $\overline{\psi}$ and γ for different values of θ.

In the present study, we choose the initial curve to be a β-characteristic spanning the top surface of the hopper. From the results in Section 4.2, the stress characteristics in terms of polar coordinates can be determined as

$$\frac{d\theta}{dr}=\frac{1}{r}\tan\left(\overline{\psi}\pm\frac{\pi}{4}\pm\frac{\phi}{2}\right), \tag{4.54}$$

with +,- signs indicating the β- ,α- characteristics. For the radial stress field, integration of the β-characteristic gives

$$r=r_0\exp\left[\int_{\theta_0}^{\theta}\cot\left(\overline{\psi}+\tfrac{\pi}{4}+\tfrac{\phi}{2}\right)d\theta\right]\ ,\ \ \theta_0\le\theta\le\theta_w. \tag{4.55}$$

Although there is no known analytical solution of Eq. (4.55), the integration can be easily handled using a numerical integration scheme such as the *composite Simpson's rule*. Therefore, for each θ, from Eq. (4.55) and by solving the two-point boundary value problem, we can obtain the corresponding r-coordinate. Since the solution proceeds in (x,y)-coordinates, we convert all values to this system. Thus, we have

$$x=r\cos\theta\ ,\ y=r\sin\theta\ ,\ \psi=\overline{\psi}+\theta\ ,\ p=\frac{r\rho g\gamma}{\sin\phi}. \tag{4.56}$$

In summary, the initial curve and the p and $\overline{\psi}$ values on the curve can be derived using a combination of the shooting method, the Runge-Kutta method and the Simpson's rule.

4.6 SOLUTION PROCEDURE FOR CHARACTERISTIC MESH AND STRESS FIELDS

We now describe how to obtain the solution throughout the domain of the hopper. The method starts by generating data at the N+1 points on the initial curve using the radial stress field solution. This curve is a β-characteristic spanning the top surface of the hopper. The data is then used, together with the boundary conditions at the wall, to generate region one bounded by lines AB, BC and CA as shown in Fig. 4.5.

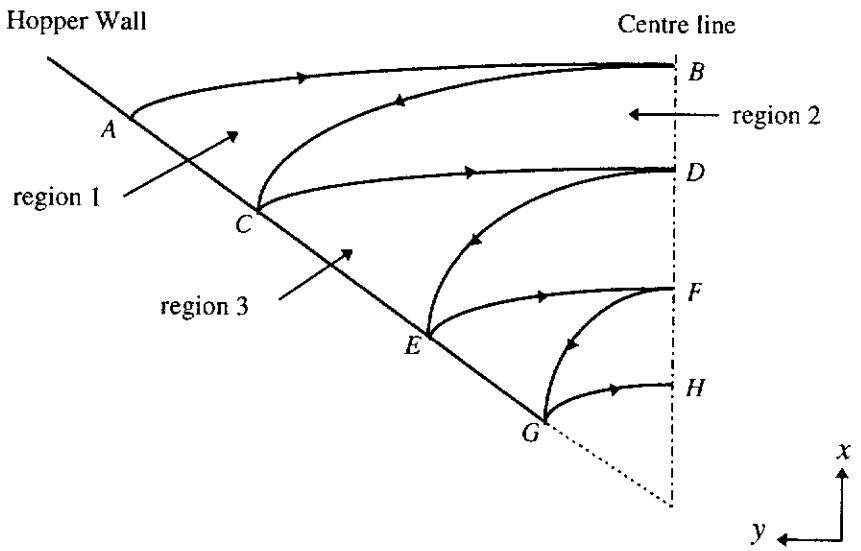

Fig. 4.5 Computational regions

Next, region two (bounded by BC, CD and DB) is calculated using the solution on BC (initial curve) together with the conditions on the centre-line. Region three is calculated in a similar way to region one except that the initial curve is now CD. The process continues until data in all desired regions has been calculated.

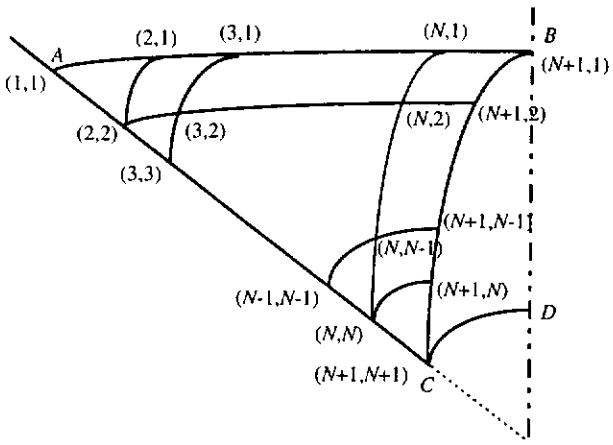

Fig. 4.6 Computation scheme for region one

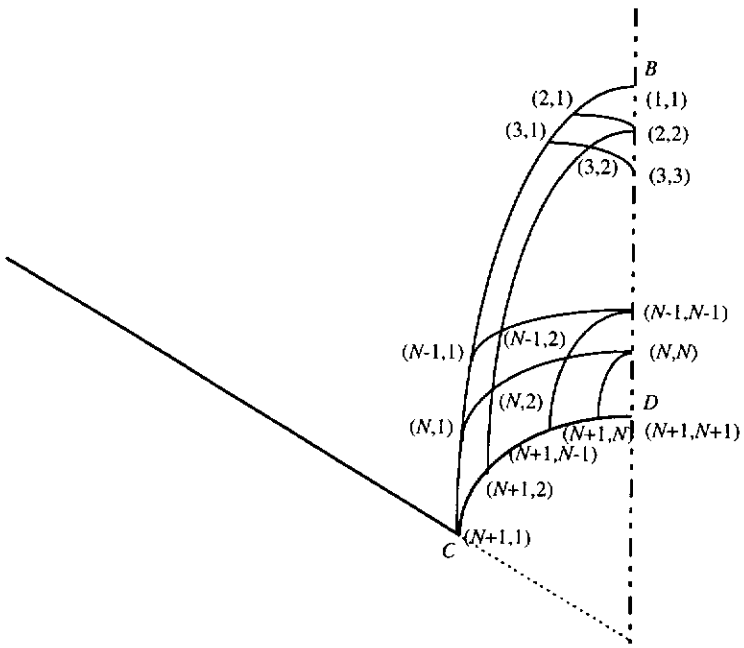

Fig. 4.7 Computation scheme for region two

The schemes for regions one and two are shown in Fig. (4.6) and (4.7) respectively. For region one, starting with data on the initial curve (nodes $(i,1)_{i=1}^{N+1}$), we first generate solution at the grid point (2,2) by integrating along the α characteristic passing through P (2,1). Then, we generate solution at point (3,2) using data at (3,1) and (2,2). Then we continue generating solutions at all grid points on the second layer, and then at points on the third layer and so on until we obtain the solution at

the grid point (N+1,N+1). Similarly, for region two, we generate solutions in the following order, $(i,2)_{i=2}^{N+1}$, then $(i,3)_{i=3}^{N+1}$ and so on. A computer program has been written implementing the method of characteristics. The algorithm is given below.

ALGORITHM

Let $\boldsymbol{x} = (x, y, p, \psi)^T$

Initial step: specify $\boldsymbol{x}$ along the β characteristic spanning top of hopper by solving Eqs. (4.51) and (4.52)

Step 1 For l=1,2,...,*Maxl* do Steps 2-26

Step 2 For j=1,2,...,N-1 do Steps 3-9 {*domain1*}

Step 3 Set $\boldsymbol{x}_p = \boldsymbol{x}(j+1, j)$

Step 4 Calculate data $\boldsymbol{x}_R$ at grid point (j+1,j+1) using Eqs. (4.36), (4.37), (4.38), (4.39)
{*wall*}

Step 5 Set $\boldsymbol{x}(j+1, j+1) = \boldsymbol{x}_R$

Step 6 For i=j+2,...,N+1 do Steps 7-9 {*inner points*}

Step 7 Set $\boldsymbol{x}_P = \boldsymbol{x}(i, j)$

$\boldsymbol{x}_Q = \boldsymbol{x}(i-1, j+1)$

Step 8 Calculate data $\boldsymbol{x}_R$ at grid point (i,j+1) using Eqs. (4.28), (4.29), (4.32), (4.33)

Step 9 Set $\boldsymbol{x}(i, j+1) = \boldsymbol{x}_R$

Step 10 Set $\boldsymbol{x}_P = \boldsymbol{x}(N+1, N)$ {*wall*}

Step 11 Calculate data $\boldsymbol{x}_R$ at grid point (N+1,N+1) using Eqs. (4.36), (4.37), (4.38), (4.39)

Step 12 Set $\boldsymbol{x}(N+1, N+1) = \boldsymbol{x}_R$

Step 13 Save data in global array

Step 14 Set up initial curve for domain 2 by renumbering points (Fig. 4.7)

Step 15 For j=1,2,...,N-1 do Steps 16-22 {domain 2}

Step 16 Set $x_Q = x(j+1, j)$

Step 17 Calculate data x_R at grid point (j+1,j+1) using Eqs. (4.34), (4.35)

Step 18 Set $x(j+1, j+1) = x_R$

Step 19 For i=j+2,...,N+1 do Steps 20-22

Step 20 Set $x_Q = x(i, j)$

$x_P = x(i-1, j+1)$

Step 21 Calculate data x_R at grid point (i,j+1) using Eqs.(4.28), (4.29), (4.32), (4.33)

Step 22 Set $x(i, j+1) = x_R$

Step 23 Set $x_Q = x(N+1, N)$

Step 24 Calculate data x_R at grid point (N+1,N+1) using Eqs. (4.34), (4.35)

Step 25 Set $x(N+1, N+1) = x_R$

Step 26 Save data in global array

4.7 SOLUTION PROCEDURE FOR THE VELOCITY FIELD

In this problem the bounding surfaces are the centre line and the hopper wall. The normal component can be written in terms of the x and y components as follows

$$v_n = v_y \cos\theta - v_x \sin\theta, \quad \theta_0 \le \theta \le \theta_w \tag{4.57}$$

Therefore, we can find the relation of the two velocity components on the centre-line and the wall using the velocity boundary condition (2.28). Substituting (3.18) and (3.19) into (4.57) and then using (2.28), we have

$$v_\alpha = -v_\beta \frac{\sin(\psi + \varepsilon - \theta)}{\sin(\psi - \varepsilon - \theta)}, \tag{4.58}$$

where $\theta = \theta_0 = 0$ on the centre-line and $\theta = \theta_w$ on the wall.

To solve for velocity at the grid points generated in the previous section, we use the equations in steady-state form as given by Eqs. (3.30) and (3.31). These equations can be discretised using the following first order derivative approximations at R

$$\left.\frac{\partial v_\alpha}{\partial s_\alpha}\right|_R \approx \frac{v_\alpha^R - v_\alpha^P}{\delta s_\alpha}, \left.\frac{\partial v_\alpha}{\partial s_\beta}\right|_R \approx \frac{v_\alpha^R - v_\alpha^Q}{\delta s_\beta}, \left.\frac{\partial v_\beta}{\partial s_\alpha}\right|_R \approx \frac{v_\beta^R - v_\beta^P}{\delta s_\alpha},$$

$$\left.\frac{\partial v_\beta}{\partial s_\beta}\right|_R \approx \frac{v_\beta^R - v_\beta^Q}{\delta s_\beta}, \left.\frac{\partial \psi}{\partial s_\alpha}\right|_R \approx \frac{\psi_R - \psi_P}{\delta s_\alpha}, \left.\frac{\partial \psi}{\partial s_\beta}\right|_R \approx \frac{\psi_R - \psi_Q}{\delta s_\beta},$$

where δs_α and δs_β are the arc lengths PR and QR as shown in Fig. 4.8 and, from Eq. (4.19), can be approximated by

$$\delta s_\alpha \approx \frac{y_R - y_P}{\sin(\psi_R - \varepsilon)}, \delta s_\beta \approx \frac{y_R - y_Q}{\sin(\psi_R + \varepsilon)}.$$

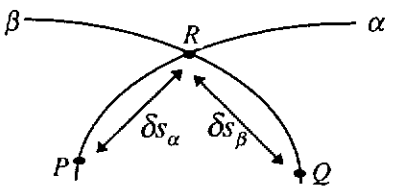

Fig. 4.8 Approximations to arcs PR and QR

Substituting the above approximations into Eq. (3.31) leads to

$$v_\alpha^R - v_\beta^R(m + d_\alpha) + v_\beta^P m - v_\alpha^P = 0. \tag{4.59}$$

From Eq. (3.30) we have

$$v_\beta^R - v_\alpha^R(m - d_\beta) + v_\alpha^Q m - v_\beta^Q = 0, \tag{4.60}$$

where

$$d_\alpha = \frac{1}{\cos(\phi - \nu)}\left[(\psi_R - \psi_P)\cos\nu + (\psi_R - \psi_Q)\sin(\phi - \nu)\frac{\delta s_\alpha}{\delta s_\beta}\right],$$

$$d_\beta = \frac{1}{\cos(\phi - \nu)}\left[(\psi_R - \psi_Q)\cos\nu + (\psi_R - \psi_P)\sin(\phi - \nu)\frac{\delta s_\beta}{\delta s_\alpha}\right],$$

$$m = \frac{\sin\nu}{\cos(\phi - \nu)}.$$

4.7.1 Velocity at inner mesh points

Eqs. (4.59) and (4.60) are two equations in two unknowns v_α^R and v_β^R whose direct solution is given by

$$v_\alpha^R = \frac{(m + d_\alpha)(v_\beta^Q - m v_\alpha^Q) + v_\alpha^P - v_\beta^P m}{1 - m^2 + m(d_\beta - d_\alpha) + d_\alpha d_\beta}, \tag{4.61}$$

$$v_\beta^R = \frac{(v_\alpha^P - v_\beta^P m)(m - d_\beta) - m v_\alpha^Q + v_\beta^Q}{1 - m^2 + m(d_\beta - d_\alpha) + d_\alpha d_\beta}. \tag{4.62}$$

4.7.2 Velocity at points on centre line

Substituting Eq. (4.58) into Eq. (4.60) and noting that $\psi_0 = 0$ and $\theta_0 = 0$ on the centre-line, we have

$$v_\beta^R = \frac{v_\beta^Q - v_\alpha^Q m}{1 - m + d_\beta}, \tag{4.63}$$

$$v_\alpha^R = v_\beta^R.$$

4.7.3 Velocity at points on the wall

Substitution of Eq. (4.58) into Eq. (4.59) gives

$$v_\alpha^R = -v_\beta^R \frac{\sin(\psi_w + \varepsilon - \theta_w)}{\sin(\psi_w - \varepsilon - \theta_w)}, \tag{4.64}$$

$$v_\beta^R = \frac{v_\beta^P m - v_\alpha^P}{\frac{\sin(\psi_w + \varepsilon - \theta_w)}{\sin(\psi_w - \varepsilon - \theta_w)} + m + d_\alpha}. \tag{4.65}$$

4.7.4 Velocity on initial curve

The initial curve is calculated using the radial velocity field. We first present Eqs. (3.30) and (3.31) in polar coordinates. Using

$$v_x = v_r \cos\theta - v_\theta \sin\theta, \tag{4.66}$$

$$v_y = v_r \sin\theta + v_\theta \cos\theta, \tag{4.67}$$

$$\frac{\partial}{\partial r} = \cos\theta \frac{\partial}{\partial x} + \sin\theta \frac{\partial}{\partial y}, \tag{4.68}$$

$$\frac{1}{r}\frac{\partial}{\partial \theta} = -\sin\theta \frac{\partial}{\partial x} + \cos\theta \frac{\partial}{\partial y}, \tag{4.69}$$

$$\psi = \overline{\psi} + \theta,$$

where v_r and v_θ are the velocity components in the r and θ directions respectively, then equations (2.21) and (2.22) can be expressed as

$$\left(\frac{\partial v_r}{\partial r} - \frac{1}{r}\frac{\partial v_\theta}{\partial \theta} - \frac{1}{r}v_r\right)\cos 2\overline{\psi} + \left(\frac{\partial v_\theta}{\partial r} + \frac{1}{r}\frac{\partial v_r}{\partial \theta} - \frac{1}{r}v_\theta\right)\sin 2\overline{\psi}$$
$$= \frac{\cos(\phi - \nu)}{\sin\nu}\left(\frac{\partial v_r}{\partial r} + \frac{1}{r}\frac{\partial v_\theta}{\partial \theta} + \frac{1}{r}v_r\right), \tag{4.70}$$

$$-\left(\frac{\partial v_\theta}{\partial r} + \frac{1}{r}\frac{\partial v_r}{\partial \theta} - \frac{1}{r}v_\theta\right)\cos 2\overline{\psi} - \left(\frac{1}{r}\frac{\partial v_\theta}{\partial \theta} - \frac{\partial v_r}{\partial r} + \frac{1}{r}v_r\right)\sin 2\overline{\psi}$$

$$= \frac{\sin(\phi - \nu)}{\cos \nu}\left(\frac{1}{r}\frac{\partial v_r}{\partial \theta} - \frac{\partial v_\theta}{\partial r} + \frac{v_\theta}{r} + 2\overline{\Omega}\right), \tag{4.71}$$

where

$$\overline{\Omega} = \frac{\partial \overline{\psi}}{\partial t} + v_r \frac{\partial \overline{\psi}}{\partial r} + \frac{v_\theta}{r}\frac{\partial \overline{\psi}}{\partial \theta}.$$

These equations admit solutions of the form $v_\theta = 0$, $\overline{\psi} = \overline{\psi}(\theta)$ for $\nu = 0$, namely radial flow. Following Jenike (1961), let

$$v_r = \frac{h(\theta)}{r}, \quad v_\theta = 0.$$

Substituting the above solution form into Eqs. (4.70) and (4.71), we have

$$h(\theta) = C\exp\left[\int_{\theta_0}^{\theta} \frac{-2\sin 2\overline{\psi}}{\cos 2\overline{\psi} + \sin\phi} d\theta\right] < 0 \quad , \quad \theta_0 \le \theta \le \theta_w \tag{4.72}$$

and $C < 0$ is an arbitrary constant.

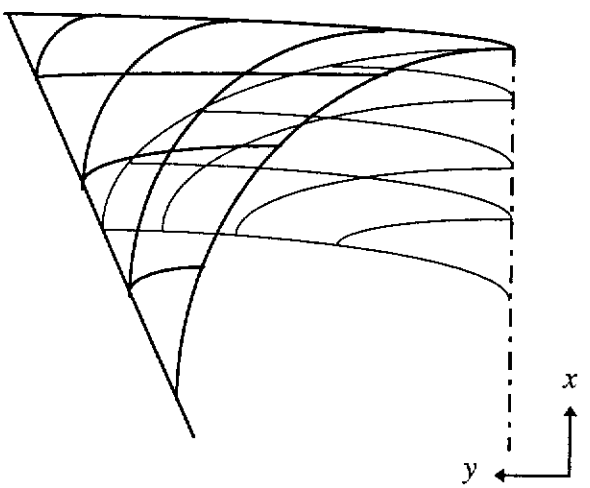

Fig. 4.9 Overlapping characteristics resulting from incompatible bc's

4.8 DETERMINATION OF DISCONTINUITY LINES

When the conditions on the top surface are not compatible with conditions on centre line, the α-characteristics emanating from the top surface will intersect the α-characteristics emanating from the centre line resulting in multivalued solutions at certain points. Hence there exists a discontinuity between the two regions emanating from the discontinuous boundary point (Nedderman, 1976) as shown in Fig. 4.9.

To determine the equations along the discontinuity, we note that for a surface whose normal is inclined at an angle η to the x-axis, the relations for the normal and tangential stresses are given by

$$\sigma_{nn} = \frac{\sigma_{xx} + \sigma_{yy}}{2} + \frac{\sigma_{xx} - \sigma_{yy}}{2}\cos(2\eta) + \sigma_{xy}\sin(2\eta), \tag{4.73}$$

$$\sigma_{nt} = \sigma_{xy}\cos(2\eta) - \frac{\sigma_{xx} - \sigma_{yy}}{2}\sin(2\eta). \tag{4.74}$$

Now for stability of a particle lying on the discontinuity, we require that the normal and shear stresses, σ_{nn} and σ_{nt}, must be continuous (Sokolovskii, 1965; Neddermann, 1992), that is

$$\begin{aligned} \sigma_{nn}^{-} &= \sigma_{nn}^{+}, \\ \sigma_{nt}^{-} &= \sigma_{nt}^{+}, \end{aligned} \tag{4.75}$$

which, on using the Coulomb-Mohr yield criterion, can be written as

$$p^{+}\left[-1 + \sin\phi\cos\left(2\psi^{+} - 2\eta\right)\right] = p^{-}\left[-1 + \sin\phi\cos\left(2\psi^{-} - 2\eta\right)\right], \tag{4.76}$$

$$p^{+}\sin\left(2\psi^{+} - 2\eta\right) = p^{-}\sin\left(2\psi^{-} - 2\eta\right), \tag{4.77}$$

where p is as defined in Chapter two. The super scripts + and - refer to regions on either side of the discontinuity as shown in Fig. 4.10.

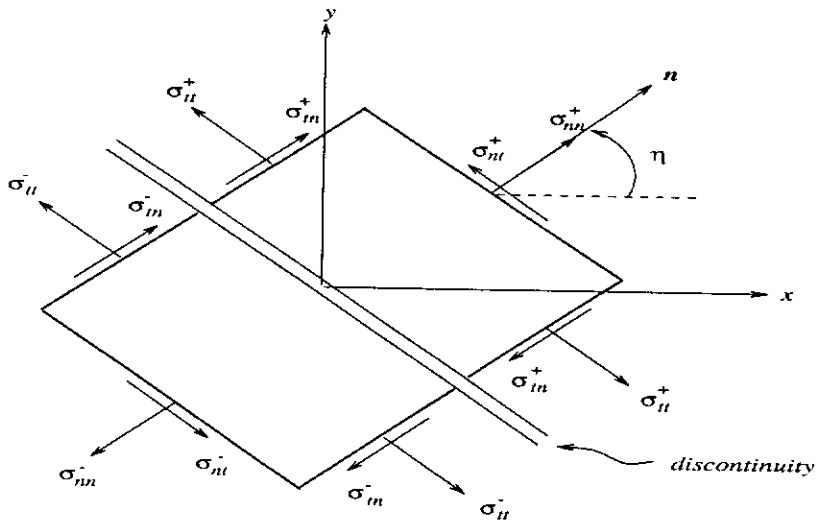

Fig. 4.10 Forces acting on an element in the presence of a discontinuity

This situation can be represented more clearly using the Mohr-Coulomb diagram shown in Fig. 4.11 in which $\xi^- = \frac{1}{2}(\pi + \Delta + \delta)$ and $\xi^+ = \frac{1}{2}(2\pi - \Delta + \delta)$. From this figure, it is seen that point D gives the normal and shear stress components, σ_{nn} and σ_{nt}, on the plane of discontinuity.

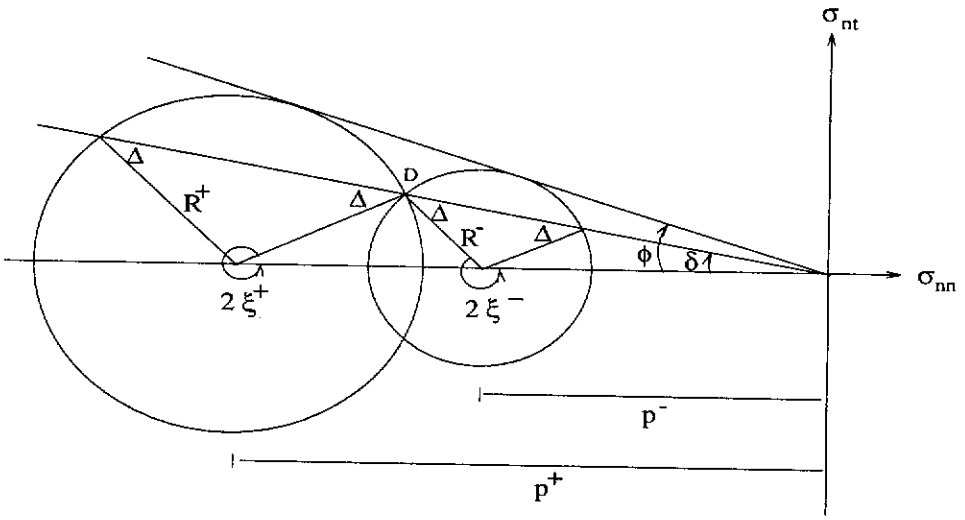

Fig. 4.11 Boundary conditions at the point of discontinuity

There are two types of discontinuities. One is generated using information on the α-line and the other is generated using information on the β-line. In both types, we have five equations for the determination of five unknowns.

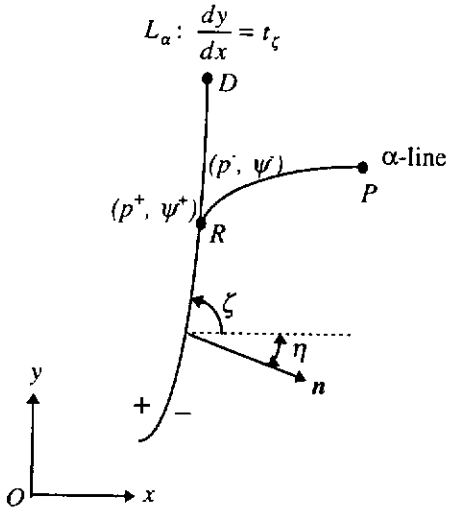

Fig. 4.12 α-discontinuity

Equations for type 1 discontinuity - α discontinuity

Consider Figure 4.12. Let L_α be a α discontinuity line defined by

$$L_\alpha: \frac{dy}{dx} = \tan\zeta,$$

where $\zeta = \zeta(x, y)$ is the angle between the x-axis and the plane of discontinuity and is related to η by

$$\zeta = \eta + \frac{\pi}{2}.$$

Assume that solutions of p^+ and ψ^+ on the '+' side have been obtained and that the α-line from the '-' side intersects the discontinuity line at a point R with coordinate (x, y). Then there are five unknowns at point R, namely, x, y, p^-, ψ^- and $\eta(x, y)$. The equations governing these unknowns include the contact Eqs.

(4.76) and (4.77), and in addition, the equation of the discontinuity line and two equations along the α-characteristic i.e.

$$\frac{dy}{dx} = t_\zeta , \tag{4.78}$$

$$\frac{dy}{dx} = t_\alpha , \tag{4.79}$$

$$\cos\phi c_\alpha \left(p^- - p_p\right) + 2c_\alpha p^- \sin\phi\left(\psi^- - \psi_p\right) = \left(Xs_\beta - Yc_\beta\right)\left(x - x_P\right), \tag{4.80}$$

where

$$t_\alpha = \tan\left(\psi^- - \varepsilon\right), \quad t_\zeta = \tan\zeta , \quad c_\alpha = \cos\left(\psi^- - \varepsilon\right), \quad c_\beta = \cos\left(\psi^- + \varepsilon\right),$$

$$s_\beta = \sin\left(\psi^- + \varepsilon\right).$$

Let D and p denote a previously calculated point on the discontinuity and the α-line respectively. Then Eqs. (4.78) and (4.79) can be approximated by

$$y - y_D = t_\zeta \left(x - x_D\right), \tag{4.81}$$

$$y - y_P = t_\alpha \left(x - x_P\right). \tag{4.82}$$

To solve the five equations, we proceed as follows. Firstly, from Eq. (4.77) we have

$$p^- = \frac{p^+ \sin\left(2\psi^+ - 2\eta\right)}{\sin\left(2\psi^- - 2\eta\right)}. \tag{4.83}$$

Substituting Eq. (4.83) into Eq. (4.76) gives

$$\left[-1 + \sin\phi\cos\left(2\psi^+ - 2\eta\right)\right]\sin\left(2\psi^- - 2\eta\right) = \left[-1 + \sin\phi\cos\left(2\psi^- - 2\eta\right)\right]\sin\left(2\psi^+ - 2\eta\right). \tag{4.84}$$

Solving Eqs. (4.81) and (4.82) for x and y, results in

$$x = \frac{x_p t_\alpha - x_D t_\zeta + y_D - y_p}{t_\alpha - t_\zeta} \tag{4.85}$$

$$y = \frac{\left[\left(x_p - x_D\right)t_\alpha - y_p\right]t_\zeta + y_D t_\alpha}{t_\alpha - t_\zeta} \tag{4.86}$$

Then, by substituting Eqs. (4.83)-(4.86) into (4.84) and (4.80), one obtains a system of two equations in two unknowns η and ψ^-, which can be written in the form of

$$\begin{aligned} F_1^\alpha\left(\eta,\psi^-,x\left(\eta,\psi^-\right),y\left(\eta,\psi^-\right),p^-\left(\eta,\psi^-\right)\right)=0,\\ F_2^\alpha\left(\eta,\psi^-,x\left(\eta,\psi^-\right),y\left(\eta,\psi^-\right),p^-\left(\eta,\psi^-\right)\right)=0, \end{aligned} \tag{4.87}$$

where x, y and p^- are as defined in (4.83), (4.85) and (4.86) and

$$\begin{aligned} F_1^\alpha &= \sin\left(2\psi^+ - 2\eta\right) - \sin\left(2\psi^- - 2\eta\right) + \sin\phi\sin\left(2\psi^- - 2\psi^+\right),\\ F_2^\alpha &= \cos\phi c_\alpha\left(p^- - p_p\right) + 2c_\alpha p^- \sin\phi\left(\psi^- - \psi_p\right) - \left(Xs_\beta - Yc_\beta\right)\left(x - x_P\right). \end{aligned} \tag{4.88}$$

Once η and ψ^- are determined from system (4.87), we can then determine x, y and p^- from (4.83), (4.85) and (4.86).

Equations for type 2 discontinuity - β discontinuity

Here, the governing equations consist of (4.83), (4.84), (4.81) and the following two relations along the β - line,

$$y - y_Q = t_\beta\left(x - x_Q\right), \tag{4.89}$$

$$\cos\phi c_\beta\left(p^- - p_Q\right) - 2c_\beta p^- \sin\phi\left(\psi^- - \psi_Q\right) = \left(Yc_\alpha - Xs_\alpha\right)\left(x - x_Q\right). \tag{4.90}$$

The solution of Eq. (4.89) and (4.81) results in

$$x = \frac{x_Q t_\beta - x_D t_\zeta + y_D - y_Q}{t_\beta - t_\zeta}, \tag{4.91}$$

$$y = \frac{\left[\left(x_Q - x_D\right)t_\beta - y_Q\right]t_\zeta + y_D t_\beta}{t_\beta - t_\zeta}, \tag{4.92}$$

where

$$t_\beta = \tan\left(\psi^- + \varepsilon\right), \quad s_\alpha = \sin\left(\psi^- - \varepsilon\right).$$

Once again, this set of equations can be written as two equations in terms of the two unknowns η and ψ^-, i.e.

$$F_1^\beta\left(\eta, \psi^-\right) = 0, \; F_2^\beta\left(\eta, \psi^-\right) = 0,$$

where

$$F_1^\beta = F_1^\alpha,$$

$$F_2^\beta = \cos\phi c_\beta\left(p^- - p_Q\right) - 2c_\beta p^- \sin\phi\left(\psi^- - \psi_Q\right) - \left(Yc_\alpha - Xs_\alpha\right)\left(x - x_Q\right). \tag{4.93}$$

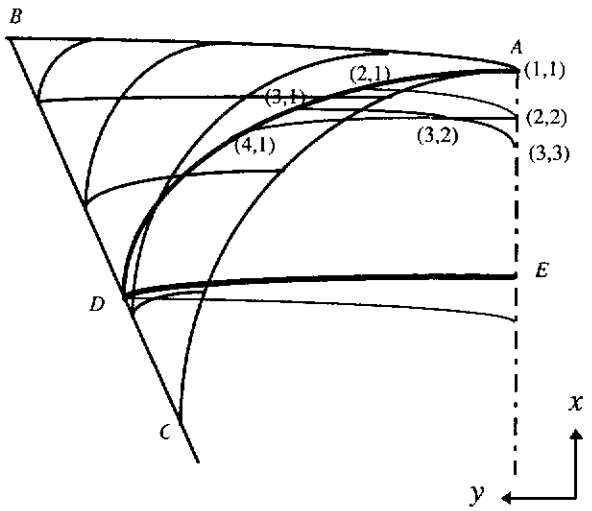

Fig. 4.13 Generation of the discontinuity

4.8.1 Generation of the line of discontinuity and stress field

To calculate the line of discontinuity, we start by finding solutions in the first domain (given by region *ABC* in Fig. 4.13) by using the initial curve and the wall condition. Then, we determine the discontinuity line *AD* and generate points (1,1), (2,1), (2,2) and etc in the region *ADE*. For clarity of presentation, the discontinuity line and the points are also shown in a separate diagram (Fig. 4.14). In the region *ADE*, we first find a point (2,1), a short distance from *A*, along the line through point *A* with slope ζ_A. The slope ζ_A can be estimated from the knowledge of ψ^- and ψ^+ at point *A*. Here we have used + to denote the region above the discontinuity and - to denote the region below the discontinuity. Therefore, ψ^+ is the value of ψ on the initial surface at *A* and ψ^- $(=0)$ is the value on the centre line, p^+ is also known. Hence we can use Eqs. (4.76) and (4.77) to obtain the two nonlinear equations in η and p^- and upon eliminating p^- we end up with the following equation

$$\sin(2\psi^+ - 2\eta) - \sin(2\psi^- - 2\eta) + \sin\phi \sin(2\psi^- - 2\psi^+) = 0\,, \qquad (4.94)$$

which can be solved for η using Newton's method. The second discontinuity (type 2), *DE*, will emanate where the first discontinuity terminates at the wall (point *D*) here $\psi^- = \psi_w$. Equation (4.94) can be used again to obtain the initial slope.

Given the coordinates of point (2,1), we can find the corresponding values of p and ψ by first locating the quadrilateral containing the point and then interpolating p and ψ at the grid points to obtain p^+ and ψ^+ using the procedure described in Section 4.8.1.1. Then assigning η the value at point (1,1), we can use Eq. (4.84) to solve for ψ^- and then Eq. (4.83) to solve for p^-. We note, however, that this equation has always at least one root, namely $\psi^- = \psi^+$, hence there must be a check that this does not happen. Next, point (2,2) is found as the intersection of

the β-characteristic through point (2,1) and the centre-line. For type 2 discontinuity it is the intersection of an α-characteristic and the wall. Next, we interpolate at points (2,1) and (2,2) resulting in P_I (Fig. 4.14), i.e.

$$P_I = P_1 + (P_2 - P_1) \times scale$$

where P_I, P_1, P_2 represent any of x, y, p, ψ values and $0 \le scale \le 1$ is chosen so that P_I is close to P_1, otherwise the solution may not exist. These interpolation points are necessary to prevent the mesh from expanding during the solution.

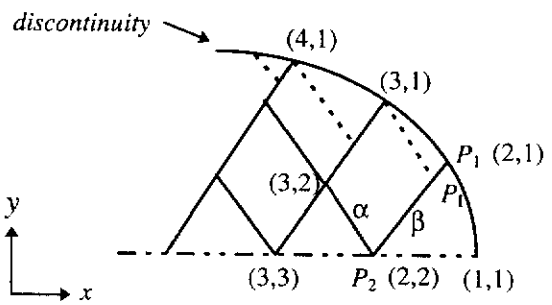

Fig. 4.14 Mesh generation using the interpolation point P_I

Then, using information at points P_I and (2,1), we solve system (4.87) using a combination of the steepest descent and Newton-Raphson method to obtain point (3,1) on the discontinuity. Within the steepest descent iteration, the values of x and y will vary, therefore we will need to interpolate to obtain the corresponding values of p^+ and ψ^+. Point (3,2) is calculated by finding the solution to the intersection of the β-characteristic through (3,1) and the α-characteristic through (2,2) using a similar procedure described in Section 4.5. Point (3,3) is calculated by finding the solution to the intersection of the β-characteristic through (3,2) and the centre-line. Similarly, from points (3,1) and (3,2), we can generate point (4,1) and so on.

For the steepest descent method the following derivatives are required for the Jacobian.

Type 1 discontinuity:

$$\frac{\partial F_1^{\alpha}}{\partial \eta} = 2\left[\cos\left(2\psi^- - 2\eta\right) - \cos\left(2\psi^+ - 2\eta\right)\right], \tag{4.95}$$

$$\frac{\partial F_1^{\alpha}}{\partial \psi^-} = 2\left[\sin\phi\cos\left(2\psi^+ - 2\psi^-\right) - \cos\left(2\psi^- - 2\eta\right)\right], \tag{4.96}$$

$$\frac{\partial F_2^{\alpha}}{\partial \eta} = c_{\alpha}\frac{\partial p^-}{\partial \eta}\left[\cos\phi + 2\sin\phi\left(\psi^- - \psi_p\right)\right] - \left(Xs_{\beta} - Yc_{\beta}\right)\frac{\partial x}{\partial \eta}, \tag{4.97}$$

$$\begin{aligned}\frac{\partial F_2^{\alpha}}{\partial \psi^-} = {} & c_{\alpha}\left(\cos\phi\frac{\partial p^-}{\partial \psi^-} + 2\sin\phi p^-\right) - s_{\alpha}\left(p^- - p_p\right)\cos\phi \\ & + 2\left(\psi^- - \psi_p\right)\sin\phi\left[c_{\alpha}\frac{\partial p^-}{\partial \psi^-} - s_{\alpha}p^-\right] - \left(x - x_p\right)\left(Xc_{\beta} + Ys_{\beta}\right) \\ & - \frac{\partial x}{\partial \psi^-}\left(Xs_{\beta} - Yc_{\beta}\right),\end{aligned} \tag{4.98}$$

where

$$\frac{\partial x}{\partial \eta} = \frac{\sec^2\zeta\left[\left(x_p - x_D\right)t_{\alpha} + y_D - y_p\right]}{\left(t_{\alpha} - t_{\zeta}\right)^2}, \quad \frac{\partial p^-}{\partial \psi^-} = \frac{-2p^+\cos\left(2\psi^- - 2\eta\right)\sin\left(2\psi^+ - 2\eta\right)}{\sin^2\left(2\psi^- - 2\eta\right)},$$

$$\frac{\partial x}{\partial \psi^-} = \frac{\sec^2\left(\psi^- - \varepsilon\right)\left[\left(x_D - x_p\right)t_{\zeta} - y_D + y_p\right]}{\left(t_{\alpha} - t_{\zeta}\right)^2}, \quad \frac{\partial p^-}{\partial \eta} = \frac{2p^+\sin\left(2\psi^+ - 2\psi^-\right)}{\sin^2\left(2\psi^- - 2\eta\right)}.$$

Type 2 discontinuity:

$$\frac{\partial F_2^{\beta}}{\partial \eta} = c_{\beta}\frac{\partial p^-}{\partial \eta}\left[\cos\phi - 2\sin\phi\left(\psi^- - \psi_Q\right)\right] - \left(Yc_{\alpha} - Xs_{\alpha}\right)\frac{\partial x}{\partial \eta}, \tag{4.99}$$

$$\frac{\partial F_2^{\beta}}{\partial \psi^-} = c_\beta\left(\cos\phi\frac{\partial p^-}{\partial \psi^-} - 2\sin\phi p^-\right) - s_\beta\left(p^- - p_Q\right)\cos\phi$$
$$-2\left(\psi^- - \psi_Q\right)\sin\phi\left[c_\beta\frac{\partial p^-}{\partial \psi^-} - s_\beta p^-\right] + \left(x - x_Q\right)\left(Xc_\alpha + Ys_\alpha\right) \quad (4.100)$$
$$-\frac{\partial x}{\partial \psi^-}\left(Yc_\alpha - Xs_\alpha\right),$$

where

$$\frac{\partial x}{\partial \eta} = \frac{\sec^2\zeta\left[\left(x_Q - x_D\right)t_\beta + y_D - y_Q\right]}{\left(t_\beta - t_\zeta\right)^2}, \frac{\partial x}{\partial \psi^-} = \frac{\sec^2\left(\psi^- + \varepsilon\right)\left[\left(x_D - x_Q\right)t_\zeta - y_D + y_Q\right]}{\left(t_\beta - t_\zeta\right)^2},$$

When calculating the type 2 discontinuity, numerical difficulties occur when $\psi^- + \varepsilon \to \pi/2$. In this instance, the function F_2^{β} is dominated by $\tan\left(\psi^- + \varepsilon\right)$ and hence can be considered to be independent of η (η, being a finite number, becomes negligible) so instead, we consider the equation

$$F_2^{\beta *} = \frac{F_2^{\beta}}{c_\beta} = 0. \quad (4.101)$$

Now,

$$\lim_{\psi^- + \varepsilon \to \pi/2}\frac{x - x_Q}{c_\beta} = -\left[\left(x_D - x_Q\right)t_\zeta - y_D + y_Q\right],$$

therefore

$$F_2^{\beta *} = \cos\phi\left(p^- - p_Q\right) - 2\sin\phi p^-\left(\psi^- - \psi_Q\right) + \left(Yc_\alpha - Xs_\alpha\right)\left[\left(x_D - x_Q\right)t_\zeta - y_D + y_Q\right]. \quad (4.102)$$

We also have

$$\lim_{\psi^- + \varepsilon \to \pi/2}\frac{\partial x}{\partial \eta}\frac{1}{c_\beta} = \sec^2\left(x_Q - x_D\right),$$

$$\lim_{\psi^- + \varepsilon \to \pi/2}\frac{1}{c_\beta^2}\left(c_\beta\frac{\partial x}{\partial \psi^-} + s_\beta\left(x - x_Q\right)\right) = t_\zeta\left[t_\zeta\left(x_D - x_Q\right) - y_D + y_Q\right],$$

resulting in the following derivatives

$$\frac{\partial F_2^{\beta^*}}{\partial \eta} = \frac{\partial p^-}{\partial \eta}\left[\cos\phi - 2\sin\phi\left(\psi^- - \psi_Q\right)\right] - \left(Yc_\alpha - Xs_\alpha\right)\sec^2\zeta\left(x_Q - x_D\right), \quad (4.103)$$

$$\begin{aligned}\frac{\partial F_2^{\beta^*}}{\partial \psi^-} = \cos\phi\frac{\partial p^-}{\partial \psi^-} - 2\sin\phi\left[\frac{\partial p^-}{\partial \psi^-}\left(\psi^- - \psi_Q\right) + p^-\right] \\ -\left[\left(x_D - x_Q\right)t_\zeta - y_D + y_Q\right]\left[Ys_\alpha + Xc_\alpha + \left(Yc_\alpha - Xs_\alpha\right)t_\zeta\right].\end{aligned} \quad (4.104)$$

Therefore, when calculating the discontinuity of type 2, whenever

$$\left|\psi^- + \varepsilon - \pi/2\right| \le 0.005,$$

we use Eqs. (4.102) to (4.104) instead of Eqs. (4.93), (4.99) and (4.100).

4.8.1.1 Locating the quadrilateral

Given P we can find the quadrilateral in which it is contained. Consider Fig. 4.15, we first find the closest point O to P. This can be done simply using the distance formula.

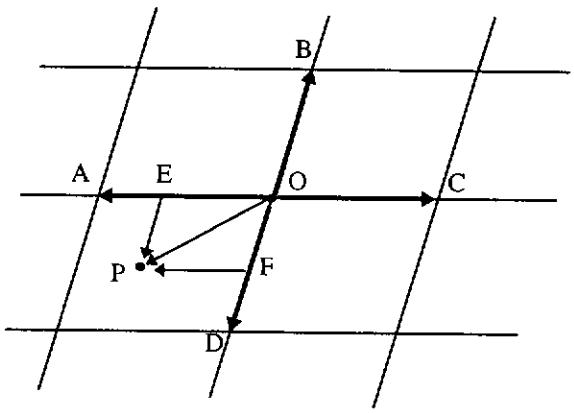

Fig. 4.15 Location of a point within quadrilateral

Once point O has been located, it is easy to find points A, B, C, and D around it. The next step is to find a vector $\vec{EP}$ parallel to $\vec{OD}$ and a vector $\vec{FP}$ parallel to $\vec{OA}$. Then, if the Euclidean inner products

$$\vec{EP}\cdot\vec{OD} > 0 \text{ and } \vec{FP}\cdot\vec{OA} > 0 \tag{4.105}$$

then P is located in the quadrilateral defined by AOD, otherwise we search for P in the other three quadrilaterals.

4.8.1.2 Interpolation within quadrilaterals

Let Φ represent either the mean stress p or ψ. Now we assume that within each quadrilateral, Φ is a smooth function that can be represented by a simple polynomial such as the bilinear function

$$\Phi = a_1 + a_2 x + a_3 y + a_4 xy . \tag{4.106}$$

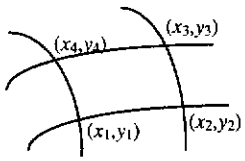

Fig. 4.16 A typical quadrilateral

The constants a_i can be expressed in terms of Φ_i's which are the values of Φ at the four nodes. Equation (4.106) represents an interpolation of function Φ in terms of the position (x, y) within an element (Fig. 4.16). That is, when the a_i's have been determined in terms of the grid point values Φ_i by solving

$$\begin{pmatrix} \Phi_1 \\ \Phi_2 \\ \Phi_3 \\ \Phi_4 \end{pmatrix} = \begin{bmatrix} 1 & x_1 & y_1 & x_1 y_1 \\ 1 & x_2 & y_2 & x_2 y_2 \\ 1 & x_3 & y_3 & x_3 y_3 \\ 1 & x_4 & y_4 & x_4 y_4 \end{bmatrix} \begin{pmatrix} a_1 \\ a_2 \\ a_3 \\ a_4 \end{pmatrix},$$

Eq. (4.106) defines Φ within an element in terms of Φ_i's and the coordinates. For a fine discretisation, Φ is a good approximation away from the grid points. For points on the boundary (wall or centre-line) the adjacent elements are triangular, so instead of Eq. (4.106) we use

$$\Phi = a_1 + a_2 x + a_3 y.$$

4.8.2 Generation of the corresponding velocity field

A knowledge of the velocity field is important in the prediction of the mixing properties of silos, rate of wall wear and the type of discharge. There is no effective method for solving the velocity problem coupled with a discontinuous stress field (Michalowski, 1984).

In the calculation of the velocity field in the presence of a discontinuous stress field, we assume that the velocity is continuous across the stress discontinuity. However, we note that discontinuous velocity fields are possible even within continuous stress fields. We calculate the velocity field within each computational domain separately. Therefore, the velocity is first calculated within the continuous region then we interpolate along the line of discontinuity and use these values as initial values for the next region.

4.9 NUMERICAL RESULTS

In this section, we first compare the accuracy of our solution scheme with that of Bradley (1991) for continuous stress fields and we also present the velocity field which was not presented by Bradley. Secondly, we study the stress and velocity fields in the presence of stress discontinuity. Finally, we investigate the effect of various physical parameters on the normal pressures on the wall and centre-line of a hopper.

4.9.1 Investigation of continuous stress fields

Bradley (1991) compared the solution of the Method of Characteristics with the radial stress field solution. To achieve this, he used the radial stress field solution to specify the values of $x, y, p,$ and ψ at 21 and 41 points along the initial curve which was taken to be a β characteristic spanning the outlet of the hopper. In his analysis, he considered two examples. In the first example the physical parameters were given by $\theta_w = 23^o$, $\phi_w = 11.5^o$ and $\phi = 30^o$. He found that, when compared to the radial stress field solution, the error in the computed values of p increases as the distance from the apex increases; and that the error in the numerical solution increases when the number of points along the initial curve is increased. In the second example the physical parameters are $\theta_w = 57^o$, $\phi_w = 14.5^o$ and $\phi = 30^o$. He found that there was a significant error in the computed values of ψ (by comparing the corresponding meshes) at large distances from the apex; and that the error in p increases significantly with distance. In this example, however, the results become more accurate when the number of points along the initial curve is increased. Bradley thus concluded that the mesh size has no significant effect on the accuracy of the numerical solution and that using double precision might result in a more accurate solution.

In this section, we test his claims using our numerical scheme. Also, we compare the results of our method in which the initial curve spans the top surface of the hopper rather that the outlet. Our model hopper has vertical height of seven metres. Figures 4.17-4.20 show respectively the solution of p, the characteristic mesh, the stress and velocity fields. The results are qualitatively correct based on our knowledge. The comparison of solution by the present scheme with the radial stess solution clearly indicates that the numerical scheme is robust.

Figures 4.21 and 4.22 show the relative errors in p for the case when $\theta_w = 23^o$, $\phi_w = 11.5^o$ and $\phi = 30^o$. The graph compares the results of solutions generated by starting from the outlet and the top surface. It can be noted that when

the calculations proceed upwards from the outlet, the error in p increases exponentially. On the other hand, if the calculation proceeds from the top surface, the error actually vanishes at the outlet. Figures 4.23 and 4.24 show the relative errors corresponding to $\theta_w = 57^o$, $\phi_w = 14.5^o$ and $\phi = 30^o$. It can be noted that the errors follow a similar pattern, except that when the top surface is used as the initial curve, the behaviour is a little erratic close to the outlet. Again an increase in mesh size results in a considerable reduction in error.

Therefore, based on our results, it seems reasonable to conclude that all calculations should start from the top surface and proceed towards the outlet of the hopper. It can be noted that with our scheme, the error in p decreases substantially when the number of points along the outlet is increased which is a contradiction to Bradley's result. However, we believe that a proper scheme should have the feature that accuracy can be improved by refining the mesh. The conclusion that mesh size has no significant effect on the numerical solution has been shown to be false.

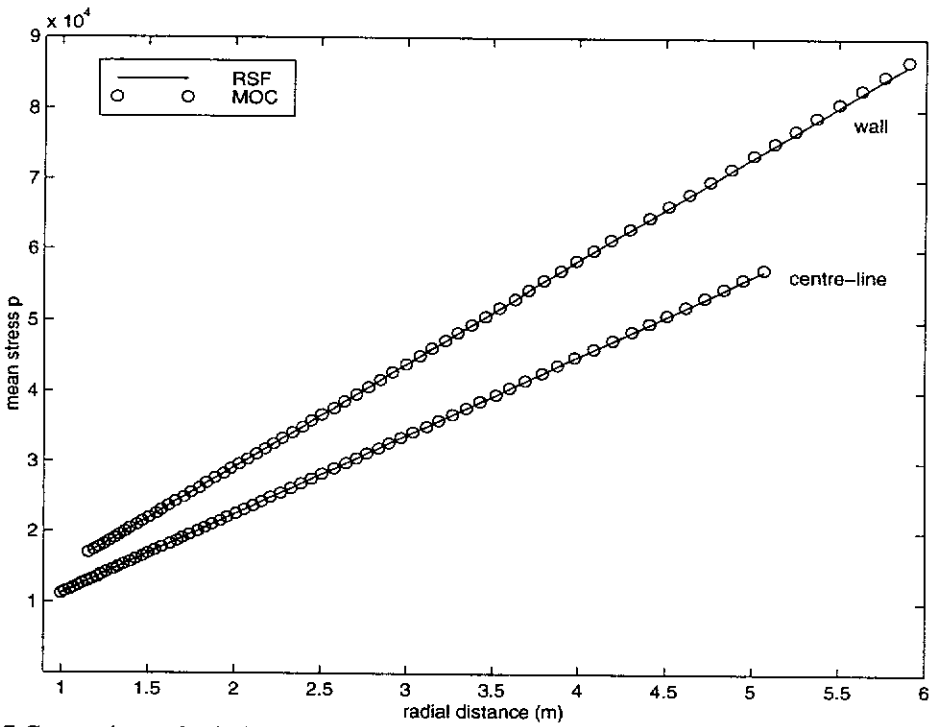

Fig. 4.17 Comparison of solutions obtained by the present numerical scheme (MOC) and radial stress solution (RSF) (θ_w=23°, ϕ_w=11.5°, ϕ=30°)

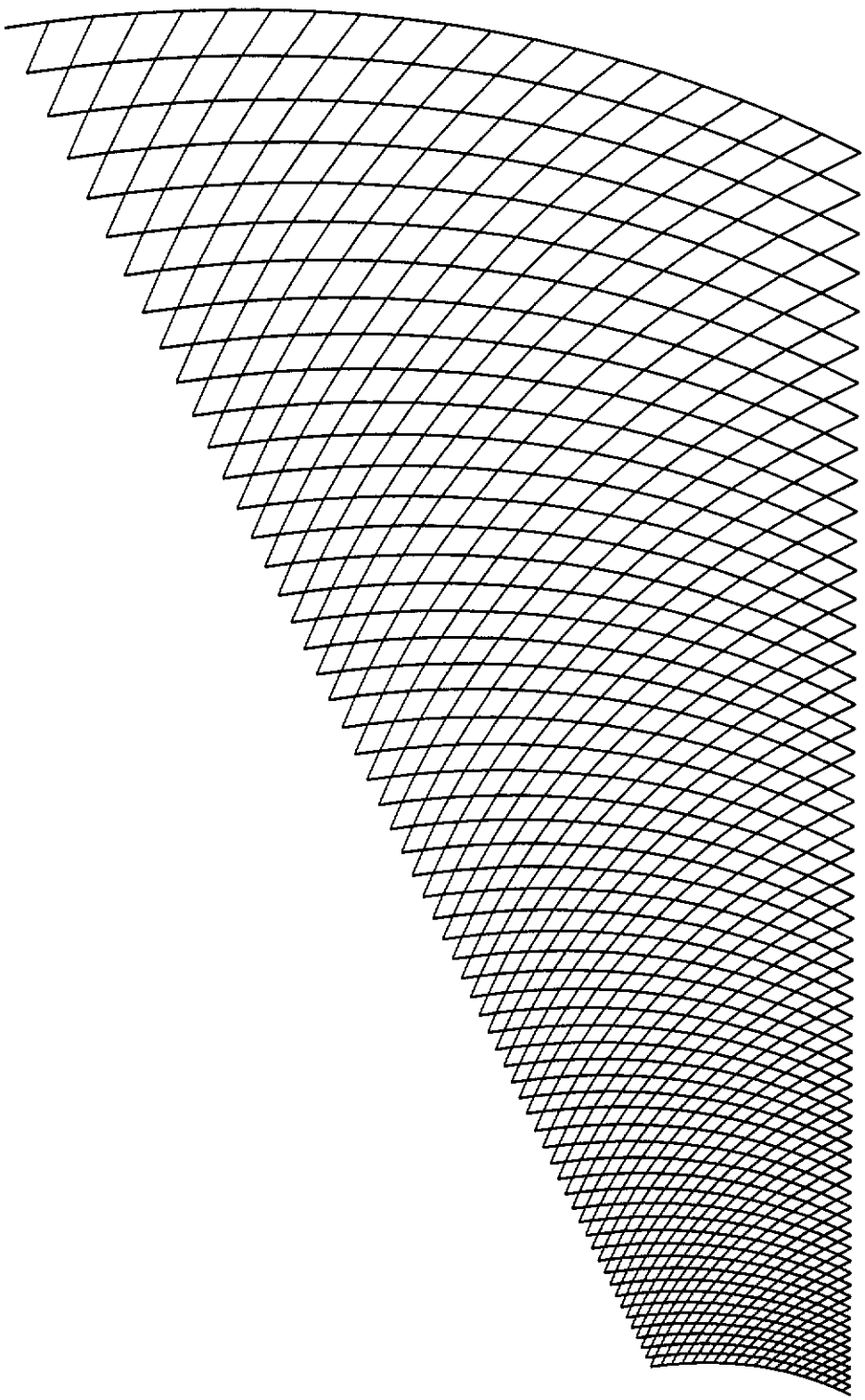

Fig. 4.18 Characteristic mesh (θ_w=23°, ϕ_w=11.5°, ϕ=30°)

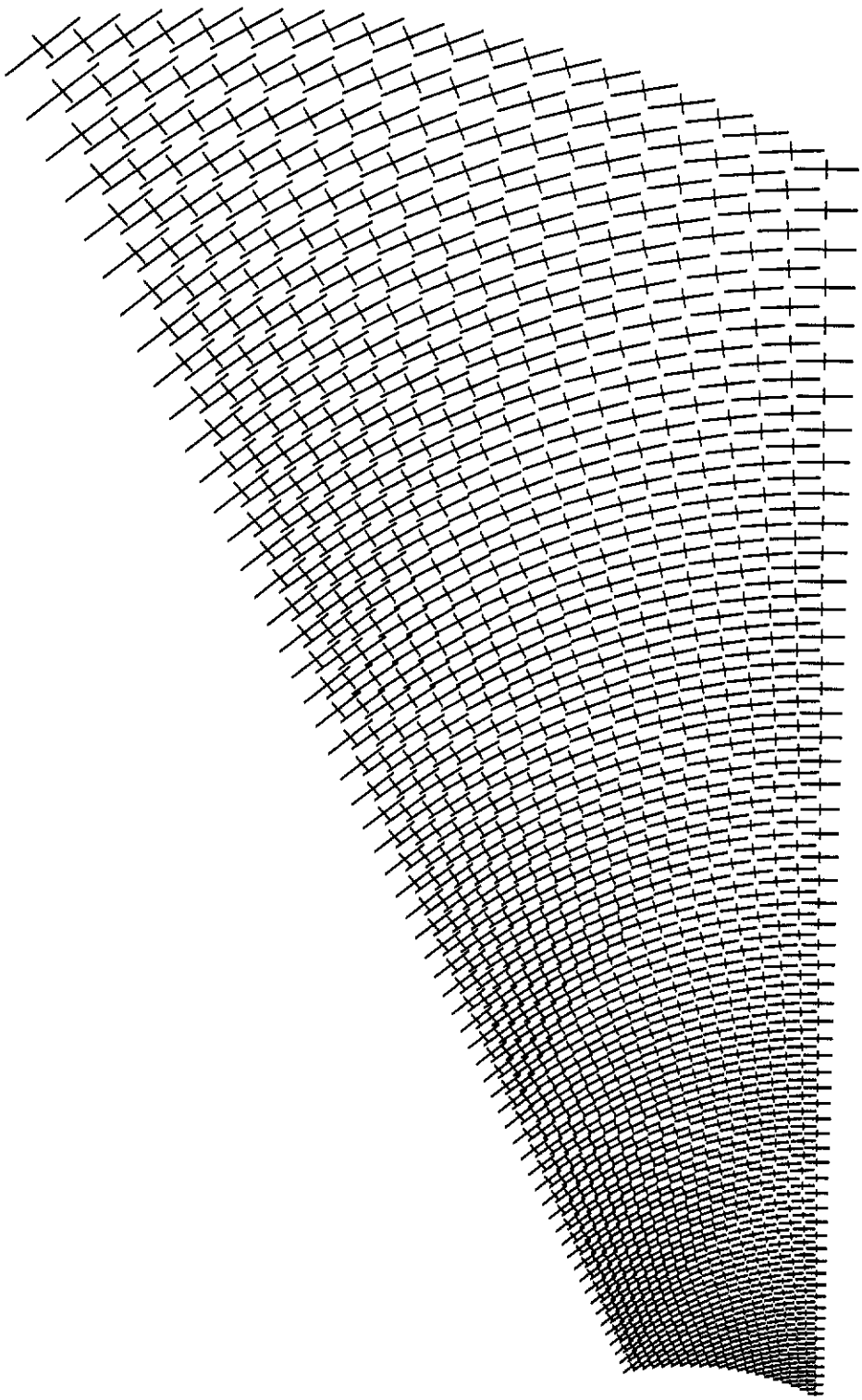

Fig. 4.19 Principal stress field (θ_w=23°, ϕ_w=11.5°, ϕ=30°)

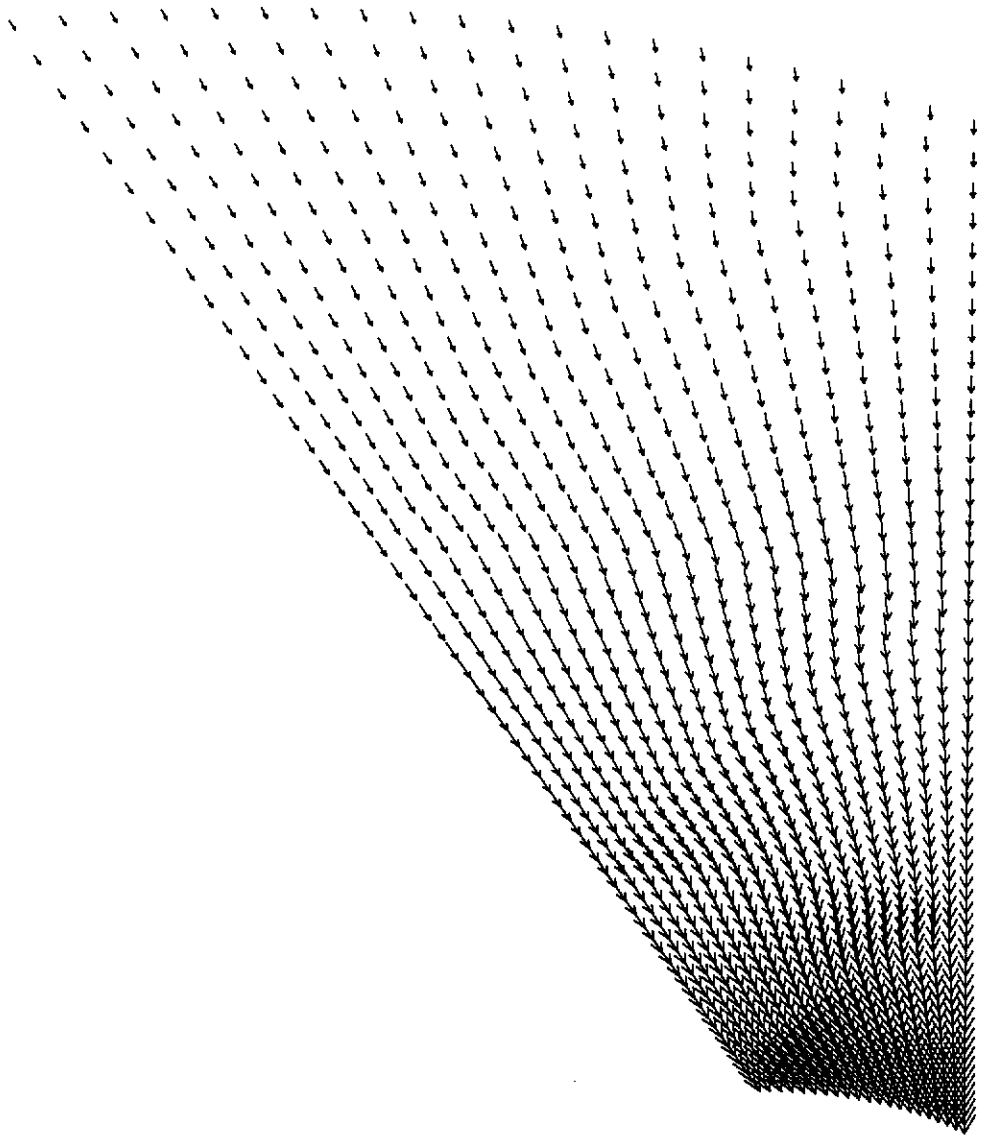

Fig. 4.20 Velocity field (θ_w=23°, ϕ_w=11.5°, ϕ=30°)

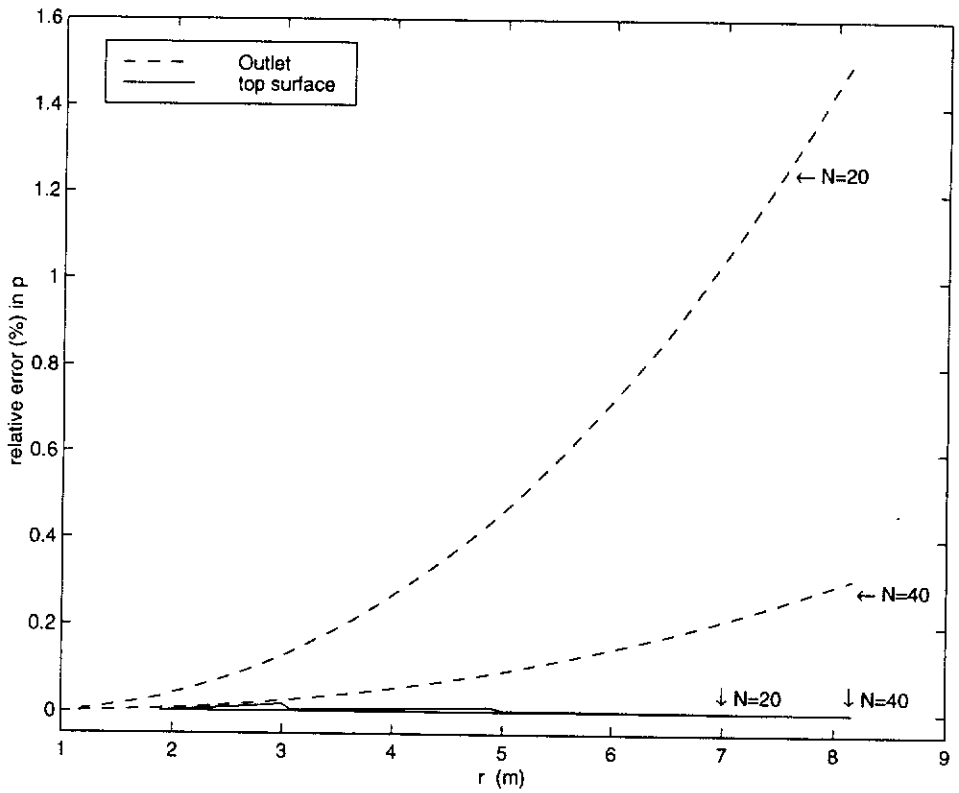

Fig. 4.21 Error of p at the wall for solutions generated from outlet and top surface (θ_w=23°, ϕ_w=11.5°, ϕ=30°)

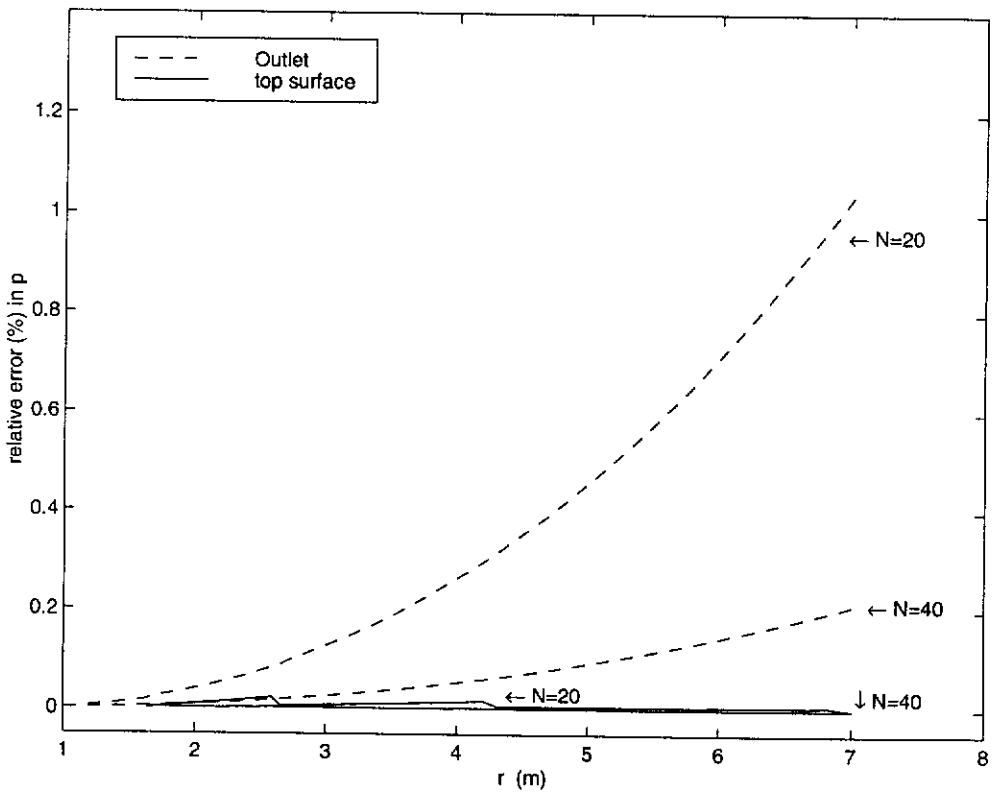

Fig. 4.22 Error of p at the centre-line for solutions generated from outlet and top surface (θ_w=23°, ϕ_w=11.5°, ϕ=30°)

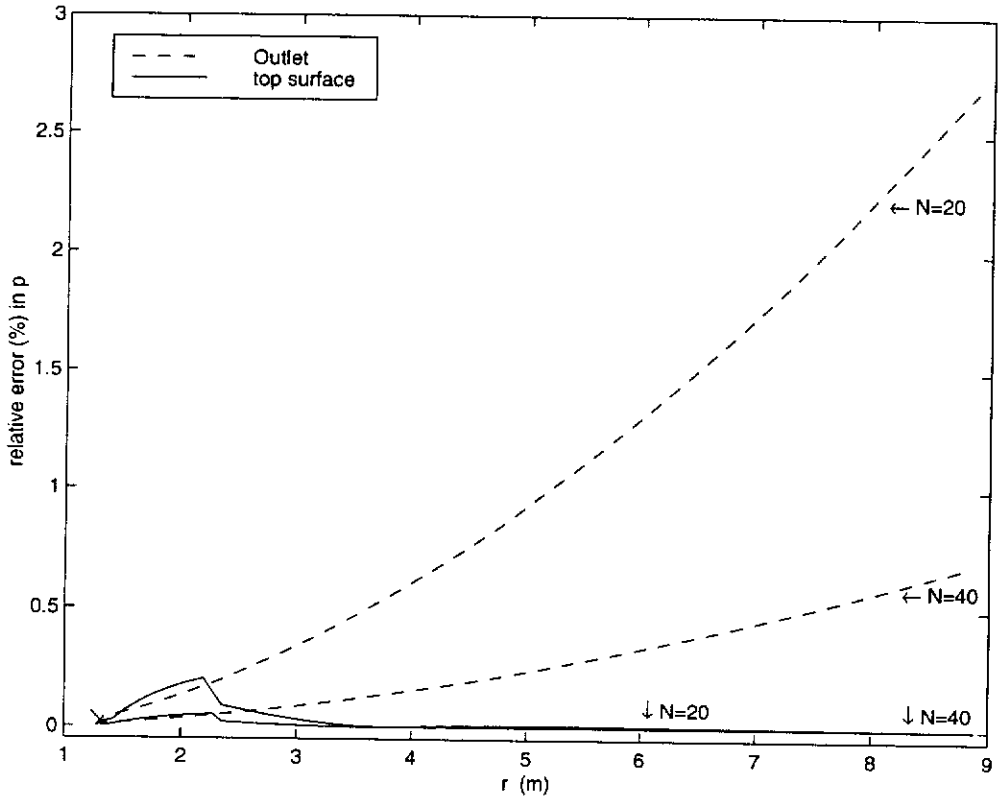

Fig. 4.23 Error of p at the wall for solutions generated from outlet and top surface (θ_w=57°, ϕ_w=14.5°, ϕ=30°)

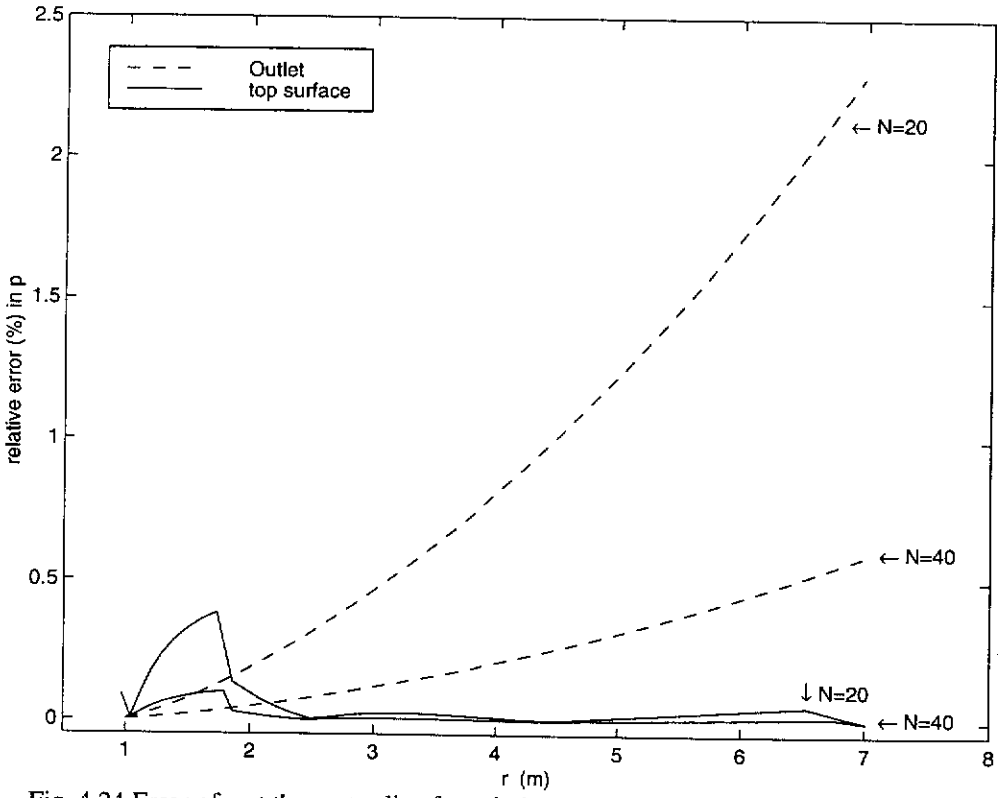

Fig. 4.24 Error of p at the centre-line for solutions generated from outlet and top surface (θ_w=57°, ϕ_w=14.5°, ϕ=30°)

4.9.2 Stress and velocity pattern in the presence of stress discontinuity

The numerical scheme developed is applied to study the stress distribution and velocity pattern of granular material in hoppers, in the presence of stress discontinuity. The values of parameters used in each computation scheme are as shown in table 4.1. Figures 4.25 and 4.26 show the characteristic mesh and stress distribution corresponding to $\theta_w = 23^o$, $\phi = 30^o$ and $\phi_w = 11.5^o$. It is obvious that the stress discontinuity propagates over the whole region. The velocity field shown in Fig. 4.27 is typical of the fields calculated using parameters in Table 4.1. This figure shows two kinds of distinct flow zones. The first kind of flow zone corresponds to the computational region adjacent to the wall. It can be seen that the velocity is almost parallel to the wall. The second kind of flow zone corresponds to the regions adjacent to the centre-line. Here, the velocity is almost vertical.

Table 4.1 Physical parameters

θ_w (°)	ϕ (°)	ϕ_w (°)
23	30	11.5, 13, 14.5
23	20	11.5, 13, 14.5
23	35	11.5, 13, 14.5
15	30	11.5, 13, 14.5
15	20	11.5, 13, 14.5
15	35	11.5, 13, 14.5
30	30	11.5, 13, 14.5
30	20	11.5, 13, 14.5
30	35	11.5, 13, 14.5

As many investigators such as Bransby & Blair-Fish (1973) and Michalowski (1984) have observed non-steady discontinuous velocity fields during discharge in a plane wedge-shaped hopper, the current analysis is limited to steady state cases.

4.9.3 Effect of various parameters on stress in the presence of stress discontinuity

This section deals with the application of the numerical technique to a parametric study of granular flows in hoppers. We investigate the effect of varying several parameters on the normal pressure. The values of parameters used are as shown in Table 4.1 (note that each row corresponds to three sets of parameters). The results presented are typical for values in the table. We may think of the initial surface as the surface formed in the transition region between the bin section and the hopper. Again, the hopper is assumed to be symmetrical and so we restrict the computation region to just one half of the hopper.

Effect of hopper half-angle

The hopper half-angle θ_w is varied while the angle of internal friction ϕ and the angle of wall friction ϕ_w are constant throughout the calculations. Figures 4.28 and 4.29 show the results for $\theta_w = 15^o, 23^o, 30^o$ while $\phi = 30^o$ and $\phi_w = 11.5^o$. It can be noted that increasing θ_w has the effect of increasing σ_{nn} on the wall and centre-line. Also, the jump in σ_{nn} across the discontinuity is bigger. This result is correct from a qualitative analysis. For a hopper with smaller half-angle, the material is confined in a narrower region and thus wall friction plays a more significant effect and the normal wall pressure will consequently be smaller.

Effect of angle of internal friction

The angle of internal friction ϕ is varied while the values of θ_w and ϕ_w are kept constant. Figures 4.30 and 4.31 show that a decrease in ϕ results in a substantial increase in σ_{nn} along the wall and an increase in the jump across the discontinuity. Also, it can be seen that σ_{nn} increases more rapidly between two successive discontinuities.

Effect of the angle of wall friction

The angle of wall friction is varied for each set of θ_w and ϕ. Figures 4.32 and 4.33 show the results for $\phi_w = 11.5^o, 13^0, 14.5^o$ and the fixed values $\theta_w = 13^o$, $\phi = 30^o$. We can see that increasing the angle of wall friction will result in a decrease in p while there seems to be no effect on the jump. Our knowledge of hopper pressure distribution also indicates that this result is correct.

4.10 CONCLUDING REMARKS

A numerical technique has been developed to solve the hyperbolic partial differential equations arising from the formulation of the so-called double-shearing theory for granular flows. The essential features of stress distribution and velocity pattern in hoppers are computed in the presence of stress discontinuity. The importance of this development is that it will facilitate the development of the double-shearing theory. The double-shearing theory has been proposed and developed for many decades. However, due to the high nonlinearity of the underlying equations, very few real problems can be solved using this theory, which makes it impossible to identify its application domain. The development of the numerical technique will make it possible to generate numerical solutions for many problems using the perfect plasticity theory based on the double shearing assumption and thus to identify the application domain of the double shearing theory by comparing mathematical solutions with experimental results or measurements. In addition, the present numerical technique is capable of determining the stress discontinuity, which is important because stress discontinuity is one of the special features of granular flows, but existing continuum numerical techniques are not able to determine such discontinuities.

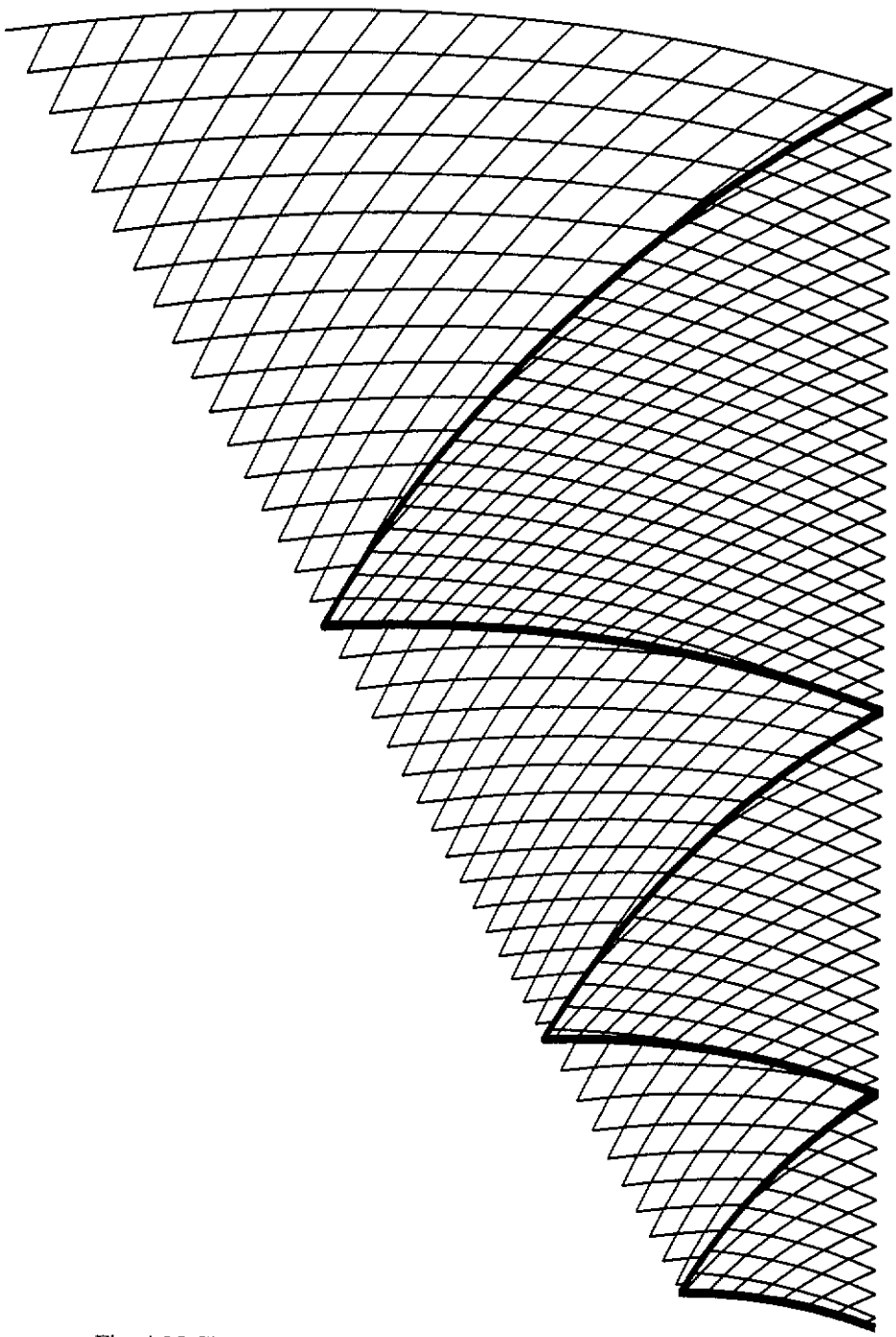

Fig. 4.25 Characteristic mesh (thick lines indicate discontinuities)

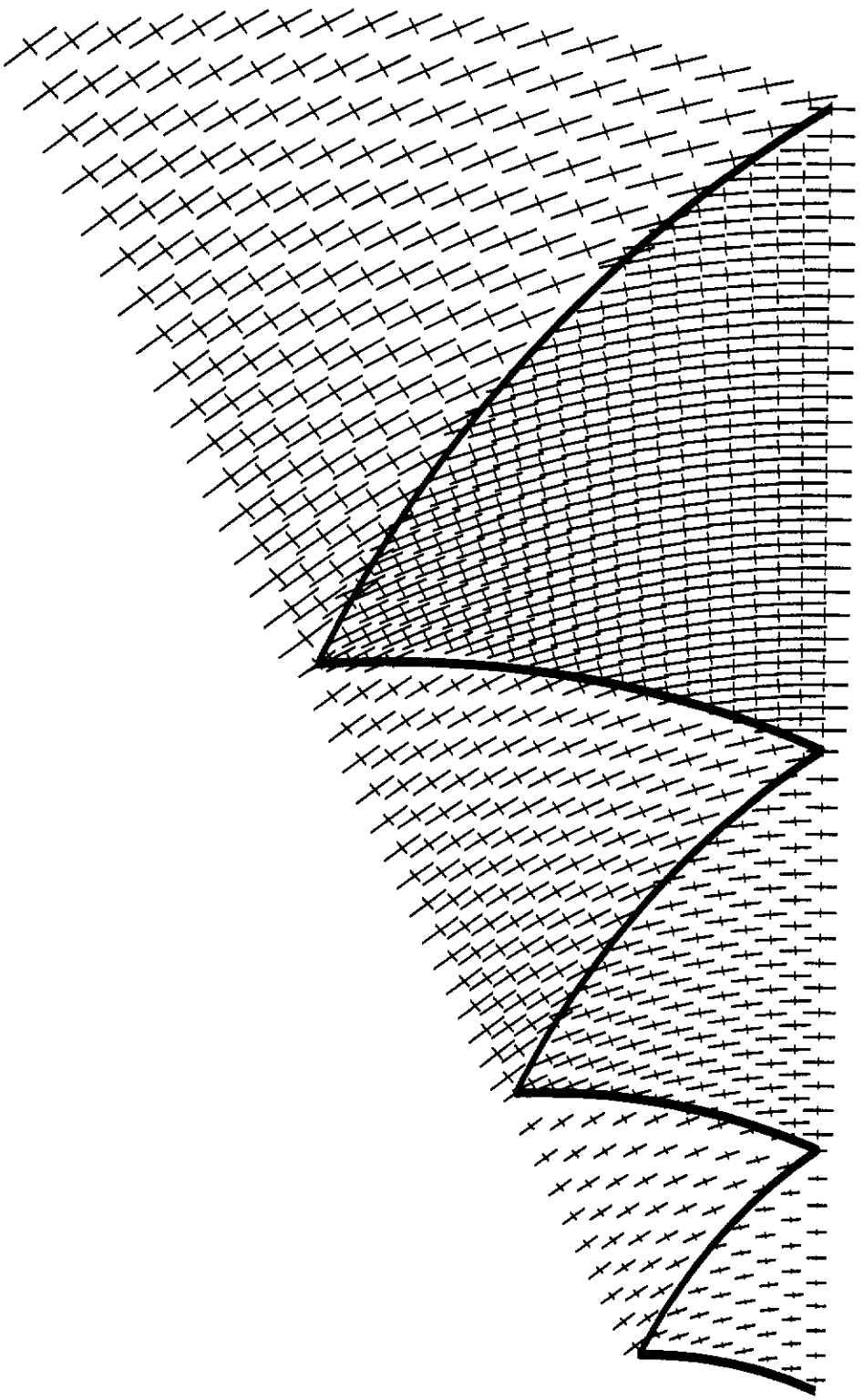

Fig. 4.26 Principal stress field in the presence of discontinuities (θ_w=23°, ϕ_w=11.5°, ϕ=30°)

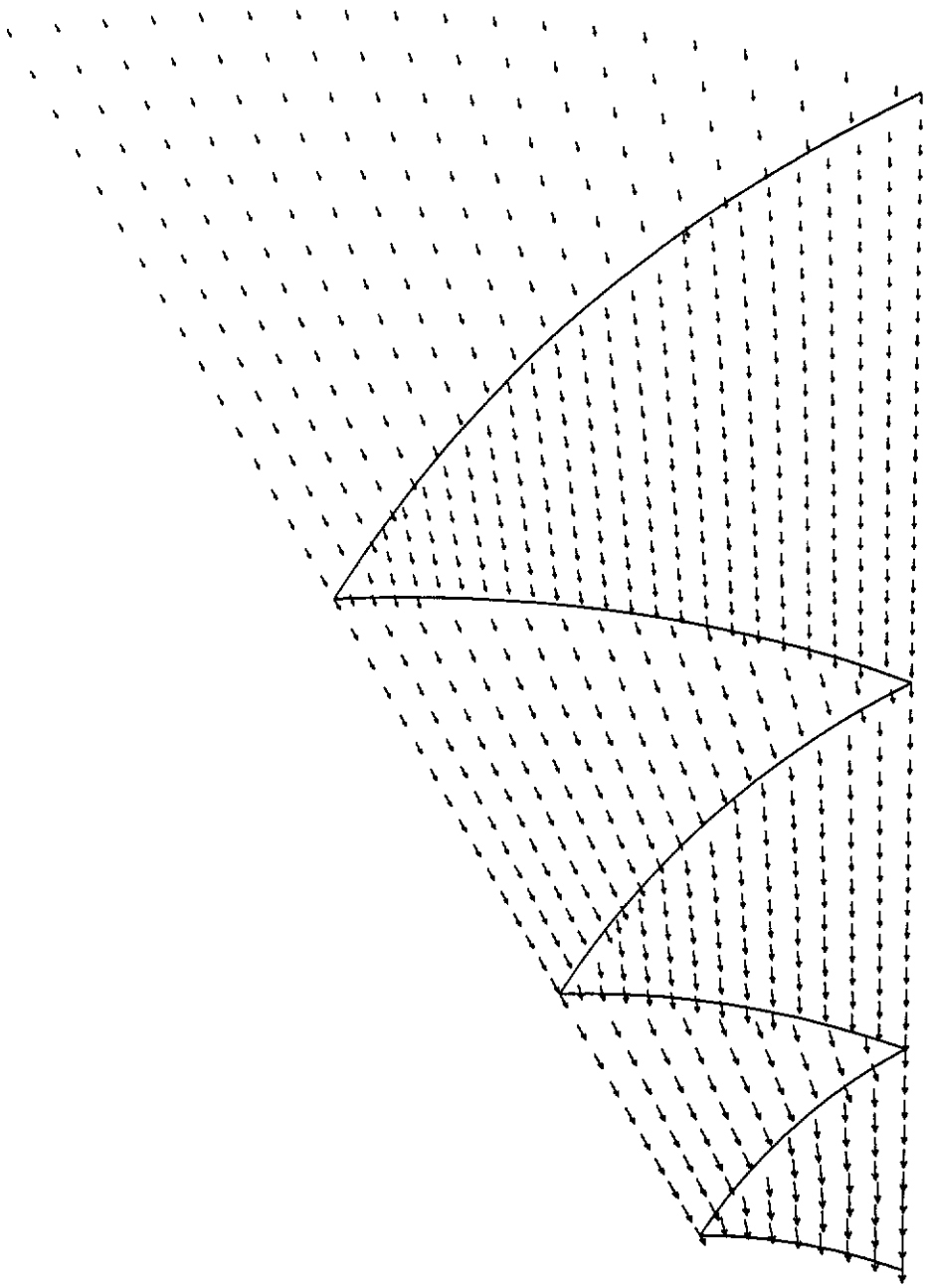

Fig. 4.27 Velocity field in the presence of discontinuities (θ_w=23°, ϕ_w=11.5°, ϕ=30°)

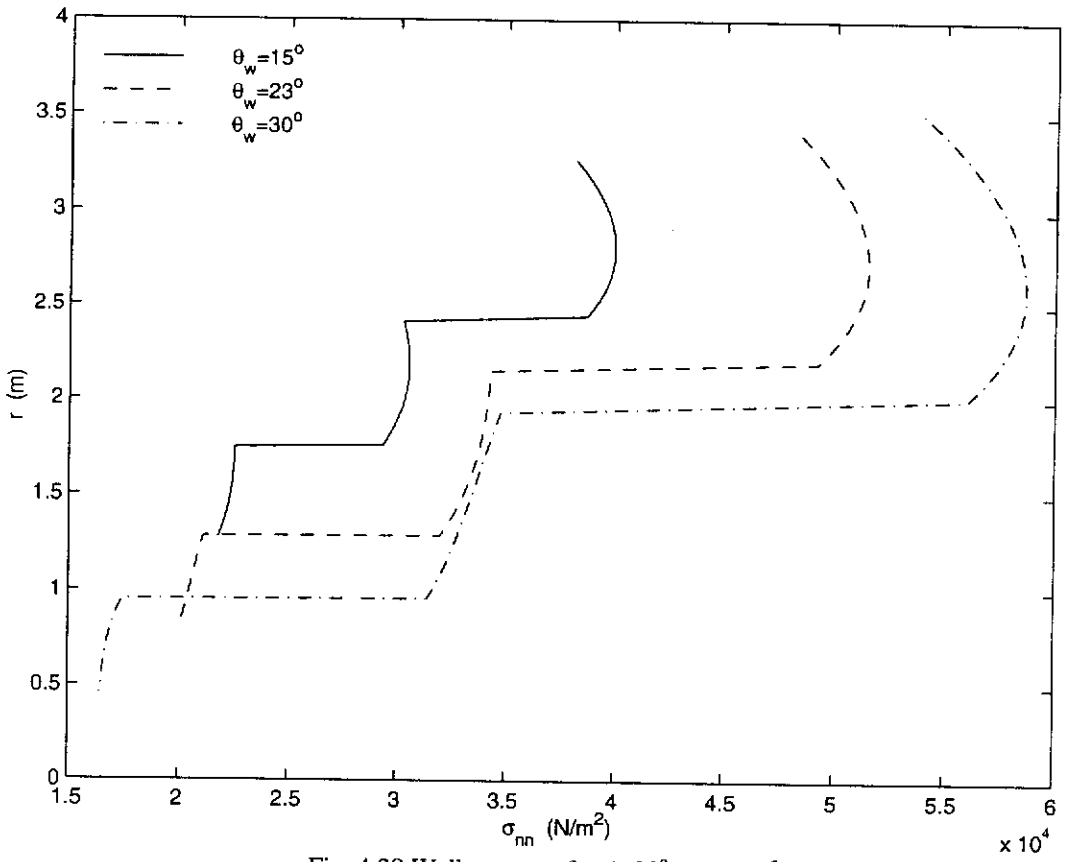

Fig. 4.28 Wall pressure for ϕ=30°, ϕ_w=11.5°

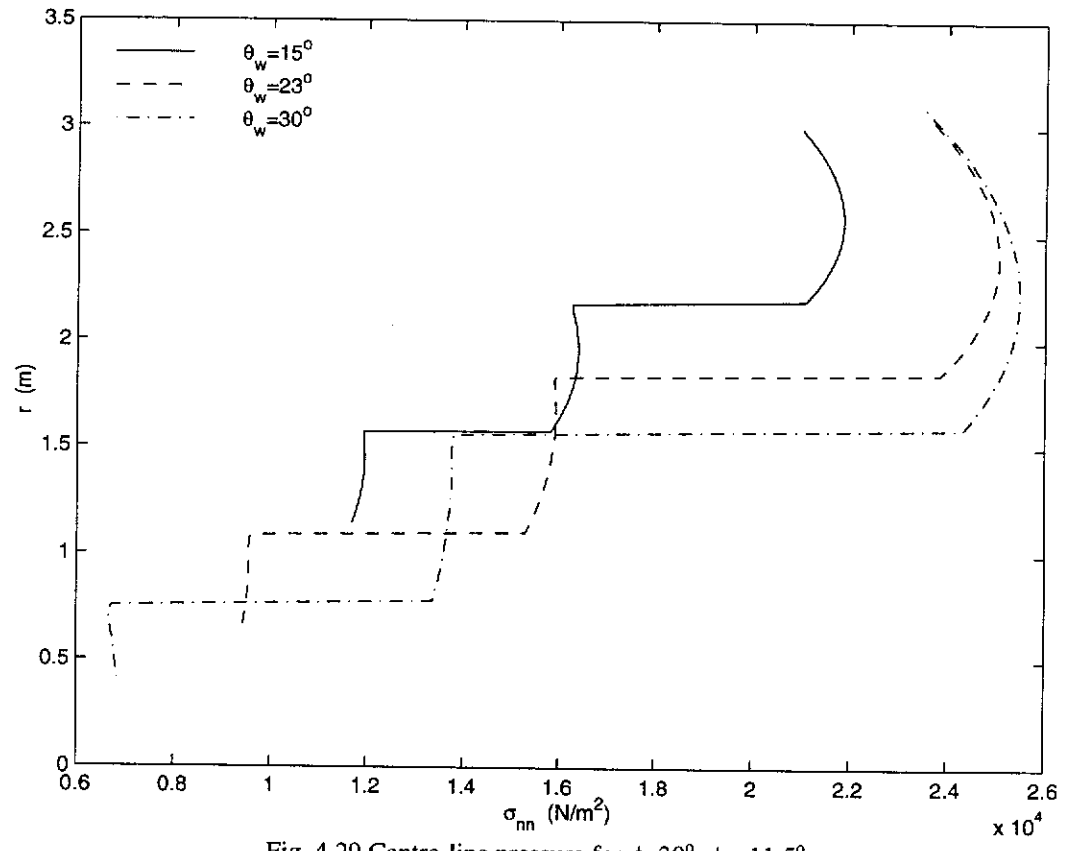

Fig. 4.29 Centre-line pressure for ϕ=30°, ϕ_w=11.5°

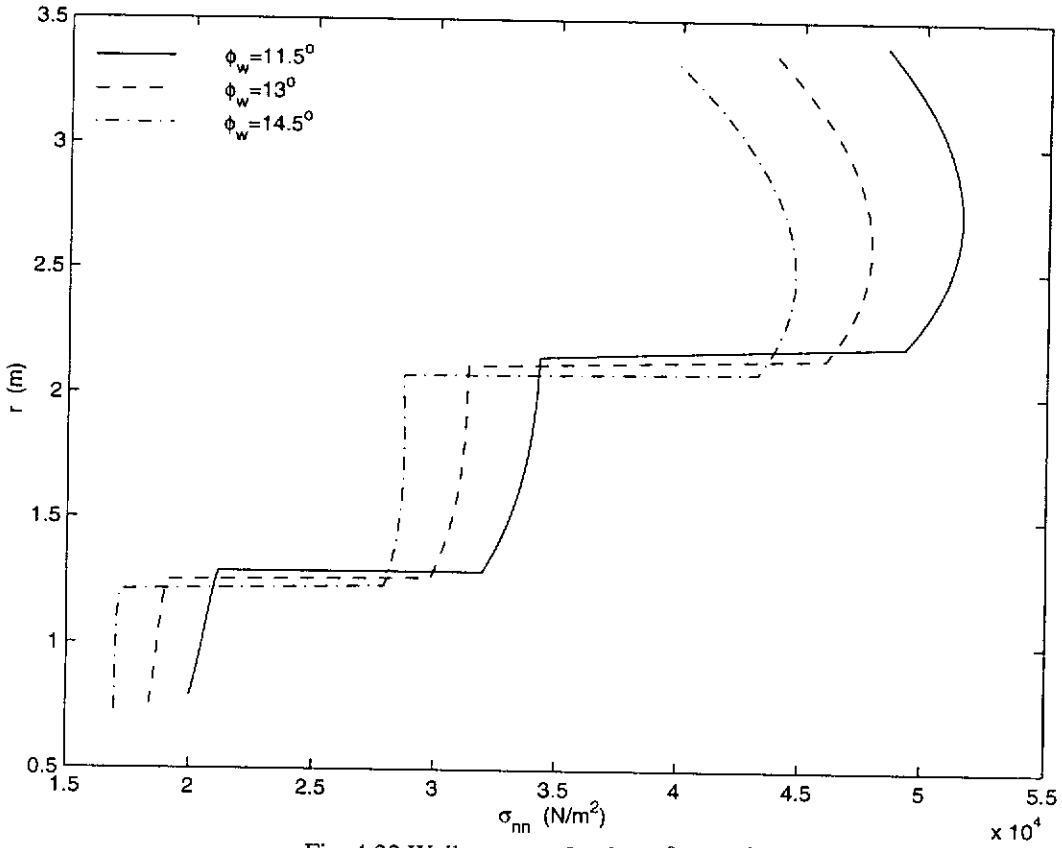

Fig. 4.32 Wall pressure for θ_w=13°, ϕ=30°

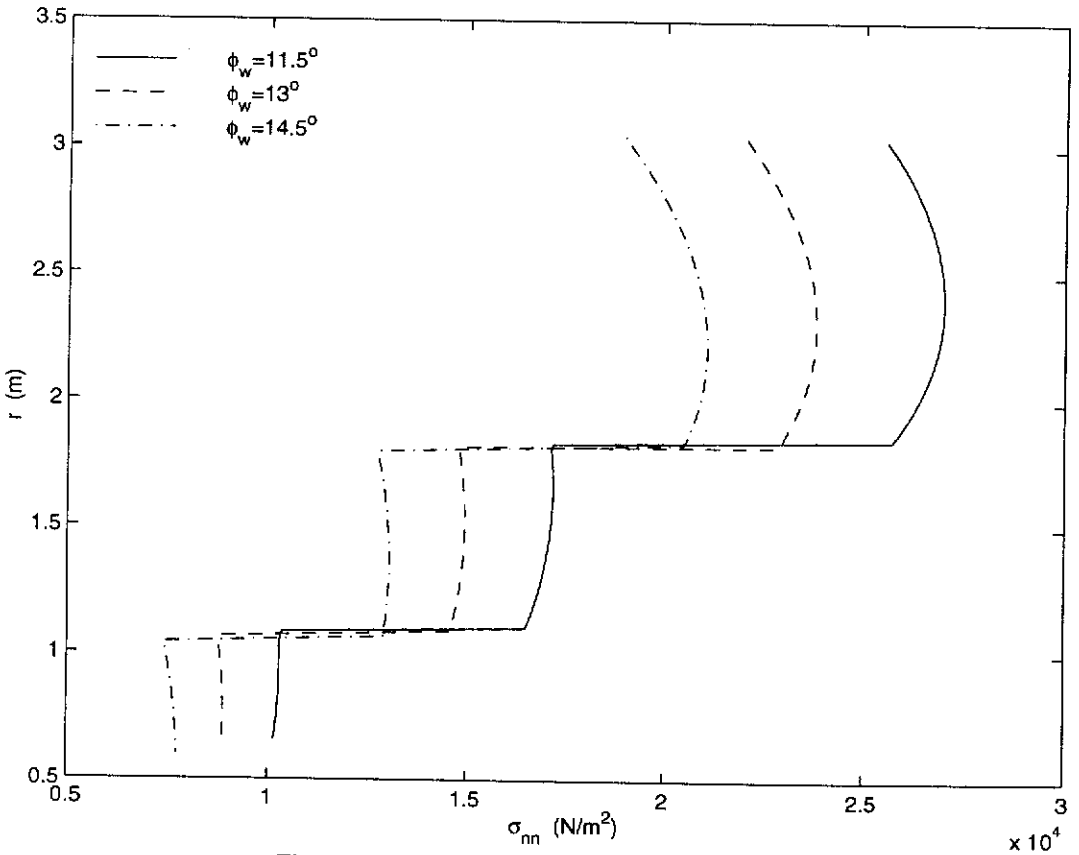

Fig. 4.33 Centre-line pressure for θ_w=13°, ϕ=30°

CHAPTER FIVE

FINITE ELEMENT SOLUTION OF THE DOUBLE SHEARING-BASED MODEL

5.1 GENERAL

Over the last two decades, many attempts have been made to develop general granular flow models with both the elasto-plasticity feature of solids and the viscous behaviour of fluids (Rombach & Eibl, 1995; Schmidt & Wu, 1989). This type of model is usually referred to as a viscous elasto-plasticity model. Sophisticated numerical methods such as the *finite element method* and the *boundary element method* have been developed to implement these models. However, most researchers concentrate only on models with the plastic deformation governed by the so-called plastic flow rule theory. Very few attempts have been made to develop general numerical techniques for granular flow associated with the double-shearing flow mechanism.

The formulation of the double shearing theory in Sections 3.3 and 3.4 has made it possible to develop a general numerical method for simulating the viscous elasto-plasticity flow obeying the double shearing flow mechanism. As proposed by many authors, the stress tensor is assumed to consist of a rate dependent part σ_v and a rate independent part σ_s, thus

$$\overset{\circ}{\sigma} = \overset{\circ}{\sigma}_v + \overset{\circ}{\sigma}_s, \tag{5.1}$$

where $\overset{\circ}{\sigma}$ is the corotational rate of stress, namely

$$\overset{\circ}{\sigma} = \frac{\partial \sigma}{\partial t} + v \cdot \nabla \sigma + \sigma w - w \sigma . \tag{5.2}$$

The rate dependent part is due to the viscous effect and is assumed to be linearly proportional to the corotational rate of deformation, namely

$$\overset{\circ}{\boldsymbol{\sigma}}_{v} = G\overset{\circ}{\boldsymbol{d}}, \tag{5.3}$$

where G is a viscous matrix. The rate independent part is due to the elastic-plastic deformation and is determined as shown in Sec. 3.3 by

$$\overset{\circ}{\boldsymbol{\sigma}}_{s} = H\boldsymbol{d}. \tag{5.4}$$

Therefore, the stress and velocity fields in such a model are governed by the standard equations of motion, a set of viscous-elastic-plastic constitutive equations, and a set of boundary conditions.

The purpose of this Chapter is to present a finite element formulation within a proper mathematical framework for the flow of an idealised granular material whose constitutive relations can be described in the form of Eq. (5.1). The rest of this chapter is organised as follows. In section 5.2, three different kinds of boundary conditions for granular flows are introduced. In section 5.3, a variational statement for the boundary value problem governing the viscous elasto-plasticity flow is developed. In section 5.4, the variational statement is posed in N-dimensional function subspace and then discretised by the finite element method. Sections 5.5 and 5.6 concern the computational aspect. A numerical example is then presented in section 5.7 and some concluding remarks are given in section 5.8.

5.2 GENERAL BOUNDARY CONDITIONS

The boundary conditions at each boundary point are specified as either essential (both components of displacement are specified), natural (both components of stress are specified), or mixed. For a well-posed boundary-value problem we must specify displacements or velocities at various points to prevent rigid-body motion of the structure. This is because the governing equations only describe relative motion

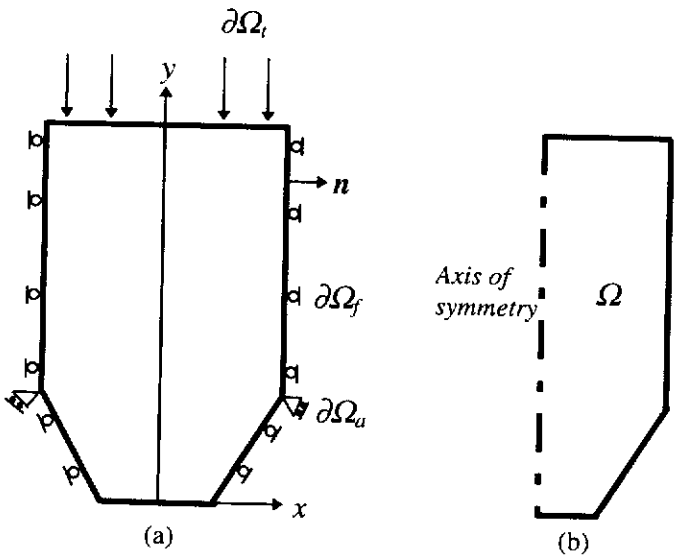

Fig. 5.1 Plane strain silo and computational region

between points in the body. If the structure is not sufficiently constrained to prevent rigid-body motions, then there are infinitely many solutions to the governing equations, each having the same deformation but at different location in space.

Consider a silo as shown in Fig. 5.1. The structure is symmetric about the y-axis. Within each half, the physical properties and boundary conditions are identical and hence the solutions will be identical in the right half and the left half (Fig. 5.1b). This simplifies the problem because we will only need to find solution in one half.

Although it is generally accepted that, unlike in fluids, the no-slip boundary condition does not apply to granular materials, the behaviour at the solid boundary interface is not fully understood (Zheng and Hill, 1996). We assume that the frictional force at the boundary surface, which is one of the most influential factors affecting the performance of silos (Roberts, 1991), obeys Coulomb's Law of friction, namely the frictional force is proportional to the pressure exerted by the material on the wall. Hence,

$$|\sigma_t| = |\sigma_n| \tan \phi_w \tag{5.5}$$

where σ_n is the component of stress normal to the boundary, σ_t denotes the tangential component, and ϕ_w denotes the angle of wall friction. In general, the

angle of wall friction ϕ_w decreases as the normal pressure increases (Roberts, 1991) as shown in Fig. 5.2.

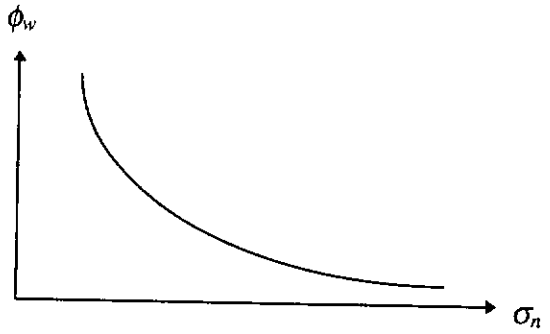

Fig. 5.2 Relationship between wall friction and normal pressure

The boundary of the stored granular material can be classified into three types (Wu, 1990): a free/surface boundary $\partial\Omega_t$, an adhesion contact boundary $\partial\Omega_a$ and a frictional contact region $\partial\Omega_f$. Therefore, since Eq. (5.5) represents the critical value of the shear traction at which slip occurs, we have

$$|\sigma_t| \geq |\sigma_n| \tan\phi_w \quad \text{on} \quad \partial\Omega_f$$
$$|\sigma_t| < |\sigma_n| \tan\phi_w \quad \text{on} \quad \partial\Omega_a .$$

In the slip region $\partial\Omega_f$, the boundary condition includes natural boundary conditions and an essential boundary condition, namely

$$\sigma_t = (-\tan\phi_w \frac{v_t}{|v_t|})(-\sigma_n), \tag{5.6}$$

$$v_n = 0 . \tag{5.7}$$

In the adhesion region $\partial\Omega_a$, we have two essential boundary conditions

$$v_t = 0, \; v_n = 0 , \tag{5.8}$$

where v_t and v_n are the components of velocity tangential and normal to the boundary.

The boundary condition on the top surface and the outlet in the discharging phase is simply that the tractions are zero, that is $\sigma_{nn} = \sigma_{nt} = 0$. Along the axis of symmetry, the boundary condition is $\sigma_{xy} = 0$, $v_x = 0$.

5.3 VARIATIONAL STATEMENT OF THE PROBLEM

Consider the flow of a granular material which occupies the spatially fixed region Ω with a boundary $\partial\Omega$ consisting of three parts: $\partial\Omega_a$ with rigid constraints, $\partial\Omega_t$ with the prescribed tractions $\overline{f}$, and $\partial\Omega_f$ with rigid constraints in the normal direction and frictional forces along the tangential direction, as shown in Fig. 5.1. From Chapter 3 and Fig. 5.1, the stress and velocity fields of granular flow are governed by the following boundary value problem (BVP).

BVP : Find v and σ such that

$$\sigma_{ij,i} + X_j - \rho\frac{Dv_j}{Dt} = 0 \quad \text{in } \Omega, \tag{5.9}$$

$$\overset{\circ}{\sigma}_{ij} = H_{ijrs}d_{rs} + G_{ijrs}\overset{\circ}{d}_{rs} \quad \text{in } \Omega, \tag{5.10}$$

$$v_i\big|_{t=0} = v_i^0 \,, \quad \sigma_{ij}\big|_{t=0} = \sigma_{ij}^0 \quad \text{in } \Omega, \tag{5.11}$$

$$v_i = 0 \quad \text{on } \partial\Omega_a, \tag{5.12}$$

$$f_i = \sigma_{ji}n_j = \overline{f}_i \quad \text{on } \partial\Omega_t, \tag{5.13}$$

$$v_i n_i = 0, f_t = -\text{sgn}(v_t)f_n\mu_w \quad \text{on } \partial\Omega_f, \tag{5.14}$$

where $\Omega \in R^2$, $\partial\Omega = \partial\Omega_a \cup \partial\Omega_t \cup \partial\Omega_f$ is the boundary of Ω, $\boldsymbol{n}$ denotes the unit vector in the outward normal direction of $\partial\Omega$, v_i^0 and σ_{ij}^0 are the initial values of

velocity and stress respectively. In the above equations, we have used the so-called index notation in which the comma represents differentiation and repeated indices indicate summation over the index range. The material derivative is given by

$$\frac{D(\ )_{ij}}{Dt} = \frac{\partial(\ )_{ij}}{\partial t} + v_k \frac{\partial(\ )_{ij}}{\partial x_k}.$$

In what follows, $L^2(\Omega)$ and $H^1(\Omega)$ denote respectively the square integrable function space and the usual sobolev space with the Euclidean norm $\|\cdot\|_2$, namely

$$L^2(\Omega) = \left\{v: \int_\Omega v^2 d\Omega < \infty\right\},$$

$$H^1(\Omega) = \left\{v \in L^2(\Omega): v|_{\partial\Omega_a} = 0 \text{ and } v_i n_i\big|_{\partial\Omega_f} = 0\right\}.$$

To solve the BVP problem numerically, it is necessary to derive a corresponding variational boundary value problem. For this purpose we first find the weak form of Eqs. (5.9) by making the sum of residuals orthogonal to all weight functions ω_j in the test space $H^1(\Omega)$, hence multiplying Eq. (5.9) by ω_j and integrating over the domain Ω results in

$$\int_\Omega \left(\sigma_{ij,i} + X_j - \rho \frac{Dv_j}{Dt}\right)\omega_j d\Omega = 0. \tag{5.15}$$

Now, noting that

$$\sigma_{ij,i}\omega_j = \left(\sigma_{ij}\omega_j\right)_{,i} - \omega_{j,i}\sigma_{ij},$$

integrating Eqs. (5.19) by parts and using Green's theorem in the plane, leads to the following weak form

$$\int_\Omega \left(-\omega_{j,i}\sigma_{ij} + X_j\omega_j - \rho \frac{Dv_j}{Dt}\omega_j\right) d\Omega + \int_{\partial\Omega^f} \overline{f}_j \omega_j ds = 0. \tag{5.16}$$

where $\partial\Omega^1 = \partial\Omega_t \cup \partial\Omega_f$ and s is the coordinate along the boundary $\partial\Omega^1$.

Therefore, the BVP problem has now been converted to the following variational boundary value problem.

VBVP: Find $v_j \in H^1(\Omega)$ such that, with relations (5.10) and condition (5.11), equations (5.16) are satisfied for all $\omega_j \in H^1(\Omega)$.

5.4 FINITE ELEMENT DISCRETISATION

To solve the VBVP problem numerically, we pose the problem in the N-dimensional subspace of $H^1(\Omega)$. The variable t is fixed while the space variables are discretised. Thus

$$\omega_j \approx \omega_j^h = \sum_{k=1}^{N} \beta_{jk}\phi_k(x,y), \tag{5.17}$$

$$v_j \approx v_j^h = \sum_{k=1}^{N} \phi_k(x,y)a_j^k(t), \tag{5.18}$$

where ϕ_k are the interpolating or shape functions. Substituting Eq. (5.17) into Eqs. (5.16) yields

$$\sum_{k=1}^{N}\left[\int_\Omega\left(-\phi_{k,i}\sigma_{ij} - \rho\frac{Dv_j}{Dt}\phi_k + X_j\phi_k\right)d\Omega + \int_{\partial\Omega^1}\overline{f}_j\phi_k ds\right]\beta_{jk} = 0. \tag{5.19}$$

At interior points and points on $\partial\Omega_t$, we can choose $\omega_1 = \phi_k$ and $\omega_2 = 0$ or $\omega_2 = \phi_k$ and $\omega_1 = 0$ for all k, namely

$$\beta_{mn} = \begin{cases} 1 & \text{if } n = k \text{ and } m = j, \\ 0 & \text{otherwise.} \end{cases} \tag{5.20}$$

Thus we have for $k = 1,\ldots, N - N_b$ and $j = 1,2$,

$$\int_\Omega \left(\phi_{k,i}\sigma_{ij} + \rho \frac{Dv_j}{Dt}\phi_k \right) d\Omega = \int_\Omega X_j \phi_k d\Omega + \int_{\partial\Omega^1} \overline{f}_j \phi_k ds, \tag{5.21}$$

where N_b denotes the number of nodes on $\partial\Omega_a$ and $\partial\Omega_f$.

At points on $\partial\Omega_f$, we need to choose ω_j properly such that it is in the function space $H^1(\Omega)$. Let $\boldsymbol{n} = (n_1, n_2)$ be the outward unit normal at a point on $\partial\Omega_f$, then to satisfy the condition that $\omega_i n_i = 0$, ω_j must be chosen as follows:

$$\omega_1 = n_2 f_k, \omega_2 = -n_1 f_k.$$

In other words, the β_{mn} in (5.19) must be chosen such that

$$\beta_{1n} = \begin{cases} n_2 & \text{if } n = k, \\ 0 & \text{if } n \neq k, \end{cases}$$

$$\beta_{2n} = \begin{cases} -n_1 & \text{if } n = k, \\ 0 & \text{if } n \neq k. \end{cases} \tag{5.22}$$

Substituting (5.22) into (5.19) yields

$$\int_\Omega \left(\phi_{k,i}\sigma_{ij} + \rho\phi_k \frac{Dv_j}{Dt} - X_j\phi_k \right) d\Omega = \int_{\partial\Omega^1} \overline{f}_j \phi_k ds, \quad k = N - N_b + 1,\ldots, N. \tag{5.23}$$

The next step is to approximate v by v^h. Substituting (5.18) into (5.21) yields

$$\sum_{l=1}^{N} \left\{ \left[\int_\Omega \rho\phi_k\phi_l d\Omega \right] \frac{\partial a_j^l}{\partial t} + \left[\int_\Omega \rho v_i \frac{\partial \phi_l}{\partial x_i} \phi_k d\Omega \right] a_j^l \right\}$$

$$+ \int_\Omega \phi_{k,i}\sigma_{ij} d\Omega - \int_\Omega X_j\phi_k d\Omega - \int_{\partial\Omega^1} \overline{f}_j \phi_k ds = 0 \tag{5.24}$$

$$k = 1,\ldots, N - N_b,$$

which gives

$$\sum_{l=1}^{N}\left\{\begin{bmatrix} M_{kl} & 0 \\ 0 & M_{kl} \end{bmatrix}\begin{bmatrix} \dfrac{da_1^l}{dt} \\ \dfrac{da_2^l}{dt} \end{bmatrix}+\begin{bmatrix} M_{ckl} & 0 \\ 0 & M_{ckl} \end{bmatrix}\begin{bmatrix} a_1^l \\ a_2^l \end{bmatrix}+\begin{bmatrix} r_{1k}-p_{1k} \\ r_{2k}-p_{2k} \end{bmatrix}\right\}=0\,, \qquad (5.25)$$

where

$$M_{kl}=\int_{\Omega}\rho\phi_k\phi_l d\Omega\,,$$

$$M_{ckl}=\int_{\Omega}\rho v_i\phi_{l,i}\phi_k d\Omega\,,$$

$$r_{jk}=\int_{\Omega}\phi_{k,i}\sigma_{ij}d\Omega\,,$$

$$p_{jk}=\int_{\Omega}X_j\phi_k d\Omega+\int_{\partial\Omega^l}\overline{f}_j\phi_k ds\,.$$

Similarly, by substituting (5.18) into (5.23), we have

$$\sum_{l=1}^{N}\left\{\begin{bmatrix} M_{kl}n_1 & M_{kl}n_2 \end{bmatrix}\begin{bmatrix} \dfrac{da_1^l}{dt} \\ \dfrac{da_2^l}{dt} \end{bmatrix}+\begin{bmatrix} M_{ckl}n_1 & M_{ckl}n_2 \end{bmatrix}\begin{bmatrix} a_1^l \\ a_2^l \end{bmatrix}-\begin{bmatrix} (r_{1k}+p_{1k})n_1 & (r_{2k}+p_{2k})n_2 \end{bmatrix}\right\}$$

$$=0. \qquad (5.26)$$

Equations (5.25) and (5.26) can be written in the general form

$$\boldsymbol{M}\frac{d\boldsymbol{a}}{dt}+\boldsymbol{M}_c\boldsymbol{a}+\boldsymbol{r}=\boldsymbol{p}\,. \qquad (5.27)$$

For the actual calculations to be carried out, the next step of the finite element approximation involves the discretisation of the integral equation (5.25). The domain of the problem, Ω, is partitioned into a finite number of simple shaped regions Ω_e called elements . Adjacent elements touch without overlapping, and there are no gaps between the elements. The boundary $\partial\Omega$ of the domain Ω is divided into segments called boundary elements denoted by $\partial\Omega_b$. These elements

are assumed to be fixed in space. The velocity field v_i, strain rate d_{rs}, and weighting functions ω_i are interpolated within each element by functions of compatible order in terms of values to be determined (referred to as degrees of freedom) at a set of nodal points. Denote $\boldsymbol{a}^{(e)}$ and $\boldsymbol{\omega}^{(e)}$ as vectors of element nodal point values of v_j and ω_j respectively; $\boldsymbol{\phi}^{(e)}(\boldsymbol{x}, y)$ as the interpolation functions, and $\boldsymbol{B}^{(e)}(x, y)$ the partial derivative of $\boldsymbol{\phi}^{(e)}$. Then we have,

$$\omega_j^{(e)} = \sum_{k=1}^{n} \beta_{jk} \phi_k^{(e)}(x, y), \tag{5.28}$$

$$v_j^{(e)} = \sum_{k=1}^{n} \phi_k^{(e)}(x, y) a_j^k(t), \tag{5.29}$$

where n denotes the number of nodes in the element, and within each element the velocity field, strain rate and the weight function have the following vector representations

$$\boldsymbol{v} = \boldsymbol{\phi}^{(e)} \boldsymbol{a}^{(e)}(t),\ \boldsymbol{d} = \boldsymbol{B}^{(e)}(x, y) \boldsymbol{a}^{(e)}(t),\ \boldsymbol{\omega} = \boldsymbol{\phi}^{(e)} \boldsymbol{\omega}^{(e)}. \tag{5.30}$$

Now for each element, we have the following matrices

$$\boldsymbol{M}^{(e)} = \int_{\Omega_e} \boldsymbol{\phi}^{(\varepsilon)^T} \boldsymbol{\phi}^{(\varepsilon)} \rho d\Omega_e \ , \tag{5.31}$$

$$M_{kl}^{(e)} = \int_{\Omega_e} \rho \phi_k^{(e)} \phi_l^{(e)} d\Omega_e ,$$

$$\boldsymbol{M}_c^{(e)} = \int_{\Omega_e} \boldsymbol{\phi}^{(\varepsilon)^T} \nabla v \boldsymbol{\phi}^{(\varepsilon)} \rho d\Omega_e , \tag{5.32}$$

$$\left(M_c^{(e)}\right)_{kl} = \int_{\Omega_e} \rho v_j^{(e)} \phi_{l,i}^{(e)} \phi_k^{(e)} d\Omega_e ,$$

$$\boldsymbol{r}^{(e)} = \int_{\Omega_e} \boldsymbol{B}^T \sigma d\Omega , \tag{5.33}$$

$$r_{jk}^{(e)} = \int_{\Omega_e} \phi_{k,i}^{(e)} \sigma_{ij} d\Omega_e ,$$

$$\boldsymbol{p}^{(e)} = \int_{\Omega_e} X \phi^{(e)} d\Omega_e + \int_{\partial\Omega_e^1} \overline{f} \phi^{(e)} ds , \tag{5.34}$$

$$p_{jk}^{(e)} = \int_{\Omega_e} X_j \phi_k^{(e)} d\Omega_e + \int_{\partial\Omega_e^1} \overline{f}_j \phi_k^{(e)} ds .$$

By using a standard finite element assembling procedure, Eqs. (5.31)-(5.34) can be expressed in the matrix form of equations (5.27), where $\boldsymbol{M}$ and $\boldsymbol{M}_c$ are the assembled mass and convective mass matrices respectively; $\boldsymbol{r}$ and $\boldsymbol{p}$ are the assembled internal and external load vectors respectively. The assembled matrices can be expressed as

$$\boldsymbol{M}_{ij} = \sum_{e_{ij}} \boldsymbol{M}_{ij}^{(e)} , \quad \boldsymbol{M}_{cij} = \sum_{e_{ij}} \boldsymbol{M}_{cij}^{(e)} , \quad \boldsymbol{r}_{ij} = \sum_{e_{ij}} \boldsymbol{r}_{ij}^{(e)} , \quad \boldsymbol{p}_{ij} = \sum_{e_{ij}} \boldsymbol{p}_{ij}^{(e)} .$$

Therefore, Eq. (5.27) represents a system of $2N$ nonlinear first order ordinary differential equations in terms of $2N$ nodal unknown values $\boldsymbol{a}$.

Although velocities $\boldsymbol{a}$ are discrete functions of space, they are still continuous functions of time. Therefore Eq. (5.27) is discretised in time using a finite difference scheme to obtain a sequence of simultaneous algebraic equations. We approximate the time derivative in Eq. (5.27) by the following differentiation scheme

$$\left(\frac{\partial \boldsymbol{a}}{\partial t}\right)_{n+1} = \frac{\boldsymbol{a}^{n+1} - \boldsymbol{a}^{n}}{\Delta t} ,$$

which is known as the backward difference equation. It is unconditionally stable which means that stability (but not accuracy) is guaranteed as Δt becomes indefinitely small. Therefore, Eq. (5.27) can be rewritten at the t^{n+1} time step as

$$\boldsymbol{M}^{n+1}\frac{\boldsymbol{a}^{n+1}-\boldsymbol{a}^{n}}{\Delta t}+\boldsymbol{M}_{c}^{n+1}\boldsymbol{a}^{n+1}+\boldsymbol{r}^{n+1}=\boldsymbol{p}^{n+1}, \tag{5.35}$$

where

$$r^{n+1}=\int_{\Omega}\phi_{k,i}\sigma_{ij}^{n+1}d\Omega\,.$$

As from (5.10) and (5.2),

$$\sigma_{ij}^{n+1}=\sigma_{ij}^{n}+\left(H_{ijrs}d_{rs}^{n+1}\Delta t+G_{ijrs}\left(d_{rs}^{n+1}-d_{rs}^{n}\right)+\tau_{ij}^{n+1}\Delta t\right), \tag{5.36}$$

where

$$\tau_{ij}=-\left(\sigma_{ik}w_{kj}-w_{ik}\sigma_{kj}+\frac{\partial\sigma_{ij}}{\partial x_{k}}v_{k}\right)+G\left(d_{ik}w_{kj}-w_{ik}d_{kj}+\frac{\partial d_{ij}}{\partial x_{k}}v_{k}\right),$$

we have

$$r_{k}^{n+1}=r_{k}^{n}+\sum_{l}\begin{bmatrix}K_{kl}^{11} & K_{kl}^{12}\\ K_{kl}^{21} & K_{kl}^{12}\end{bmatrix}\begin{bmatrix}a_{1}^{l}\\ a_{2}^{l}\end{bmatrix}\Delta t+\sum_{l}\begin{bmatrix}G_{kl}^{11} & G_{kl}^{12}\\ G_{kl}^{21} & G_{kl}^{12}\end{bmatrix}\begin{bmatrix}\Delta a_{1}^{l}\\ \Delta a_{2}^{l}\end{bmatrix}$$

$$=r_{k}^{n}+K^{n+1}a^{n+1}\Delta t+C\Delta a^{n+1}+r_{n}^{n+1}\Delta t\ , \tag{5.37}$$

where

$$K_{kl}^{j1}=\int_{\Omega}\begin{bmatrix}\phi_{k,1} & \phi_{k,2}\end{bmatrix}\begin{bmatrix}H_{1j11} & \frac{1}{2}\left(H_{1j12}+H_{1j21}\right)\\ H_{2j11} & \frac{1}{2}\left(H_{2j12}+H_{2j21}\right)\end{bmatrix}\begin{bmatrix}\phi_{l,1}\\ \phi_{l,2}\end{bmatrix}d\Omega\,,$$

$$K_{kl}^{j2}=\int_{\Omega}\begin{bmatrix}\phi_{k,1} & \phi_{k,2}\end{bmatrix}\begin{bmatrix}\frac{1}{2}\left(H_{1j21}+H_{1j12}\right) & H_{1j22}\\ \frac{1}{2}\left(H_{2j21}+H_{2j12}\right) & H_{2j22}\end{bmatrix}\begin{bmatrix}\phi_{l,1}\\ \phi_{l,2}\end{bmatrix}d\Omega\,,$$

$$\left(r_{n}^{n+1}\right)_{k}=\begin{bmatrix}\left(r_{n}^{n+1}\right)_{k1}\\ \left(r_{n}^{n+1}\right)_{k2}\end{bmatrix},\quad\left(r_{n}^{n+1}\right)_{kj}=\int_{\Omega}\phi_{k,i}\tau_{ij}^{n+1}d\Omega\,.$$

The formula for G_{kl}^{ji} is similar to that for K_{kl}^{ji} and will not be repeated here.

5.5 ELEMENT CHARACTERISTICS - COMPUTATIONAL ASPECTS

The computation domain of the problem is discretised into a finite number of isoparametric quadrilateral elements, as outlined in Zienkiwicz and Taylor (1994). These are the most frequently used and reliable elements available. In formulating isoparametric elements, a local coordinate system is used (system $\xi\eta$ in Fig. 5.3a). The local coordinates ξ and η are dimensionless and range from -1 to +1 for convenience in later applying the Gauss-Legendre quadrature formulas (which integrate from -1 to +1). Although the element is distorted in the global Cartesian system, it is perfectly square with sides parallel to the axes when referred to the local coordinate system.

For an isoparametric mapping we have

$$x = \sum_{i=1}^{4} \phi_i^{(e)}(\xi,\eta) x_i \tag{5.38}$$

$$y = \sum_{i=1}^{4} \phi_i^{(e)}(\xi,\eta) y_i \tag{5.39}$$

which provides continuity between adjacent elements, that is there are no gaps or overlapping because of the C^0- continuity of shape functions ϕ_i.

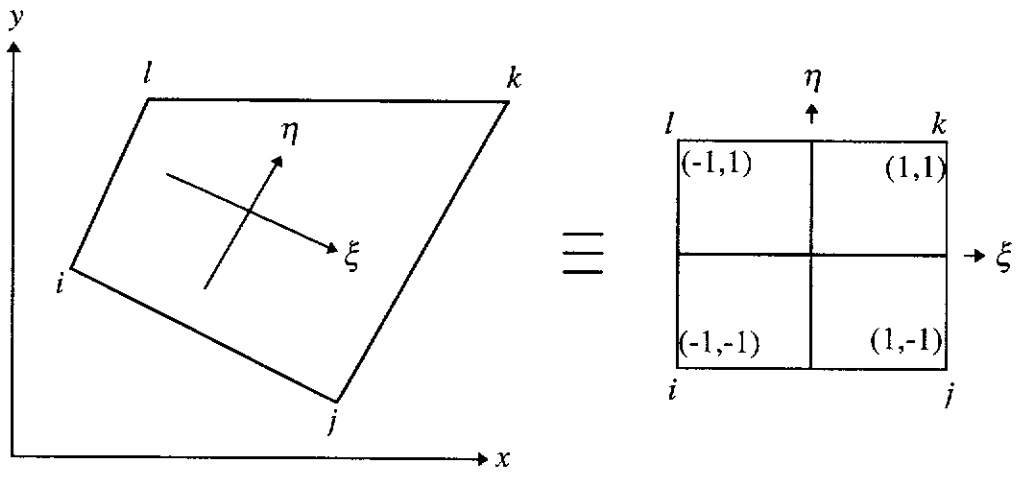

(a) (b)

Fig. 5.3 Mapping of a four node element

Consider a quadrilateral element with nodes i, j, k, and l, as shown in Fig. 5.3. The global coordinates and local coordinates of node i, for example, are (x_i,y_i) and (ξ_i,η_i) respectively. The local coordinate interpolation functions used for the element are

$$\phi_1 = \frac{1}{4}(1-\xi)(1-\eta),\ \phi_2 = \frac{1}{4}(1+\xi)(1-\eta),$$

$$\phi_3 = \frac{1}{4}(1+\xi)(1+\eta),\ \phi_4 = \frac{1}{4}(1-\xi)(1+\eta).$$

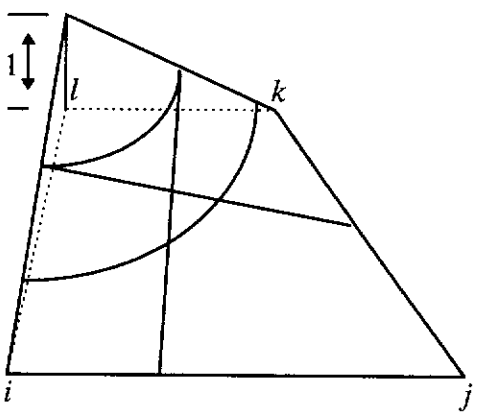

Fig. 5.4 Variation of shape function ϕ_l within an element

Figure 5.4 shows the variation of shape function ϕ_l over a typical element. It can be seen that the shape function is linear along each side which ensures C^0-continuity between elements. Within the element, ϕ_i may vary quadratically. Also the interpolation property that it is unity at the corner node and zero at the other nodes is satisfied.

In the following sub-sections the variation of velocity (or displacement), strain and stress within an element is described using the above shape functions.

5.5.1 Velocity

The velocities in the x and y directions are analysed independently, and hence each node has two degrees of freedom. Therefore, the nodal velocity $\boldsymbol{a}_i$, as shown in Fig. 5.5, is given by

$$\boldsymbol{a}_i = \begin{pmatrix} a_{ix} \\ a_{iy} \end{pmatrix}. \tag{5.40}$$

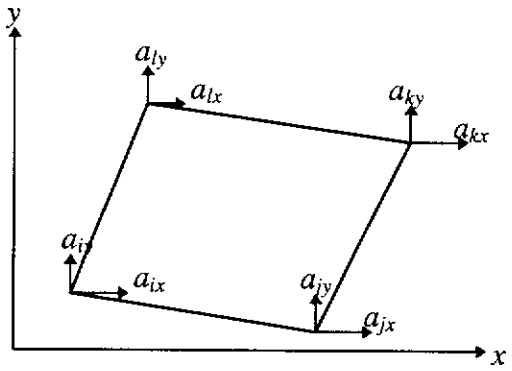

Fig. 5.5 Degrees of freedom required to define a two-dimensional element

Since the element has a total of eight degrees of freedom, the element velocity vector $\boldsymbol{a}_e$ has eight components and is given by

$$\boldsymbol{a}_e = \begin{pmatrix} \boldsymbol{a}_i \\ \boldsymbol{a}_j \\ \boldsymbol{a}_k \\ \boldsymbol{a}_l \end{pmatrix} = \begin{pmatrix} a_{ix} \\ a_{iy} \\ a_{jx} \\ a_{jy} \\ a_{kx} \\ a_{ky} \\ a_{lx} \\ a_{ly} \end{pmatrix}. \tag{5.41}$$

The element requires two interpolation functions, one for each direction. In other words,

$$v_x = \phi_i a_{ix} + \phi_j a_{jx} + \phi_k a_{kx} + \phi_l a_{lx},$$
$$v_y = \phi_i a_{iy} + \phi_j a_{jy} + \phi_k a_{ky} + \phi_l a_{ly}. \tag{5.42}$$

Equations (5.42) can be written in terms of the shape function matrix as follows

$$\boldsymbol{v} = \begin{pmatrix} v_x \\ v_y \end{pmatrix} = \boldsymbol{\phi}^{(e)} \boldsymbol{a}_e = \begin{bmatrix} \phi_i & 0 & \phi_j & 0 & \phi_k & 0 & \phi_l & 0 \\ 0 & \phi_i & 0 & \phi_j & 0 & \phi_k & 0 & \phi_l \end{bmatrix} \boldsymbol{a}_e. \tag{5.43}$$

The velocity gradient in Eq. (5.32) also has to be evaluated. It is given by

$$\nabla \boldsymbol{v} = \begin{bmatrix} \dfrac{\partial v_x}{\partial x} & \dfrac{\partial v_x}{\partial y} \\ \dfrac{\partial v_y}{\partial x} & \dfrac{\partial v_y}{\partial y} \end{bmatrix}. \tag{5.44}$$

From Eq. (5.43), the components of Eq. (5.44) can be evaluated by

$$\begin{pmatrix} \dfrac{\partial v_x}{\partial x} \\ \dfrac{\partial v_y}{\partial x} \end{pmatrix} = \frac{\partial \boldsymbol{\phi}}{\partial x} \boldsymbol{a}_e = \begin{bmatrix} \dfrac{\partial \phi_i}{\partial x} & 0 & \dfrac{\partial \phi_j}{\partial x} & 0 & \dfrac{\partial \phi_k}{\partial x} & 0 & \dfrac{\partial \phi_l}{\partial x} & 0 \\ 0 & \dfrac{\partial \phi_i}{\partial x} & 0 & \dfrac{\partial \phi_j}{\partial x} & 0 & \dfrac{\partial \phi_k}{\partial x} & 0 & \dfrac{\partial \phi_l}{\partial x} \end{bmatrix} \boldsymbol{a}_e,$$

$$\begin{pmatrix} \dfrac{\partial v_x}{\partial y} \\ \dfrac{\partial v_y}{\partial y} \end{pmatrix} = \frac{\partial \boldsymbol{\phi}}{\partial y} \boldsymbol{a}_e = \begin{bmatrix} \dfrac{\partial \phi_i}{\partial y} & 0 & \dfrac{\partial \phi_j}{\partial y} & 0 & \dfrac{\partial \phi_k}{\partial y} & 0 & \dfrac{\partial \phi_l}{\partial y} & 0 \\ 0 & \dfrac{\partial \phi_i}{\partial y} & 0 & \dfrac{\partial \phi_j}{\partial y} & 0 & \dfrac{\partial \phi_k}{\partial y} & 0 & \dfrac{\partial \phi_l}{\partial y} \end{bmatrix} \boldsymbol{a}_e. \tag{5.45}$$

5.5.2 Strain rate

The strain rate for plane strain conditions is determined by three components at each point, that is

$$\boldsymbol{d} = \begin{pmatrix} d_x \\ d_y \\ 2d_{xy} \end{pmatrix} = \begin{pmatrix} \dfrac{\partial v_x}{\partial x} \\ \dfrac{\partial v_y}{\partial y} \\ \dfrac{\partial v_x}{\partial y} + \dfrac{\partial v_y}{\partial x} \end{pmatrix}. \tag{5.46}$$

From Eq. (5.45), the strain rate can be expressed in the following compact form

$$\boldsymbol{d} = \boldsymbol{B}\boldsymbol{a}_e,$$

where

$$\boldsymbol{B} = \begin{bmatrix} \dfrac{\partial \phi_i}{\partial x} & 0 & \dfrac{\partial \phi_j}{\partial x} & 0 & \dfrac{\partial \phi_k}{\partial x} & 0 & \dfrac{\partial \phi_l}{\partial x} & 0 \\ 0 & \dfrac{\partial \phi_i}{\partial y} & 0 & \dfrac{\partial \phi_j}{\partial y} & 0 & \dfrac{\partial \phi_k}{\partial y} & 0 & \dfrac{\partial \phi_l}{\partial y} \\ \dfrac{\partial \phi_i}{\partial y} & \dfrac{\partial \phi_i}{\partial x} & \dfrac{\partial \phi_j}{\partial y} & \dfrac{\partial \phi_j}{\partial x} & \dfrac{\partial \phi_k}{\partial y} & \dfrac{\partial \phi_k}{\partial x} & \dfrac{\partial \phi_l}{\partial y} & \dfrac{\partial \phi_l}{\partial x} \end{bmatrix}.$$

5.5.3 Rotation rate

Under plane strain conditions, the rotation rate tensor has two non-zero components, namely w_{xy} and $w_{yx} = -w_{xy}$ where

$$w_{xy} = \frac{1}{2}\left(\frac{\partial v_x}{\partial y} - \frac{\partial v_y}{\partial x} \right).$$

In matrix form

$$\boldsymbol{w} = \begin{bmatrix} 0 & w_{xy} & 0 \\ -w_{xy} & 0 & 0 \\ 0 & 0 & 0 \end{bmatrix},$$

and from Eq. (5.45)

$$w_{xy} = \frac{1}{2}\left(\frac{\partial \phi_i}{\partial y} \quad -\frac{\partial \phi_i}{\partial x} \quad \frac{\partial \phi_j}{\partial y} \quad -\frac{\partial \phi_j}{\partial x} \quad \frac{\partial \phi_k}{\partial y} \quad -\frac{\partial \phi_k}{\partial x} \quad \frac{\partial \phi_l}{\partial y} \quad -\frac{\partial \phi_l}{\partial x} \right) \boldsymbol{a}_e.$$

5.5.4 Stress gradient

The gradient of each component of the stress tensor is given by

$$\nabla \sigma_{ij} = \left(\frac{\partial \sigma_{ij}}{\partial x} \quad \frac{\partial \sigma_{ij}}{\partial y} \right),$$

where

$$\begin{pmatrix} \frac{\partial \sigma_{ij}}{\partial x} \\ \frac{\partial \sigma_{ij}}{\partial y} \end{pmatrix} = \begin{bmatrix} \frac{\partial \phi_i}{\partial x} & \frac{\partial \phi_j}{\partial x} & \frac{\partial \phi_k}{\partial x} & \frac{\partial \phi_l}{\partial x} \\ \frac{\partial \phi_i}{\partial y} & \frac{\partial \phi_j}{\partial y} & \frac{\partial \phi_k}{\partial y} & \frac{\partial \phi_l}{\partial y} \end{bmatrix} \begin{pmatrix} \sigma_{iji} \\ \sigma_{ijj} \\ \sigma_{ijk} \\ \sigma_{ijl} \end{pmatrix}.$$

The vector on the right hand side denotes nodal stress values at nodes i, j, k, and l respectively.

5.5.5 Coordinate transformation

The shape functions are defined as functions of the local coordinates, therefore we must make a transformation of coordinates to allow the calculation of the $\boldsymbol{B}$ matrix and $\nabla \boldsymbol{v}$. Hence, we must express the global derivatives $\frac{\partial \phi_i}{\partial x}$ and $\frac{\partial \phi_i}{\partial y}$ in terms of the local derivatives $\frac{\partial \phi_i}{\partial \xi}$ and $\frac{\partial \phi_i}{\partial \eta}$. It is well known that these derivatives are related by the Jacobian. Recalling that from the chain rule of calculus we can write

$$\frac{\partial \phi_i}{\partial \xi} = \frac{\partial \phi_i}{\partial x}\frac{\partial x}{\partial \xi} + \frac{\partial \phi_i}{\partial y}\frac{\partial y}{\partial \xi},$$

with similar expressions for $\frac{\partial \phi_i}{\partial \eta}$. In matrix form, this relationship can be expressed as

$$\begin{pmatrix} \frac{\partial \phi_i}{\partial \xi} \\ \frac{\partial \phi_i}{\partial \eta} \end{pmatrix} = \begin{bmatrix} \frac{\partial x}{\partial \xi} & \frac{\partial y}{\partial \xi} \\ \frac{\partial x}{\partial \eta} & \frac{\partial y}{\partial \eta} \end{bmatrix} \begin{pmatrix} \frac{\partial \phi_i}{\partial x} \\ \frac{\partial \phi_i}{\partial y} \end{pmatrix} = \boldsymbol{J} \begin{pmatrix} \frac{\partial \phi_i}{\partial x} \\ \frac{\partial \phi_i}{\partial y} \end{pmatrix}.$$

This implies that the global derivatives are given by

$$\begin{pmatrix} \frac{\partial \phi_i}{\partial x} \\ \frac{\partial \phi_i}{\partial y} \end{pmatrix} = \boldsymbol{J}^{-1} \begin{pmatrix} \frac{\partial \phi_i}{\partial \xi} \\ \frac{\partial \phi_i}{\partial \eta} \end{pmatrix},$$

where

$$\begin{pmatrix} \frac{\partial \phi_i}{\partial \xi} \\ \frac{\partial \phi_i}{\partial \eta} \end{pmatrix} = \frac{1}{4} \begin{pmatrix} \xi_i(1+\eta\eta_i) \\ \eta_i(1+\xi\xi_i) \end{pmatrix},$$

and $\boldsymbol{J}$ is the Jacobian matrix. It is a function of ξ and η and an explicit inverse might not exist. Therefore $\boldsymbol{J}$ and $\boldsymbol{J}^{-1}$ are evaluated numerically as follows. Using the definition for x and y for an isoparametric element (Eqs. 5.38 and 5.39), we have

$$\boldsymbol{J} = \begin{bmatrix} J_{11} & J_{12} \\ J_{21} & J_{22} \end{bmatrix} = \begin{bmatrix} \sum_{i=1}^{4} \frac{\partial \phi_i}{\partial \xi} x_i & \sum_{i=1}^{4} \frac{\partial \phi_i}{\partial \xi} y_i \\ \sum_{i=1}^{4} \frac{\partial \phi_i}{\partial \eta} x_i & \sum_{i=1}^{4} \frac{\partial \phi_i}{\partial \eta} y_i \end{bmatrix}, \tag{5.47}$$

and

$$\boldsymbol{J}^{-1} = \frac{1}{J} \begin{bmatrix} J_{22} & -J_{12} \\ -J_{21} & J_{11} \end{bmatrix}, \tag{5.48}$$

where J is the determinant of the Jacobian matrix, namely

$$J = |\boldsymbol{J}| = (J_{11}J_{22} - J_{21}J_{12}).$$

By using Eq. (5.47) and Eq. (5.48), we can define $\boldsymbol{J}$ and $\boldsymbol{J}^{-1}$ at any integration point (ξ, η) inside a typical element.

5.5.6 Changing the variable of integration

The calculation of the element equations will require a change of integration variable. The relationship between the global coordinates (x,y) and the local coordinates (ξ, η) for a given element can be stated as follows

$$\int_{\Omega_e} f(x,y)dxdy = \int_{-1}^{1}\int_{-1}^{1} g(\xi,\eta)|J|d\xi d\eta \tag{5.49}$$

where $g(\xi,\eta)$ is the function $f(x,y)$ written in terms of the local coordinates ξ and η. As usual, this change of variable holds provided the determinant of the Jacobian J is greater than zero.

5.5.7 Numerical integration

Although the limits of integration in Eq. (5.49) are simple, the Jacobian is a function of coordinates (ξ,η) and such integrations cannot be performed exactly. Therefore numerical integration has to be used to evaluate the integrals. A nine-point Gaussian quadrature formula is used, so integrals of the form of Eq. (5.49) can be numerically integrated as

$$\sum_{i=1}^{3}\sum_{j=1}^{3} g(\xi_i,\eta_j)Jw_iw_j \tag{5.50}$$

Table 5.1 Sampling points and weights for Gauss quadrature

ξ_i and η_j	w_i and w_j
$\pm$0.77459 66692 41483	0.55555 55555 55555
0.0	0.88888 88888 88888

The values of the weight coefficients w_i and w_j and the values of sampling points ξ_i and η_j are given in Table 5.1. The locations of the integration points in a nine-point Guassian quadrature integration scheme are shown in Fig. 5.6.

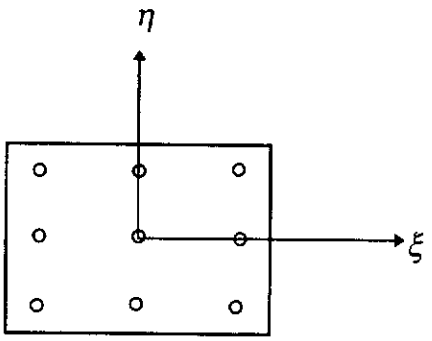

Fig. 5.6 Location of Gaussian integration points

5.5.8 Evaluation of element matrices

The matrices in Eqs. (5.31)-(5.34) can now be evaluated numerically using the above transformations in the following way.

Mass matrix:

$$\boldsymbol{M}^{(e)} = \sum_{i=1}^{3}\sum_{j=1}^{3} \boldsymbol{\phi}^{(e)T}(\xi_i,\eta_j)\boldsymbol{\phi}^{(e)}(\xi_i,\eta_j)\rho|\boldsymbol{J}|w_i w_j, \tag{5.51}$$

Convective mass matrix:

$$\boldsymbol{M}_c^{(e)} = \sum_{i=1}^{3}\sum_{j=1}^{3} \boldsymbol{\phi}^{(e)T}(\xi_i,\eta_j)\nabla v(\xi_i,\eta_j)\boldsymbol{\phi}^{(e)}(\xi_i,\eta_j)\rho|\boldsymbol{J}|w_i w_j, \tag{5.52}$$

Stiffness matrix:

$$\boldsymbol{K}^{(e)} = \sum_{i=1}^{3}\sum_{j=1}^{3} \boldsymbol{B}^{T}(\xi_i,\eta_j)\boldsymbol{H}\boldsymbol{B}(\xi_i,\eta_j)|\boldsymbol{J}|w_i w_j, \tag{5.53}$$

Load vectors:

$$\boldsymbol{r}^{(e)} = \sum_{i=1}^{3}\sum_{j=1}^{3} \boldsymbol{B}^{T}(\xi_i,\eta_j)\sigma(\xi_i,\eta_j)|\boldsymbol{J}|w_i w_j, \tag{5.54}$$

$$\boldsymbol{p}^{(e)} = \sum_{i=1}^{3}\sum_{j=1}^{3} \boldsymbol{\phi}^{(e)T}(\xi_i,\eta_j)\boldsymbol{f}\,|\boldsymbol{J}|w_i w_j, \tag{5.55}$$

$$\boldsymbol{r}_n^{(e)} = \sum_{i=1}^{3}\sum_{j=1}^{3} \boldsymbol{B}^{T}(\xi_i,\eta_j)\pi(\xi_i,\eta_j)|\boldsymbol{J}|w_i w_j. \tag{5.56}$$

5.5.9 Evaluation of the boundary integral

To evaluate the boundary integral in Eq. (5.34), we use the simple one-dimensional element with two nodes, j and k; it lies along the edge $\partial\Omega_e$ as shown in Fig. 5.7. Assuming that the prescribed tractions vary linearly along the edge jk of length L, then the shape functions are given by

$$\phi_j = 1 - \frac{s}{L}\ ,\ \ \phi_k = \frac{s}{L},$$

where the coordinate s is measured along the edge jk. Therefore, the boundary integral can be written as

$$\int_{\partial\Omega_e} \phi^{(e)T} \overline{f} d\Omega_e = \boldsymbol{F} = \int_0^L \phi^{(e)T} \overline{f} ds\,, \tag{5.57}$$

where

$$\boldsymbol{F} = \begin{pmatrix} F_{xj} & F_{yj} & F_{xk} & F_{yk} \end{pmatrix}^T,$$

$$\phi^{(e)} = \begin{bmatrix} \phi_j & 0 & \phi_k & 0 \\ 0 & \phi_j & 0 & \phi_k \end{bmatrix},$$

and

$$\overline{f} = \phi^{(e)} \overline{f}_{jk}\,, \tag{5.58}$$

with nodal values given by

$$\overline{f}_{jk} = \begin{pmatrix} f_{xj} \\ f_{yj} \\ f_{xk} \\ f_{yk} \end{pmatrix}.$$

After substitution of Eq. (5.58) into Eq. (5.57), we obtain

$$\boldsymbol{F} = \left(\int_0^L \phi^{(e)T} \phi^{(e)} ds \right) \overline{f}_{jk}\,, \tag{5.59}$$

which, upon integrating, yields

$$\begin{pmatrix} F_{xj} \\ F_{yj} \\ F_{xk} \\ F_{yk} \end{pmatrix} = \frac{L}{6}\begin{bmatrix} 2 & 0 & 1 & 0 \\ 0 & 2 & 0 & 1 \\ 1 & 0 & 2 & 0 \\ 0 & 1 & 0 & 2 \end{bmatrix}\begin{pmatrix} f_{xj} \\ f_{yj} \\ f_{xk} \\ f_{yk} \end{pmatrix}. \tag{5.60}$$

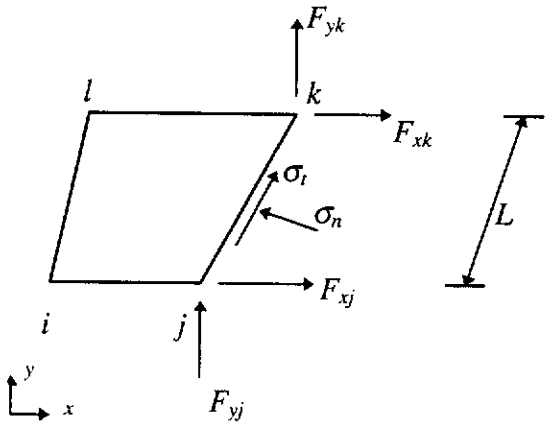

Fig. 5.7 Prescribed boundary stresses

5.6 SOLUTION PROCEDURE AND DEVELOPMENT OF A COMPUTER PROGRAM

The governing system of equations (5.27) is a nonlinear function of the nodal velocity, $\boldsymbol{a}$, as $\boldsymbol{p}^{n+1}$ and $\boldsymbol{K}^{n+1}$ depend on σ^{n+1}, $\boldsymbol{M}_c^{n+1}$ depends on $\boldsymbol{a}^{n+1}$, and $\boldsymbol{r}_n^{n+1}$ depends on σ^{n+1} and $\boldsymbol{a}^{n+1}$. This system can only be solved using an iterative numerical method. Considering that the stress σ is a nonlinear function of the velocity, $\boldsymbol{a}$, Eq. (5.27) can be rewritten as

$$\begin{aligned} \Psi\left(\boldsymbol{a}^{n+1}\right) = \boldsymbol{p}^{n+1} - \frac{1}{\Delta t}\boldsymbol{M}^{n+1}\left(\boldsymbol{a}^{n+1} - \boldsymbol{a}^{n}\right) - \boldsymbol{M}_c^{n+1}\boldsymbol{a}^{n+1} \\ - \left(\boldsymbol{r}^{n} + \Delta t\boldsymbol{K}^{n+1}\boldsymbol{a}^{n+1} + \boldsymbol{C}\left(\boldsymbol{a}^{n+1} - \boldsymbol{a}^{n}\right) + \Delta t\boldsymbol{r}_n^{n+1}\right). \end{aligned} \tag{5.61}$$

System (5.61) is a nonlinear matrix equation expressed in terms of the vector $\boldsymbol{a}^{n+1}$. The vector Ψ is known as the residual of the problem and a solution is defined as any set of nodal velocities, $\boldsymbol{a}$, for which the residual is zero. In general,

there may be more than one set of velocities that define a solution. Our aim is to find $\boldsymbol{a}^{n+1}$ such that

$$\boldsymbol{\Psi}\left(\boldsymbol{a}^{n+1}\right)=\boldsymbol{0}. \tag{5.62}$$

There are many algorithms for solving a set of nonlinear simultaneous equations. To solve the nonlinear system (5.62), we use the modified Newton-Raphson method. This method is widely used in finite-element analysis. Assuming that we know the ith approximation, ${}^{i}\boldsymbol{a}^{n+1}$, to the velocity $\boldsymbol{a}^{n+1}$, the iteration scheme for the modified Newton-Raphson algorithm is expressed as

$$\begin{aligned} \boldsymbol{A}^{i+1}\Delta\boldsymbol{a}^{n+1} &= \boldsymbol{\Psi}\left({}^{i}\boldsymbol{a}^{n+1}\right), \\ {}^{i+1}\boldsymbol{a}^{n+1} &= {}^{i}\boldsymbol{a}^{n+1}+{}^{i+1}\Delta\boldsymbol{a}^{n+1}, \end{aligned} \tag{5.63}$$

where

$$\boldsymbol{A}=-\left(\frac{\partial\boldsymbol{\Psi}}{\partial\boldsymbol{a}^{n+1}}\right)_{{}^{i}\boldsymbol{a}^{n+1}}=\frac{1}{\Delta t}{}^{i}\boldsymbol{M}^{n+1}+{}^{i}\boldsymbol{M}_{c}^{n+1}+\boldsymbol{C}+\Delta t\,{}^{i}\boldsymbol{K}^{n+1}.$$

The iteration starts with ${}^{0}\boldsymbol{a}^{n+1}=\boldsymbol{a}^{n}$. Within each iteration cycle, the matrix $\boldsymbol{A}$ is kept constant, that is

$$\boldsymbol{A}=\frac{1}{\Delta t}\boldsymbol{M}^{n}+\boldsymbol{M}_{c}^{n}+\boldsymbol{C}+\Delta t\boldsymbol{K}^{n}.$$

Next we define a convergence criterion to terminate the equilibrium iteration. At the end of each iteration cycle, the obtained solution is checked against a selected tolerance to see whether convergence has occurred. We use the Euclidean norm

$$\frac{\left\|{}^{i}\boldsymbol{a}^{n+1}-{}^{i+1}\boldsymbol{a}^{n+1}\right\|_{2}}{\left\|{}^{i}\boldsymbol{a}^{n+1}\right\|_{2}}<TOL,$$

where TOL is a user specified tolerance.

In the static case, velocities are negligible and only displacements take place. Therefore

$$\Psi\left({}^{i}\boldsymbol{a}^{n+1}\right)={}^{i}\boldsymbol{r}^{n+1}-{}^{i}\boldsymbol{p}^{n+1},$$

and

$$\boldsymbol{A}=\boldsymbol{K}^{n+1},$$

in the scheme of Eqs. (5.63).

Finally, the stresses are calculated at the centroids of the element. These are the optimum points and the stresses there are most accurate (Barlow, 1976).

The above iterative scheme is computationally expensive and therefore we exploit the sparseness of these matrices by using an efficient row-indexed sparse storage technique. For a discussion about storage schemes and equation-solving algorithms see Bathe (1982).

5.7 NUMERICAL INVESTIGATION

Over the last two decades, many numerical studies have been carried out to investigate the effect of various parameters such as silo geometry, material properties and wall friction on silo pressures (Haussler & Eibl, 1984; Schmidt & Wu, 1989). It has been well understood that wall friction has a considerable effect on the distribution and magnitude of normal silo wall pressures. However, prior work mainly focused on comparison of wall pressures for the static case only. Thus a numerical study is undertaken to investigate the influence of wall friction on the distribution of wall pressures during the dynamic process of silo discharge (from unsteady state to steady state). At $t=0$, the outlet of the silo is open and the surface tractions on the outlet are determined based on the stresses at static state. Then, the surface tractions are gradually reduced to zero to simulate the transition from the static condition to the steady-state flow condition. Figure 5.8 shows the geometry of the silo under consideration. The properties of the granular material stored in the silo are as given in Table 5.2. The coefficient of wall friction μ_w is varied from 0.1 to 0.4 while the other parameters remain unchanged. Figures 5.9 to 5.11 show the

dynamic evolution of pressure on hopper wall respectively for $\mu_w = 0.1$, 0.25 and 0.4. Variations of pressures with time at points 1 and 2, respectively, near the transition

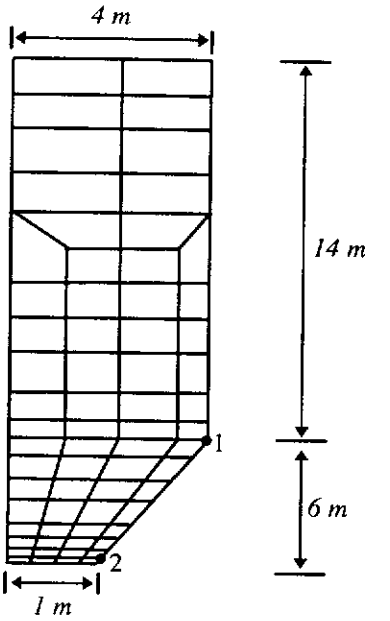

Fig. 5.8 Geometry of model silo and finite element mesh

point and the outlet for different μ_w values are also shown and compared in Figures 5.12 and 5.13. These results clearly indicate that the normal wall pressure depends on the wall friction not only under static cases but also under the steady-state flow case. Our results are generally in agreement qualitatively with results obtained by many others. Although our results also show that the hopper wall pressure near the hopper-silo transition area increases significantly, we did not predict an increase as large as predicted by others (Rombach & Eibl, 1984). This is perhaps due to the use of different models for the problem. The difference in predicted results indicates that it is important to carry out experimental investigations to identify the application domain of each theory. However, we will not proceed further as the focus of the thesis is on the mathematical and numerical aspects of granular flows. It

Table 5.2 Properties of granular material under investigation

Density	$\rho = 1800 kg/m^3$
elastic modulus	$E = 50 MPa$
Poisson's ratio	$\upsilon = 0.3$
angle of internal friction	$\phi = 30^o$
viscous constant	$\mu = 0.001 secMPa/m^2$

is also noted that wall friction also has influence on pressure distribution on the vertical wall. However, the influence is not as significant as on the hopper wall, and in addition, the variation of pressure on vertical wall with respect to time is not as significant as on hopper wall.

5.8 CONCLUDING REMARKS

The finite element method has been used by many researchers in modelling granular flows. However, existing finite element models are mainly based on the plastic flow rule theory and in addition, very few attempts have been made to implement the frictional boundary conditions within a proper mathematical framework. In the present study, we derived a set of double-shearing theory based stress-strain equations in explicit form and based on these, a general finite element method has been developed for modelling the viscous elasto-plasticity flow of granular materials obeying the double-shearing theory. The frictional boundary condition has also been implemented within a mathematical framework through the variational formulations of the boundary value problem. A numerical study has also been undertaken to study the influence of wall friction on silo wall pressures and the results indicate that wall friction has significant effects on the dynamic pressure on hopper walls.

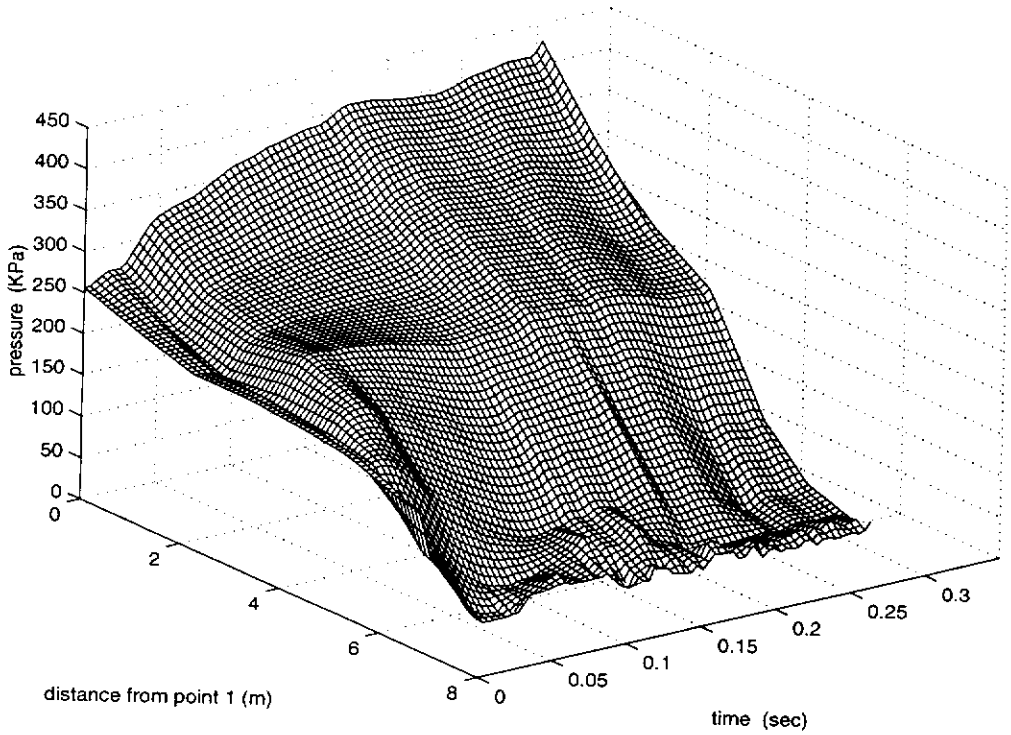

Fig. 5.9 Pressure distribution during silo discharge for μ_w=0.1

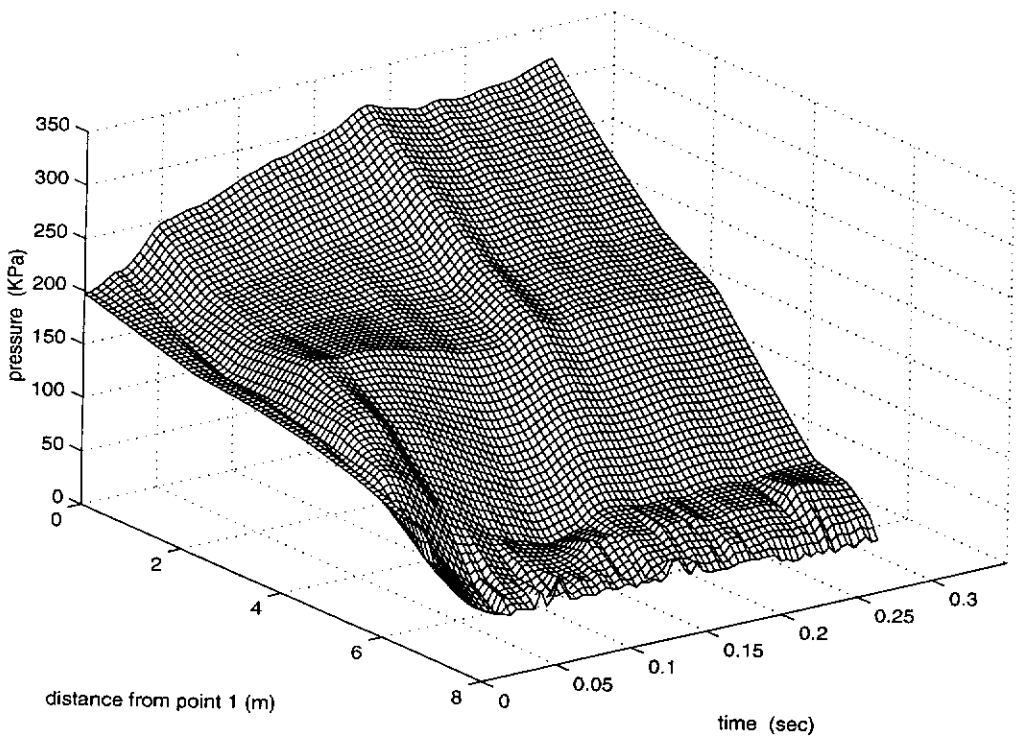

Fig. 5.10 Pressure distribution during silo discharge for μ_w=0.25

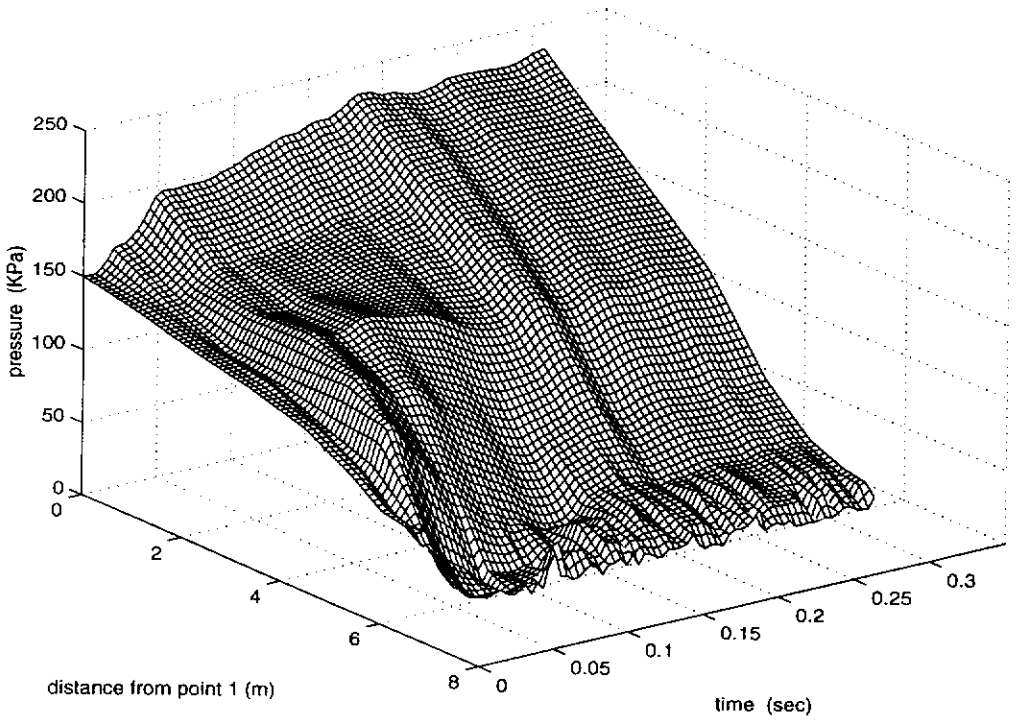

Fig. 5.11 Pressure distribution during silo discharge for μ_w=0.4

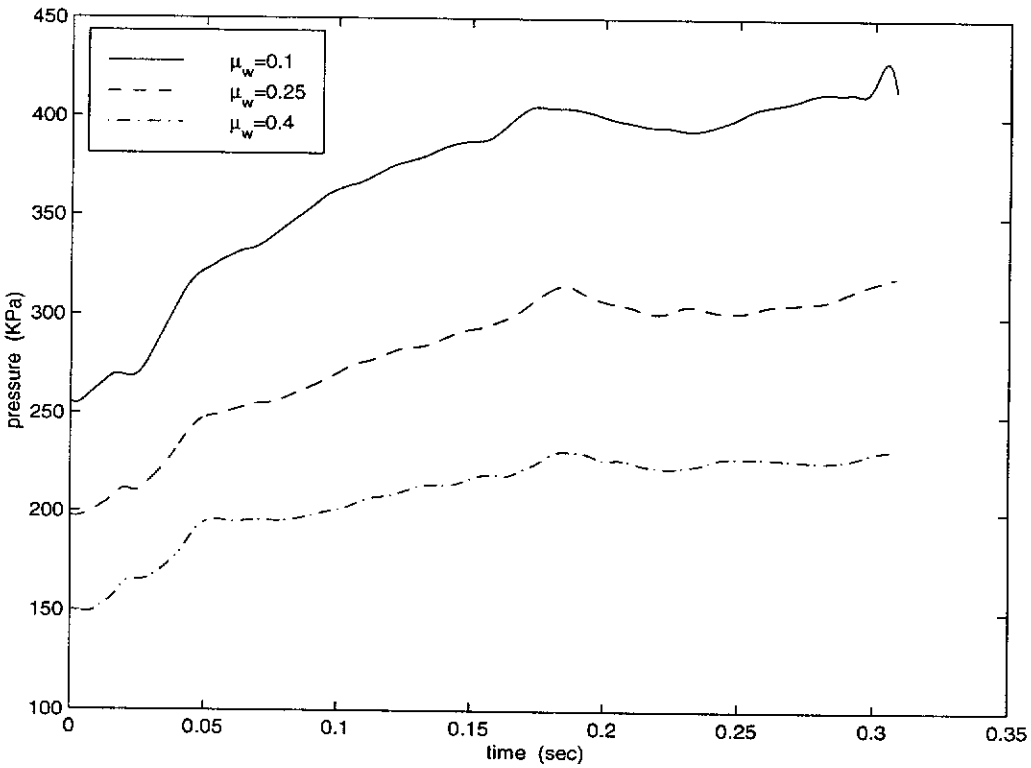

Fig. 5.12 Variation of pressure with time at the transition point of hopper wall

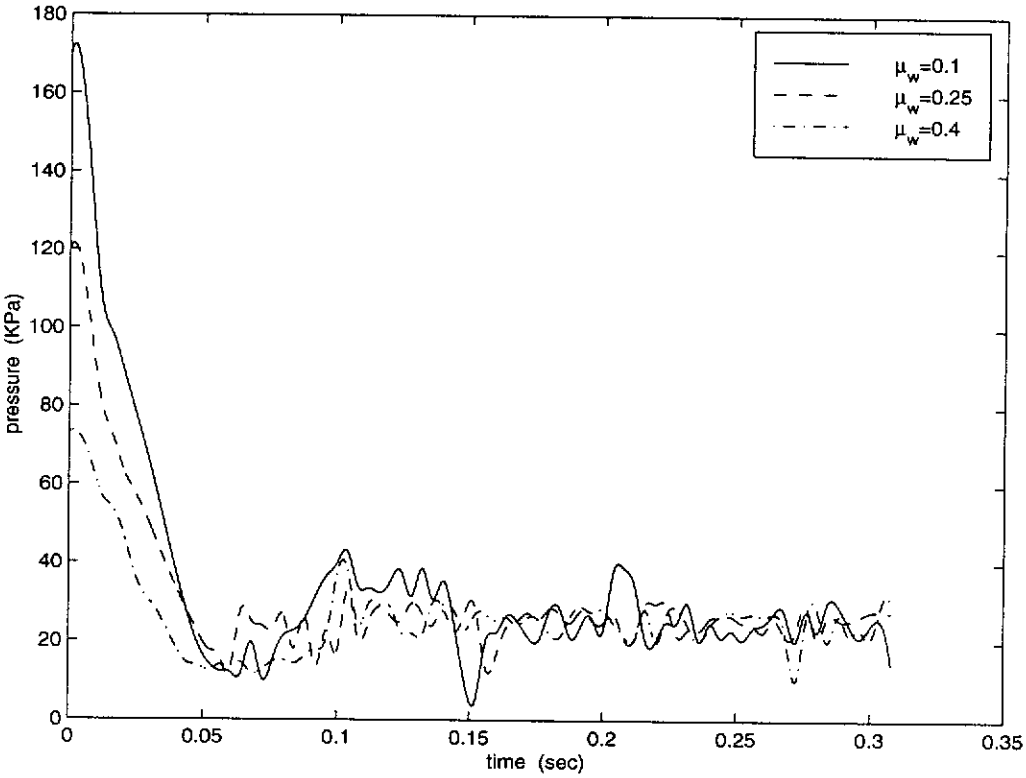

Fig. 5.13 Variation of pressure with time near the outlet on hopper wall

CHAPTER SIX

SUMMARY AND CONCLUSIONS

The project focuses on the modelling of plasticity flows of granular materials with particular emphasis on the construction of mathematical models based on the double-shearing theory and on the development of associated numerical techniques. The outcomes and conclusions gained from the research are summarised in three aspects, as follows.

(1) A sophisticated numerical technique, based on the method of characteristics, has been developed for simulating the perfect plasticity flow of granular materials obeying the so-called double-shearing theory. The underlying partial differential equations for the model have been formulated, examined and shown to be of hyperbolic type with two families of characteristics, namely the α- and β-characteristics. A robust numerical algorithm has thus been developed to determine the characteristic lines, the possible discontinuity lines and the corresponding stress and velocity fields. A numerical study has also been undertaken to demonstrate the essential features of the stress and velocity fields in the presence of a stress discontinuity, and to investigate the influence of various parameters on the distribution of hopper wall pressures. The following conclusions can be made from the numerical study.

(a) Generation of the numerical solution from the top surface of hoppers will provide more accurate results than from the outlet of the hopper. The size of the characteristic mesh is found to have significant effects on the accuracy of numerical results.

(b) The mathematical model and the associated numerical technique developed can capture the discontinuity of stresses in granular materials and the discontinuity of pressures on hopper walls. In the presence of stress discontinuities, two kinds of flow zones occur, displaying distinct flow features.

(c) In the presence of stress discontinuity, the wall friction also has considerable influence on the normal hopper wall pressure. With the increase of wall friction coefficient, the normal wall pressure decreases significantly, which is in agreement qualitatively with the case in which stress discontinuities do not occur.

(2) A finite element technique has been developed for simulating the viscous elasto-plasticity flow of granular materials. Firstly, the stress-strain constitutive equations in explicit form are constructed based on the double-shearing theory, which makes it possible to formulate the general boundary value problem within the framework of the finite element method. Consequently the governing boundary value problem is formulated as a variational boundary value problem defined in a Sobolev space, which is then posed in a N-dimensional subspace. The frictional boundary condition is implemented by choosing a proper test function on the frictional boundary. A numerical algorithm based on the finite element method is then developed. A subsequent numerical study shows that the model is robust in analysing the influence of wall friction on the distribution of wall pressure throughout the dynamic process of material discharge from silos.

(3) Two mathematical models and numerical techniques have been developed for simulating granular flows. One of the models can capture the stress discontinuity while the other cannot, which indicates that the application domain of each model is different. In fact, many researchers have suggested that different models may be required, not only for different materials but also

for the same material under different conditions, due to the complexity of granular flows. Thus, further work is recommended to examine existing models and to develop certain criteria identifying the application domain of each kind of model.

REFERENCES

Ahmadi, G. 1985, 'A turbulence model for rapid flows of granular materials. Part I: Basic theory', *Powder Technology*, vol. 44, pp. 261-268.

Ames, W. F. 1992, *Numerical Methods for Partial Differential Equations*, 3rd edn, Academic Press, Boston.

Anand, L. 1983, 'Plane deformations of ideal granular materials', *Journal of the Mechanics and Physics of Solids*, vol. 31, pp. 105-122.

Atkinson, J. H. & Bransby, P. L. 1978, *The Mechanics of Solids*, McGraw Hill, London.

Bagnold, R. A. 1954, 'Experiments on gravity-free dispersion of large solid spheres in a Newtonian fluid under shear', *Proceedings of the Royal Society of London*, Series A, vol. 225, pp. 49-63.

Balendran, B. & Nemat-Nasser, S. 1993, 'Double sliding model for cyclic deformation of granular materials, including dilatancy effects', *Journal of the Mechanics and Physics of Solids*, vol. 41, pp. 573-612.

Barlow, J. 1976, 'Optimal stress locations in finite element models', *International Journal for Numerical Methods in Engineering*, vol. 10, pp. 243-251.

Bathe, K. J. 1982, *Finite Element Procedures in Engineering Analysis*, Prentice-Hall, Englewood Cliff, NJ.

Beverloo, W. A., Leniger, H. A. & van der Velder, J. 1961, 'The flow of granular solids through orifices', *Chemical Engineering Science*, vol. 15, p. 260.

Blair-Fish, P. M. & Bransby, P. L. 1973, 'Flow patterns and wall stresses in a mass-flow bin', *Journal of Engineering for Industry*, Transactions of ASME, Series B, vol. 95, pp. 17-26.

Blinowski, A. 1978, 'On the dynamic flow of granular media', *Archives of Mechanics*, vol. 30, pp. 27-34.

Bradley, N. J. 1991, *Gravity Flows of Granular Materials*, PhD Thesis, University of Nottingham, England.

Brennen, C. & Pearce, J. C. 1978, 'Granular material flow in two-dimensional hoppers', *Journal of Applied Mechanics*, Transactions of the ASME, vol. 45, pp. 43-50.

Brey, J. J., Ruiz-Montero, M. J. & Moreno, F. 1997, 'Steady uniform shear flow in a low density granular gas', *Physical Review E*, vol. 55, p. 2846.

Butterfield, R. & Harkness, R. M. 1972, 'The kinematics of Mohr-Coulomb materials', in *Stress-Strain Behaviour of Soils*, Proceedings of the Roscoe Memorial Symposium, ed. R. H. G. Parry, G. T. Foulis, Henley-on-Thames, pp. 220-233.

Campbell, C. S. 1990, 'Rapid granular flows', *Annual Review of Fluid Mechanics*, vol. 22, pp. 57-92.

Campbell, C. S. & Brennen, C. E. 1985a, 'Computer simulation of granular shear flows', *Journal of Fluid Mechanics*, vol. 151, pp. 167-188.

Campbell, C. S. & Brennen, C. E. 1985b, 'Chute flows of granular materials: some computer simulations', *Journal of Applied Mechanics*, vol. 52, pp. 172-178.

Campbell, C. S. & Gong, A., 1986, 'The stress tensor in a two-dimensional granular shear flow', *Journal of Fluid Mechanics*, vol. 164, pp. 107-125.

Collins, I. F. 1990, 'Plane strain characteristics theory for soils and granular materials with density dependent yield criteria', *Journal of the Mechanics and Physics of Solids*, vol. 38, pp. 1-25.

Coulomb, C. A. 1773, *Coulomb's Memoir on Statics: An Essay in the History of Civil Engineering*, Cambridge University Press.

Cox, A. D., Eason, G. & Hopkins, H. G. 1961, 'Axially symmetric plastic deformations in soils', *Philosophical Transactions of the Royal Society of London*, Series A, vol. 254, pp. 1-45.

Davidson, J. F. & Nedderman, R. M. 1973, 'The hour-glass theory of hopper flow', *Transactions of the Institution of Chemical Engineers*, vol. 51, pp. 29-35.

de Josselin de Jong, G. 1959, *Statics and Kinematics of the Failable Zone of a Granular Material*, Uitgeverij Waltman, Delft.

de Josselin de Jong, G. 1971, 'The double sliding, free rotating model for granular assemblies', *Géotechnique*, vol. 21, pp. 155-163.

de Josselin de Jong, G. 1977, 'Mathematical elaboration of the double sliding, free rotating model', *Archives of Mechanics*, vol. 29, pp. 561-591.

Drescher, A. 1976, 'An experimental investigation of flow rules for granular materials using optically sensitive glass particles', *Géotechnique* , vol. 26, pp. 591-601.

Drucker, D. C., Gibson, R. E. & Henkel, D. J. 1957, 'Soil mechanics and work-hardening theories of plasticity', *Transactions of ASCE*, vol. 122, pp. 338-346.

Drucker, D.C. & Prager, W. 1952, 'Soil mechanics and plastic analysis or limit design', *Quarterly of Applied Mathematics*, vol. 10, pp. 157-165.

Farley, R. & Valentin, F.H. 1968, 'Effect of particle size upon the strength of powders', *Powder Technology*, vol 1, p. 344.

Goldstein, A. & Shapiro, M. 1995, 'Mechanics of collisional motion of granular materials, part1, general hydrodynamic equations', *Journal of Fluid Mechanics*, vol. 282, pp. 75-114.

Green, A. E. & Adkinson, J. E. 1960, *Large Elastic Deformations*, Claredon Press, Oxford.

Haff, P. K. 1983, 'Grain flow as a fluid-mechanical phenomenon', *Journal of Fluid Mechanics*, vol. 134, pp. 401-430.

Harris, D. 1985, 'A derivation of the Mehrabadi-Cowin equations', *Journal of the Mechanics and Physics of Solids*, vol. 33, pp. 51-59.

Harris, D. 1992, 'Plasticity models for soil, granular and jointed rock materials', *Journal of the Mechanics and Physics of Solids*, vol. 40, pp. 273-290.

Harris, D. 1993, 'Constitutive equations for planar deformations of rigid-plastic materials', *Journal of the Mechanics and Physics of Solids*, vol. 41, pp. 1515-1531.

Harris, D. 1995, 'A unified formulation for plasticity models of granular and other materials', *Proceedings of the Royal Society of London*, Series A, vol. 450, pp. 37-49.

Haussler, U. & Eibl, J. 1984, 'Numerical investigations on discharging silos', *Journal of Engineering Mechanics*, vol. 110, pp. 957-971.

Hill, R. 1950, *The Mathematical Theory of Plasticity*, Clarendon Press, Oxford.

Hill, J.M. & Wu, Y.H., 1992, 'Some axially symmetric flows of Mohr-Coulomb compressible granular materials', *Proceedings of the Royal Society of London*, Series A, vol. 438, pp. 67-93.

Hill, J.M. & Wu, Y.H. 1993, 'Plastic flows of granular materials of shear index n: Part I yield functions', *Journal of the Mechanics and Physics of Solids*, vol. 41, pp. 77-94.

Hopkins, M. A. & Shen, H. H. 1988, 'A monte Carlo simulation of a simple shear flow of granular materials' in *Micromechanics of Granular Materials*, eds M. Satake & J. T. Jenkins, Elsevier Science Publications, Amsterdam.

Hutter, K. & Rajagopal, K. R. 1994, 'On flows of granular materials', *Continuum Mechanics and Thermodynamics*, vol. 6, pp. 81-139.

Jackson, R. 1983, 'Some mathematical and physical aspects of continuum models for the motion of granular materials', in *The Theory of Dispersed Multiphase Flow*, ed. R. Meyer, Academic Press, New York, pp. 291-337.

Jaeger, H. M., Nagel, S. R. & Behringer, R. P. 1996, 'The physics of granular materials', *Physics Today*, vol. 49, pp. 32-38.

Jenike, A. W. 1961, 'Gravity flow of bulk solids', *Utah Engineering Experiment Station, Bulletin 108*, University of Utah, Salt Lake City, Utah.

Jenkins, J. T. & Savage, S. B. 1983, 'A theory for the rapid flow of identical, smooth, nearly elastic, spherical particles', *Journal of Fluid Mechanics*, vol. 130, pp. 187-202.

Johanson, J. R. 1964, 'Stress and velocity fields in the gravity flow of bulk solids', *Journal of Applied Mechanics*, Transactions of the ASME, Series E, vol. 31, pp. 499-505.

Johnson, P. C. & Jackson, R. 1987, 'Frictional-collisional constitutive relations for granular material, with application to plane shearing', *Journal of Fluid Mechanics*, vol. 176, pp. 67-93.

Kingston, M. R. & Spencer, A. J. M. 1970, 'General yield conditions in plane deformations of granular media', *Journal of the Mechanics and Physics of Solids*, vol. 18, pp. 233-243.

Kitamura, R. 1980, 'Analysis of deformation mechanism of particulate material based on the probability theory', Faculty of Engineering, Kagoshima University, Japan.

Lade, P. V. 1977, 'Elasto-plastic stress-strain theory for cohesionless soil with curved yield surfaces', *International Journal of Solids and Structures*, vol. 13, pp. 1019-1035.

Langston, P. A., Tüzün, U. & Heyes, D. M. 1995, 'Discrete element simulation of granular flow in 2D and 3D hoppers: dependence of discharge rate and wall stress on particle interactions', *Chemical Engineering Science*, vol. 50, pp. 967-987.

Lee, J., Cowin, S. C. & Templeton, J. S. 1974, 'An experimental study of the kinematics through hoppers', *Transactions of the Society of Rheology*, vol. 18, pp. 247-269.

Mandl, G. & Fernández Luque, R. 1970, 'Fully developed plastic shear flow of granular materials', *Géotechnique*, vol. 20, pp. 277-307.

Matsuoka, H. 1984, 'Deformation and strength of granular materials based on the compounded mobilized planes and spatial mocilized plane', in *Advances in the Mechanics and the Flow of Granular Materials*, vol. 2, ed. M. Shahinpoor, Bulf Publishing Company, U.S.A., pp. 814-836.

McLean, A. G. 1979, *Flow Rate of Simple Bulk Solids From Mass Flow Bins*, PhD Thesis, University of Wollonggong, Australia.

McLean, A. G. 1985, 'Initial stress fields in converging channels', *International Journal of Bulk Solids Handling*, vol. 5

McTigue, D. F. 1978, 'A model for stresses in shear flow of granular material', in *Proceedings of U. S. - Japan Seminar on Continnum-Mechanical and Statistical Approaches in the Mechanics of Granular Material*, eds J. T. Jenkins & S. Cowin pp. 266-271.

Mehrabadi, M. M. & Cowin, S. C. 1978, 'Initial planar deformation of dilatant granular materials', *Journal of the Mechanics and Physics of Solids*, vol. 26, pp. 269-284.

Mehrabadi, M. M. & Cowin, S. C. 1981, 'On the double-sliding free-rotating model for the deformation of granular materials', *Journal of the Mechanics and Physics of Solids*, vol. 29, pp. 269-282.

Michalowski, R. L. 1984, 'Flow of granular materials through a plane hopper', *Powder Technology*, vol. 39, pp. 29-40.

Morrison, H. L. & Richmond, O. 1976, 'Application of Spencer's ideal soil model to granular materials flow', *Journal of Applied Mechanics*, Transactions of the ASME, vol. 43, pp. 49-53.

Nedderman, R. M. 1992, *Statics and Kinematics of Granular Materials*, Cambridge University Press, Cambridge.

Ooi, J. Y. & Rotter, J. M. 1986, 'The effect of wall flexibility on pressures in squat silos', *2nd International Conference on Bulk Materials Storage, Handling and Transportation*, Wollongong, The Institution of Engineers, Australia, July.

Ooi, J. Y. & Rotter, J. M. 1987, 'Wall pressures in squat steel silos from simple finite element analysis', *Research Report R538*, School of Civil & Mining Engineering, University of Sydney, February.

Ostrowska-Maciejewska, J. & Harris, D. 1990, 'Three-dimensional constitutive equations for rigid/perfectly plastic granular materials', *Mathematical Proceedings of the Cambridge Philosophical Society*, vol. 108, pp. 153-169.

Pemberton, C. S. 1965, 'Flow of imponderable granular materials in wedge-shaped channels', *Journal of the Mechanics and Physics of Solids*, vol. 13, pp. 351-360.

Roberts, A. W. 1991, 'Bulk solids handling - Recent developments and future directions', *International Journal of Bulk Solids Handling*, vol. 11, pp.17-35.

Roco, M. C., Makhijani, V. & Ma, D. N. 1990, 'Probabilistic micromechanical model for two-dimensional slow particulate flow: dry friction', *Powder Technology*, vol. 60, pp. 223-243.

Rombach, G. & Eibl, J. 1995, 'Granular flow of materials in silos - Numerical results', *International Journal of Bulk Solids Handling*, vol. 15, pp. 65-70.

Rong, G. 1994, Discrete Element Modelling for Flow of Particulate Materials in Bins, PhD Thesis, University of Guelph, Canada.

Roscoe, K. H., Schofield, A. N. & Wroth, C. P. 1958, 'On the yielding of soils', *Géotechnique*, vol. 9, pp. 71-83.

Savage, S. B. 1965, 'The mass flow of granular materials from coupled velocity-stress fields', *British Journal of Applied Physics*, vol. 16, pp. 1885-1888.

Savage, S. B. 1988, 'Streaming motions in a bed of vibrationally fluidized dry granular material', *Journal of Fluid Mechanics*, vol. 194, pp. 457-478.

Schmidt, L.C. & Wu, Y.H. 1989, 'Prediction of dynamic wall pressures on silos', *International Journal of Bulk Solids Handling*, vol. 9, pp. 33-338.

Shen, H. H. & Ackermann, N. L. 1982, 'Constitutive equations for fluid-solid mixtures', *Journal of Engineering Mechanics Division*, ASCE, vol. 108, pp. 748-762.

Shen, H. & Hopkins, M. 1988, 'Stress in a rapid, simple shear flow of granular materials with multiple grain sizes', *Particulate Science and Technology*, vol. 6, pp. 1-15.

Smith, G. D. 1978, *Numerical Solution of Partial Differential Equations*, Clarendon Press, Oxford.

Sokolovskii, V. V. 1965, *Statics of Granular Media*, Pergamon Press, Oxford.

Spencer, A. J. M. 1964, 'A theory of the kinematics of ideal soils under plane strain conditions', *Journal of the Mechanics and Physics of Solids*, vol. 12, pp. 337-351.

Spencer, A. J. M. 1971, 'Fully developed plastic shear flow of granular materials', *Géotechnique*, vol. 21, pp. 190-192.

Spencer, A. J. M. 1982, 'Deformation of ideal granular materials', in *Mechanics of Solids*, The Rodney Hill 60th Anniversary Volume, eds H. G. Hopkins & M. J. Sewell, Pergamon Press, Oxford, pp. 607-652.

Spencer, A. J. M. 1986, 'Axially symmetric flow of granular materials', *Solid Mechanics Archives*, vol. 11, pp. 185-198.

Spencer, A. J. M. & Kingston, M. R. 1973, 'Plane mechanics and kinematics of compressible ideal granular materials', *Rheologica Acta*, vol. 12, pp. 194-199.

Stainforth, P. T., Ashley, R. C. & Morley, J. N. 1970, 'Computer analysis of powder flow characteristics', *Powder Technology*, vol. 4, pp. 250-256.

Teunissen, J. A. M. & Vermeer, P. A. 1988, 'Analysis of double shearing in frictional materials', *International Journal for Numerical and Analytical Methods in Geomechanics*, vol. 12, pp. 323-340.

Walker, D. M. 1966, 'An approximate theory for pressure and arching in hoppers', *Chemical Engineering Science*, vol. 21, pp. 975-997.

Walker, D. M. & Blanchard, M. H. 1967, 'Pressures in experimental coal hoppers', *Chemical Engineering Science*, vol. 22, pp. 1713-1745.

Walters, J. K. 1973a, 'A theoretical analysis of stresses in silos with vertical walls', *Chemical Engineering Science*, vol. 28, p. 13.

Walters, J. K. 1973b, 'A theoretical analysis of stresses in axially-symmetric hoppers and bunkers', *Chemical Engineering Science*, vol. 28, pp. 779-789.

Walton, O. R. & Braun, R. L. 1985, 'Viscosity, granular temperature and stress calculations for shearing assemblies of inelastic, frictional disks', *Journal of Rheology*, vol. 30, pp. 949-980.

Walton, O. R. & Braun, R. L. 1987, 'Stress calculations for assemblies of inelastic spheres in uniform shear', *Acta Mechanica*, vol. 63, pp. 73-86.

Wineman, A. S. & Pipkin, A. C. 1964, 'Material symmetry restrictions on constitutive equations', *Archive for Rational Mechanics and Analysis*, vol. 17, pp. 184-214.

Wu, Y. H. 1990, *Static and Dynamic Analysis of the Flow of Bulk Materials Through Silos*, PhD Thesis, The University of Wollongong.

Wu, Y. H. & Schmidt, L. C. 1992, 'A boundary element method for prediction of silo pressures', *Computers & Structures*, vol. 45, pp. 315-323.

Zheng, X. M. & Hill, J. M. 1996, 'Boundary effects for couette flow of granular material: Dynamical modelling', *Applied Mathematical Modelling*, vol. 20, pp. 82-92.

Zienkiewicz, O. C. & Taylor, R. L. 1994, *The Finite Element Method*, vol.1, 4th edn, McGraw-Hill, London.